

SYNTHESIS AND INTERFACIAL CHEMISTRY OF
SUPRAMOLECULAR ASSEMBLIES

A Dissertation

Presented to

The Graduate Faculty of The University of Akron

In Partial Fulfillment

of the Requirements for the Degree

Doctor of Philosophy

Jacob J. Weingart

December, 2010

SYNTHESIS AND INTERFACIAL CHEMISTRY OF
SUPRAMOLECULAR ASSEMBLIES

Jacob J. Weingart

Dissertation

Approved:

Accepted:

Advisor
Jun J. Hu

Department Chair
Kim C. Calvo

Committee Member
David A. Modarelli

Dean of the College
Chand Midha

Committee Member
Weipeng Zheng

Dean of the Graduate School
George R. Newkome

Committee Member
Yi Pang

Date

Committee Member
Qin Liu

ABSTRACT

This dissertation describes the design, synthesis, assembly, and characterization of derivatives of 7-substituted-2,4,9-trithiaadamantane (Tripod) in regards to their supramolecular chemistries. Using the synthesized Tripod ligands, 2,4,9-trithia-tricyclo[3.3.1.1^{3,7}]decane-7-dodecylamide and 2,4,9-trithia-tricyclo[3.3.1.1^{3,7}]decane-7-carboxylic acid 6-ferrocenoyl-hexanoate, the composition and interfacial properties of mixed monolayers were investigated via Polarization Modulation Infrared Reflectance Absorption Spectroscopy (PM-IRRAS), Water Contact Angle (WCA) measurements, and Cyclic Voltammetry (Cv). It was found that perturbations in the monolayers occurred, increasing the degrees of freedom for the attached functionalities with the possibility of forming defects such as tilt domain boundaries. This was verified when the increasing amount of the attached ferrocene end groups at the interface of monolayer and electrolyte solution resulted in a surface charge increase, which is in agreement with the notion that the electrolyte penetration into the monolayer increases.

2,4,9-Trithia-tricyclo[3.3.1.1^{3,7}]decane-7-carboxylic acid 6-(2-bromo-2-methylpropionyloxy)-hexyl ester was designed and synthesized as a unique tridentate surface anchor for Atom Transfer Radical Polymerization (ATRP) surface-initiated polymerization. The prepared initiator proved effective in the polymerization of *tert*-butyl acrylate (*t*-BA) and dimethylaminoethylmethacrylate (DMAEMA) producing

domains (40 ± 5 nm diameter) extending ~ 90 nm from the surfaces of gold slides. 2,4,9-Trithia-tricyclo[3.3.1.1^{3,7}]decane-7-octadecylamide was designed and synthesized as a ligand to cap gold nanoparticles. The ability of the ligand to intercalate the alkyl chains of lipids across the nanoparticle surface was investigated. Solid state thermometric analyses showed that a disruption and intercalation across the nanoparticle surface is marked by a lowering of the glass transition state (T_g) of the Tripod capping agent's alkyl chains. This notion was further confirmed via dispersion tests and ¹H NMR showing a decrease in intensity of the peaks corresponding to the CH₂ and CH₃ of the alkyl chains.

Based on the principles of supramolecular chemistry, polymer nanocapsules were also synthesized and surface modified for the study of guest molecule release. Testing nanocapsules with poly(carboxylate) and poly(ethylene)glycol functionalized surfaces, it was found that the polymer nanocapsules are more effective carriers for negatively charged small molecules in aqueous solutions at pH 7.4. The fast releasing rates of the guest molecules were mostly attributed to the small size of the polymer nanocapsules (~ 60 -100 nm) and the low percent of cross-linker used in this study.

DEDICATION

This dissertation is dedicated to my family.

To my grandparents for teaching me the value of hard work.

To my parents for teaching me the value of education.

To my beautiful wife, who I met in graduate school at UA, for supporting me and giving

me the most beautiful and inspirational gift of all,

my daughter:

Alaina Nichole Weingart

7 lbs. 6 oz., 21.5”

Born 10:11 AM

August 19, 2010

ACKNOWLEDGEMENTS

I would like to give a special thank you to Dr. Jun J. Hu, my advisor and friend, for his patience during my doctoral study and the guidance that goes well beyond the laboratory. Because of him, graduate school was truly an enriching experience with many memories and it will remain one of the highlights of my life.

Thank you to my family for all of their encouragement and support throughout the years of my education through my undergraduate and graduate studies. I would also like to thank my friends for their patience as I made myself unavailable for the past 6 months to complete my doctorate study. Thank you to my lab mates, past and present, for their help whether in the laboratory or through discussion, specifically Dr. Hui Wang, Dr. Serhan Boduroglu, Dr. Debanjan Sarkar, Tejal Deodhar, Caroline Davis, Bin Cao, and Tracy Olin.

The research presented could not have been possible without the support of the Department of Chemistry and the faculty at The University of Akron. A special thanks to the dissertation committee for their valuable input and guidance, particularly Dr. David A. Moderalli, Dr. Yi Pang, Dr. Weipeng Zheng, and Dr. Qin Liu.

TABLE OF CONTENTS

	Page
LIST OF TABLES.....	xi
LIST OF FIGURES.....	xii
LIST OF SCHEMES.....	xv
CHAPTER	
I. INTRODUCTION	1
1.1 Supramolecular Chemistry of Gold and Organosulfur Compounds.....	6
1.1.1 Background and Theory.....	6
1.1.2 Technological Applications.....	11
1.2 Objectives and Approach	15
1.3 Layout of Dissertation	18
II. ELECTROCHEMICAL INVESTIGATION OF MIXED 2,4,6-TRITHIA- ADAMANTANE (TRIPOD) MONOLAYERS ON GOLD SURFACES USING A FERROCENE-BASED DERIVATIVE.....	20
2.1 Introduction.....	20
2.1.1 Design and Approach.....	23
2.1.2 Polarization Modulation Infrared Reflectance Absorption Spectroscopy (PM-IRRAS).....	26
2.2 Experimental Section.....	27
2.2.1 Materials and Methods.....	27
2.2.2 Derivative Synthesis.....	28

2.2.2.1 Synthesis of 2,4,9-Trithia-tricyclo[3.3.1.1 ^{3,7}]decane-7-dodecylamide (2).....	29
2.2.2.2 Synthesis of Ferrocenoyl-6-bromohexanoate (3).....	30
2.2.2.3 Synthesis of 2,4,9-Trithia-tricyclo[3.3.1.1 ^{3,7}]decane-7-carboxylic acid 6-ferrocenoyl-hexanoate (4).....	30
2.2.3 Self Assembled Mixed Monolayer Preparation and Characterization.....	31
2.2.3.1 Self Assembled Mixed Monolayer Preparation on Au(111).....	31
2.2.3.2 Surface Characterization of Mixed SAMs on Au(111).....	32
2.2.3.3 Electrochemical Characterization of Mixed SAMs on Au(111).....	32
2.3 Results and Discussion.....	34
2.4 Conclusions and Future Work.....	44
III. ATRP INITIATED POLYMERIZATION OF POLYMER BRUSHES FROM A SELF ASSEMBLED MONOLAYER OF TRITHIAADAMANTANE DERIVATIVE AS AN IMMOBILIZED INITIATOR ON GOLD SUBSTRATE.....	46
3.1 Introduction.....	46
3.1.1. Design & Approach.....	48
3.2 Experimental Section.....	50
3.2.1 Materials and Methods.....	50
3.2.2 ATRP Initiator Synthesis.....	51
3.2.2.1 Synthesis of 2,4,9-Trithia-tricyclo[3.3.1.1 ^{3,7}]decane-7-carboxylic acid 6-hydroxy-hexyl ester (5).....	51
3.2.2.2 Synthesis of 2,4,9-Trithia-tricyclo[3.3.1.1 ^{3,7}]decane-7-carboxylic acid 6-(2-bromo-2- methyl-propionyloxy)-hexyl ester (6).....	52

3.2.3 Initiator Immobilization, Surface-Initiated ATRP, and Characterization.....	53
3.2.3.1 Preparation of Immobilized Initiators on Gold Substrates.....	53
3.2.3.2 Preparation of Polymer-Modified Gold Substrates.....	53
3.2.3.3 Characterization of Polymer Brushes.....	55
3.3 Results and Discussion	55
3.4 Conclusions and Future Work.....	64
 IV. SYNTHESIS AND CHARACTERIZATION OF MONOLAYER PROTECTED AU NANOPARTICLES AS FUNCTIONAL MIMICS OF SMALL CELLULAR VESICLES	65
4.1 Introduction.....	65
4.1.1 Objectives	69
4.1.1.1 Design and Approach.....	70
4.2 Experimental Section.....	72
4.2.1 Materials and Methods.....	72
4.2.2 Synthesis of Ligands and Ligand-stabilized GNPs	73
4.2.2.1 Synthesis of 2,4,9-Trithia-tricyclo[3.3.1.1 ^{3,7}]decane-7- octadecylamide (TpCONC ₁₈ , 7).....	74
4.2.2.2 Preparation of TpCONC ₁₈ Monolayer Protected Gold Nanoparticles (Au MPNs).....	75
4.2.3 Lipid Interdigitation into the Monolayer of the Au MPNs	75
4.2.3.1 Thermogravimetric and Differential Scanning Calorimetry Analyses of Lipid Interdigitation in the Solid State.....	76
4.2.3.2 Forced Lipid Interdigitation via Induced Solvent Effects.....	76

4.2.3.3 Interdigitation of TpCONC ₁₈ Au MPNs with the Alkyl Chains of 1,2-Didecanoyl- <i>sn</i> -glycerol 3-phosphate sodium salt and Extraction from CDCl ₃ to D ₂ O.....	77
4.3 Results and Discussion	77
4.4 Conclusions and Future Work.....	89
V. POST-SYNTHETIC SURFACE FUNCTIONALIZATION, ENCAPSULATION, AND RELEASING STUDIES OF A NOVEL POLYMER NANOCAPSULE	90
5.1 Introduction.....	90
5.1.1. Objectives	92
5.2 Experimental Section.....	94
5.2.1 Materials and Methods.....	95
5.2.1.1 Methods for Spectral and Thermometric Analyses.....	95
5.2.2 Polymer Nanocapsule Synthesis and Functionalization	96
5.2.2.1 Synthesis of the Polymer Nanocapsules.....	96
5.2.2.2 Hydrolyzation of the <i>t</i> -Butyl Ester of the Polymer Nanocapsule.....	97
5.2.2.3 Surface Modification of Polymer Nanocapsules with Poly(ethylene glycol).....	97
5.2.3 Encapsulation and Release Studies.....	98
5.2.3.1 Encapsulation of Fluorescein into the Polymer Nanocapsules and Release Studies	98
5.2.3.2 Encapsulation of 5-Fluorouracil into Surface Modified Polymer Nanocapsules and Release Studies.....	98
5.3 Results and Discussion	99
5.4 Conclusions and Future Work.....	110
REFERENCES.....	111

LIST OF TABLES

Table		Page
2.1	PM-FTIRRAS data for methylene stretching modes compared to varying mole fractions (based on 1×10^{-5} mols) and bulk material.....	37
2.2	The data obtained from calculating surface charge densities of the mixed monolayers.....	42
3.1	Water contact angle (WCA) and ellipsometry measurements.....	60
4.1	A list of lipid mixture weight ratios mixed with TpCONC ₁₈ Au MPNs and observations upon 72 h exposure to phosphate buffer (pH 7.4).....	85
5.1	The behavior of the polymer nanocapsules exposed to different solvents over an 8 hour period at 25°C.....	104
5.2	The releasing results fitted to $W_t/W_\infty = kt^n$ based on a non-linear fit using Microcal Origin version 6 software.....	109

LIST OF FIGURES

Figure	Page
1.1 Hydrogen bonding (---) resulting from Watson-Crick base pairing of DNA nucleotides.....	4
1.2 Space filling projection of a Au(111) crystal lattice with example binding sites (areas in gray, $\sim 21.6 \text{ \AA}^2$) centered between 3 Au atoms.....	8
1.3 Typical design of a organomercaptan ligand for nanotechnology applications.....	12
1.4 Random substituent (R) in the 7 position of the tridentate sulfur ligand 2,4,9-Trithiatricyclo[3.3.1.1 ^{3,7}]decane.....	17
2.1 Designed derivatives for the electrochemical investigation of Tripod-based self-assembled monolayers.....	24
2.2 A representation of the electrochemical cell used in the experiment.....	33
2.3 PM-FTIRRAS spectra of the mixed monolayers (TpC ₁₂ :TpFc) with increasing mole ratio of the ferrocene derivatized 2,4,9-trithiaadamantane.	35
2.4 PM-FTIRRAS spectra of the mixed monolayers (TpC ₁₂ :TpFc) with increasing mole ratio of the alkyl derivatized 2,4,9-trithiaadamantane.....	35
2.5 Water contact angle measurements with noted mole ratios (TpC ₁₂ :TpFc)...	39
2.6 Cyclic voltammograms of mixed monolayers with increasing mole ratio of TpC ₁₂ :TpFc from 1:0 to 1:1 (1.0×10^{-5} mols set as 1).....	41
2.7 Cyclic voltammograms of mixed monolayers with increasing mole ratio of TpC ₁₂ :TpFc from 1:1 to 0:1 (1.0×10^{-5} mols set as 1).....	41

2.8	A plot of charge density versus mole percent TpFc with a linear fit (standard error of data points $\pm 20\%$, data from mole ratios 1:0.25, 1:0.5, and 0.75:1 removed due to slide damage).....	43
3.1	Polarization modulation infrared reflectance absorption spectroscopic data for (a) 2,4,9-trithiaadamantane polymer brush initiator, (b) poly- <i>t</i> -BA brushes, and (c) PDMAEMA brushes on a Au slide surface.....	59
3.2	The AFM profiles of Poly- <i>t</i> -BA and PAA carboxylate polymer brushes.....	62
3.3	The AFM profiles of PDMAEMA and quaternized PDMAEMA polymer brushes.....	63
4.1	A TEM image of GNPs exposed to polar solvent and depiction of alkyl chain intercalation on the Au nanoparticle surfaces.....	70
4.2	The ligand exchange reaction of TpCONC ₁₈ with Ph ₃ P (integration values noted in red) on GNP surface monitored via ¹ H NMR spectroscopy.....	79
4.3	The thermo-gravimetric analysis (TGA) of TpCONC ₁₈	80
4.4	The DSC thermogram of TpCONC ₁₈ Au MPNs (data offset by 10 mW).....	82
4.5	The DSC thermogram of TpCONC ₁₈ Au MPCs mixed with chicken egg L- α -phosphatidylcholine (data offset by 5 mW).....	84
4.6	The DSC thermogram of TpCONC ₁₈ Au MPCs mixed with 1,2-dipalmitoyl- <i>rac</i> -glycero-3-phosphocholine hydrate (data offset by 5 mW).....	84
4.7	The chemical structures of the three lipids tested.....	86
4.8	The induced lipid interdigitation into TpCONC ₁₈ Au MPNs and transfer to D ₂ O monitored via ¹ H NMR.....	88
5.1	FT-IR of the unmodified (<i>a</i>), hydrolyzed (<i>b</i>), and PEGylated (<i>c</i>) poly(allylamine)- <i>g</i> -poly(<i>t</i> -butylacrylate) polymer nanocapsules.....	101
5.2	The DSC measurements of (<i>a</i>) hydrolyzed, and (<i>b</i>) PEGylated poly(allylamine)- <i>g</i> -poly(<i>t</i> -butylacrylate) polymer nanocapsules with arrows indicating glass transition states (<i>T_g</i> 's).....	103
5.3	The TGA measurements of (<i>a</i>) hydrolyzed and (<i>b</i>) PEGylated poly(allylamine)- <i>g</i> -poly(<i>t</i> -butylacrylate) polymer nanocapsules.....	103
5.4	Fluorescein release profile for the hydrolyzed polymer nanocapsules with range of error denoted as space between dotted lines.....	107

5.5	Fluorescein release profiles for the PEGylated polymer nanocapsules with range of error denoted as space between dotted lines.....	107
5.6	5-Fluorouracil release profiles for hydrolyzed polymer nanocapsules with range of error denoted as space between dotted lines.....	108
5.7	5-Fluorouracil release profiles for PEGylated polymer nanocapsules with range of error denoted as space between dotted lines.....	108

LIST OF SCHEMES

Scheme	Page
1.1 A schematic representation of the hierarchy of protein structure.....	3
1.2 Dissociative chemisorption process of a bifunctional organic disulfide.....	7
1.3 The formation of monolayer via conversion of thiol to thiolate.....	10
1.4 Representations of (a) spectroscopic and (b) electrochemical detection of targeted analyte binding.....	14
1.5 Synthesis of 7-methylester-2,4,9-trithiaadamantane developed by Hu and Khemtong.....	18
2.1 The synthesis of 7-dodecylamide-2,4,9-trithiaadamantane as an alkyl derivative.....	25
2.2 The synthesis of the 2,4,9-trithiaadamantane derivative with a ferrocene redox probe attached.....	25
2.3 Representation of a mixed monolayer using the designed derivatives.....	37
3.1 Comparison of the 7-substituted-2,4,9-trithiaadmantane initiator to other typically used ATRP initiators.....	49
3.2 Synthesis of the 2,4,9-trithiaadamantane ATRP surface initiator group.....	57
3.3 The synthesis of the poly- <i>t</i> -BA brushes.....	58
3.4 Synthesis of the PDMAEMA brushes.....	58

4.1	A representation of a general nanoparticle with varying functionalities.....	66
4.2	A schematic representation of gold nanoparticle stabilization and protection by an alkyl derivative of 2,4,9-trithiaadamantane and subsequent lipid intercalation.....	71
4.3	The synthesis of 2,4,9-trithia-tricyclo[3.3.1.1 ^{3,7}]decane-7-octadecylamide.....	78
5.1	The chemical modifications of the poly(allylamine)- <i>g</i> -poly(<i>t</i> -butylacrylate) nanocapsules.....	93

CHAPTER I

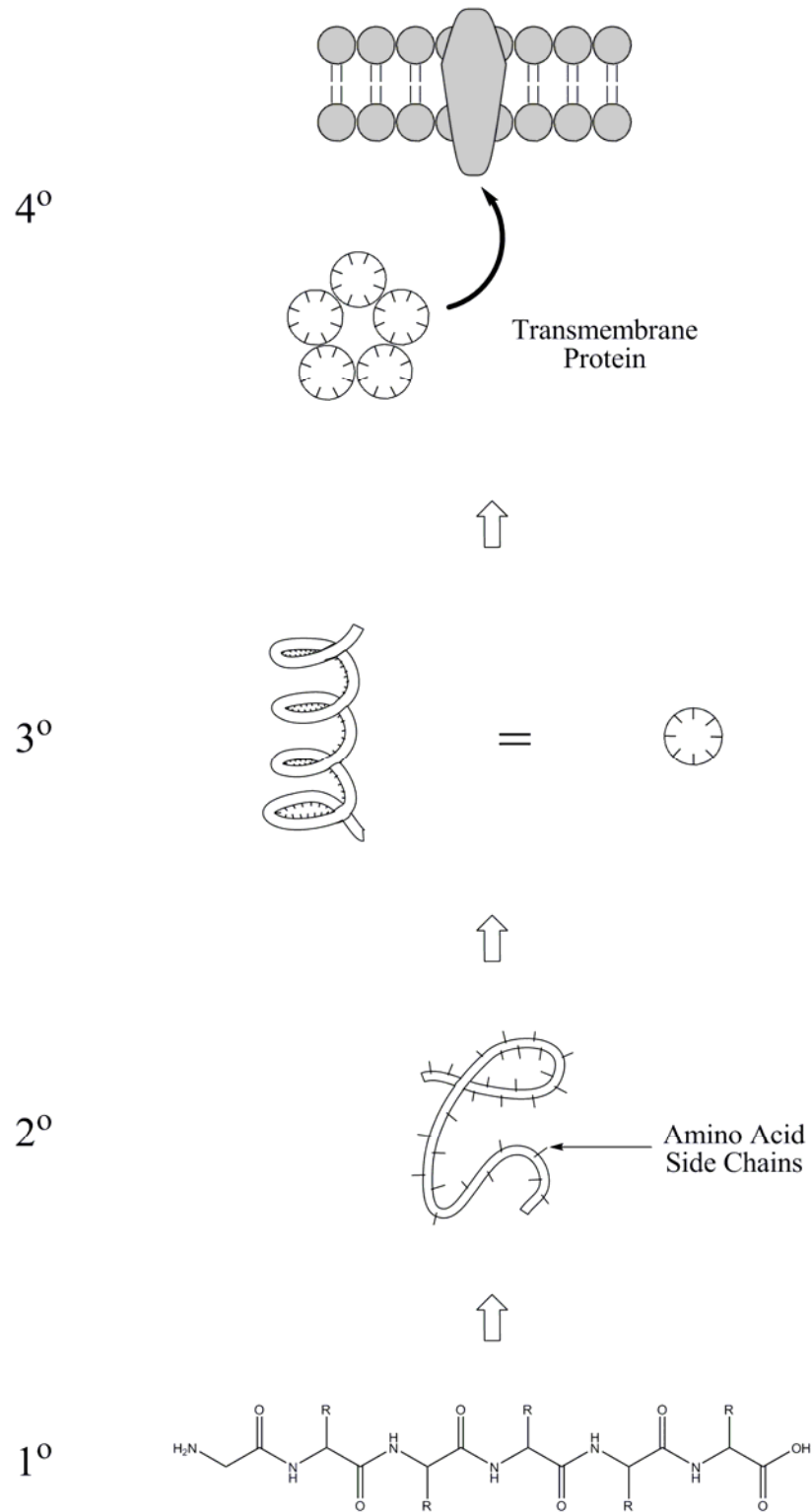
INTRODUCTION

Molecular chemistry can be defined as the chemistry of covalent bonding, the distinct sharing of electrons through inter-atomic space holding multiple atoms together to form an energetically stable molecular structure, an idea that is expressed across a wide variety of fields, especially in chemistry and physics. However, a true appreciation of the complexities of molecular chemistry can not be achieved without recognizing its mastery in nature. Nature not only creates covalent molecular structures in a thermodynamic energy efficient manner, but also uses these structures as building blocks for higher ordered structures. These higher ordered structures do not have to exist as one cohesive, covalently bound unit. Instead, the building blocks, individual molecular structures, are brought together via non-covalent intermolecular forces. The study of these intermolecular forces and their ability to form these higher ordered structures from multiple building blocks, or subunits, has lead to the birth of supramolecular chemistry.¹

Supramolecular chemistry is governed by the following types of non-covalent interactions: ionic bonding, hydrogen bonding, hydrophobic interactions, van der Waals forces and dipole-dipole bonding. These interactions are often weak, therefore it is a rarity that a single type of non-covalent interaction is solely responsible for creating a

higher ordered structure. Instead, it is often a complicated interplay between multiple types of these interactions. This is where the concept of supramolecular chemistry is employed to study and understand the phenomena and interplay of the multiple non-covalent intermolecular forces holding these higher ordered structures together. Two classical examples of supramolecular chemistry represented in nature are the formation of proteins and the formation of double stranded DNA.

Proteins often consist of two or more polypeptides that are non-covalently bound to each other to form a larger, higher ordered structure. Traditionally, proteins can be broken down into four orders of structure with three of the four being driven to form via non-covalent forces. Single peptides themselves are of primary structure. It is when these peptides begin to fold in on themselves that conformations of lower energy are achieved. These conformations, secondary and tertiary structures, are thermodynamically stable due to hydrophobic interactions on the more non-polar amino acid residue side chains causing them to avoid water as the polar amino acids favor water and hydrogen bond with each other.² When two or more of these polypeptide chains, referred to as subunits, are driven together via the same non-covalent molecular forces, the end result is the enzyme protein in quaternary structure. This process is represented in Scheme 1.1. Similarly, the formation of the double helix, double-stranded DNA, is driven by similar non-covalent forces. The three non-covalent forces driving DNA to form the stable helix structure are hydrogen bonding amongst base pairs, base stacking driven by hydrophobic interactions, and ionic interactions.³ Base pairing resulting in hydrogen bonding is singly the most important of the three and is depicted in Figure 1.1.



Scheme 1.1 A schematic representation of the hierarchy of protein structure.

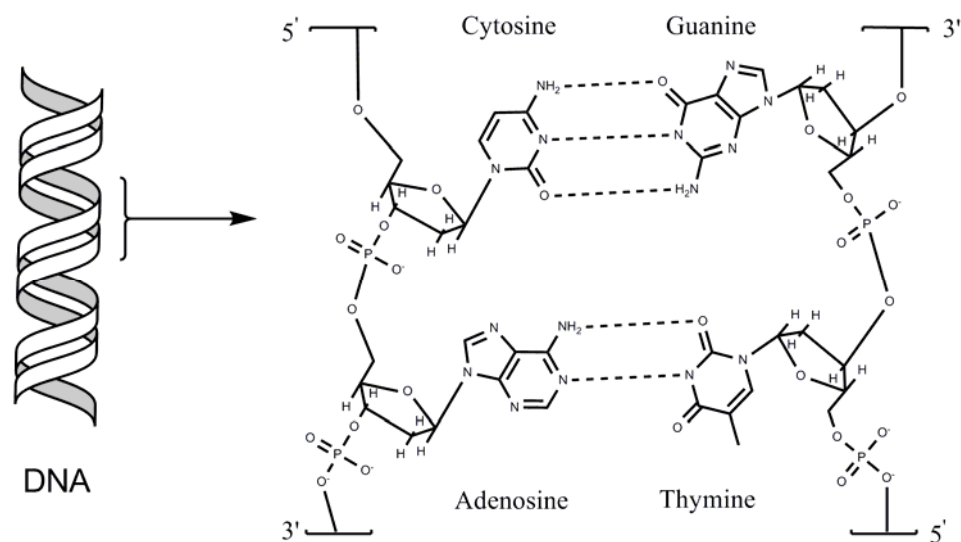


Figure 1.1 Hydrogen bonding (---) resulting from Watson-Crick base pairing of DNA nucleotides.

Prior to the observations of the previously mentioned examples in nature, supramolecular chemistry has been unknowingly used for centuries dating back to the first ancient shipwrights who used natural oils to form sufficiently ordered layers of hydrophobic molecules to preserve wood from water damage on their ships. Modern day wood protectants that are similar are referred to as varnishes.⁴ Though materials supramolecular in nature were being used, it would not be until the late years of the nineteenth entering the twentieth century that such phenomena became regularly studied upon the recognition of the existence of molecules. The most notable individual to perform systematic studies of the self-assembling of molecules was Langmuir in 1917.⁵ These molecules were amphiphilic, such as lipids, and assembled at the air/water interface. These molecules were then shown capable of being deposited on solid substrates creating organic thin films by Katherine Blodgett.⁶ Hence, these films have

come to be known as Langmuir-Blodgett films. Further studies eventually elucidated the fact that one could induce such assemblies to form monolayers in solution onto a hydrophilic substrate. This substrate then attracts the hydrophilic head group of amphiphilic molecules when they are dissolved in hydrophobic solvent.⁷ This induced phenomena led to the development of the field of self assembly creating many variations in terms of techniques applied and materials used. Understanding the self assembly process has become the driving force in the development of the field of supramolecular chemistry to produce higher ordered man-made structures.

In the last two centuries, with the recognition of supramolecular chemistry, the development and maturation of organic chemistry, the quest to mimic nature has never been so enduring. Organic chemistry, the chemistry of carbon and its unique intramolecular interactions with hydrogen and heteroatoms, such as nitrogen, oxygen, and sulfur, has become a key tool in developing new systems in the field of supramolecular chemistry. Without the ability to synthetically create the molecules used in nature, or mimics there of, it is difficult to investigate the assembly and molecular interactions of a variety of higher ordered supramolecular structures. The ability to do so has allowed the development of many new materials and has provided the platform for the field of nanotechnology. For this reason, supramolecular chemistry has become a highly interdisciplinary field with a wide range of phenomena investigated in the physical and biological sciences.

1.1 Supramolecular Chemistry of Gold and Organosulfur Compounds

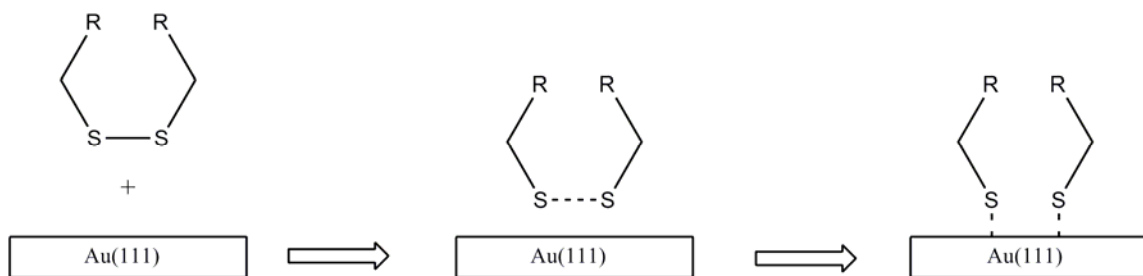
Since ancient times the precious metal gold has been highly sought after by kings and poor men alike. To this day, it is still of immense value, not just in terms of wealth, but in essence as a key component of all modern day technology. Every solid state electronic device today, relies on gold's use in its components due to the ability as a highly efficient conductor resistant to corrosion. From the smallest cellular phone to the computer that this dissertation was typed with, gold is one of the key elements which allows them to function properly. It is no wonder, that this noble transition metal has become the research focus of so many within the field of chemistry, especially in supramolecular chemistry.

The supramolecular chemistry of gold, in particular the spontaneous self assembly of heteroatom containing organic molecules onto gold surfaces, is of great interest in the development of new materials. Though a variety of organic molecules have been investigated, the study of the self assembly of organomercaptans, sulfur containing compounds, onto gold dominates the field of gold supramolecular chemistry.⁸ This in part, is owed to the pioneering work of Nuzzo and Allara,⁹ who recognized the ability of such molecules to form supported monolayer assemblies on gold substrates. These supported monolayer assemblies of specifically oriented organic molecules became of great interest and importance in thin film interfacial studies.

1.1.1 Background and Theory

In the early 1980s the ability of sulfur-based organic molecules to form oriented monolayer assemblies began to receive tremendous attention. Initial studies by Nuzzo,

Allara, and Dubois were originally performed under ultra-high vacuum (UHV) using organic disulfides and single sulfur containing thiol-based organic molecules.⁹ Gold was the transition metal of choice, the crystalline structure being closely packed and its zerovalent state rarely forming oxides in ambient conditions. Using reflectance Infrared (IR) spectroscopy, the adsorption of bifunctional organic disulfides showed no evidence of C-S cleavage on the gold surfaces, unlike silver substrates.⁹ However, there was no evidence from the results suggesting that the adsorption of the sulfur in the disulfide bond (S-S) was any different from the process associated with silver substrates, therefore it was purposed that the adsorption of disulfides may be a dissociative chemisorption process as depicted in Scheme 1.2.⁹



Scheme 1.2 Dissociative chemisorption process of a bifunctional organic disulfide.⁹

In a comparison of the chemisorption of monodentate sulfur containing thiol compounds versus that of bidentate disulfides, the formation of thin films of thiols and bifunctional disulfides on flat gold surfaces under UHV were studied via ellipsometry, scanning electron microscopy (SEM), X-ray Photon (XPS) and reflectance infrared (RIRS) spectroscopies.¹⁰ Based on XPS data and desorption studies, it was shown that the bidentate disulfides were more strongly bound having binding energies that

approximate to 30 kcal/mol, twice that of the monodentate thiols which ranged from ~12 to 14 kcal/mol.¹⁰ As for the modes of binding, XPS measurements at the S 2p core level for the bidentate sulfides exhibited large shifts and the disappearance of S-S stretching in RIRS suggest reduction of the disulfide to the thiolate species upon binding to gold. Based on crystalline gold's lattice structure, it appeared that one sulfur atom binds centering on 3 gold atoms (Figure 1.2), the area required calculated to be $\sim 21.6 \text{ \AA}^2$.¹⁰ This is a distance far too great for any disulfide, only 2.05 Å for the S-S bond length, to stretch and bind properly distributed on the gold lattice. Therefore, it was reasonable that reduction to the thiolate was the scenario that presented itself in these experiments. Though disulfides present themselves as thiolates bound to the gold surface, this is not the case for monodentate thiols. XPS shifts going from the bulk to chemisorbed states were small, suggesting that the S-H bond is not cleaved under UHV.¹⁰

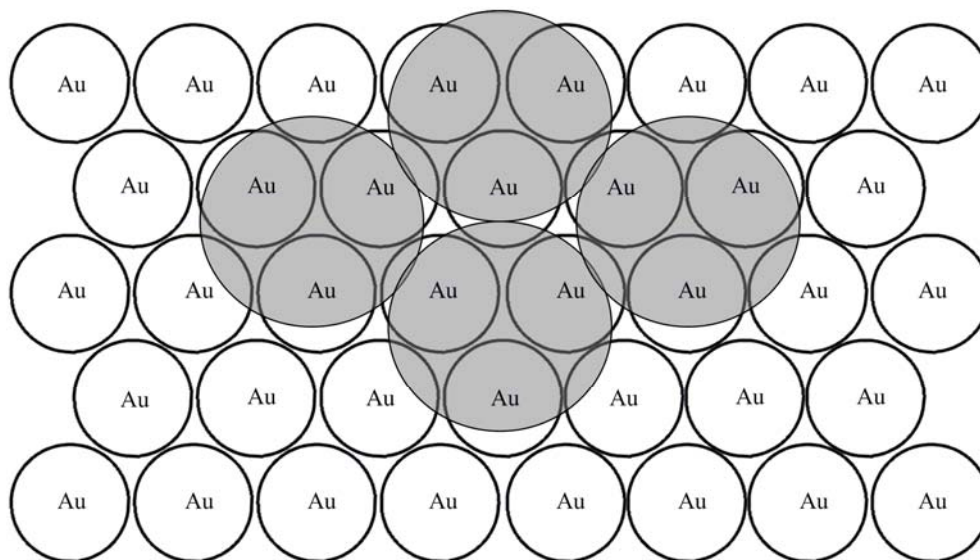
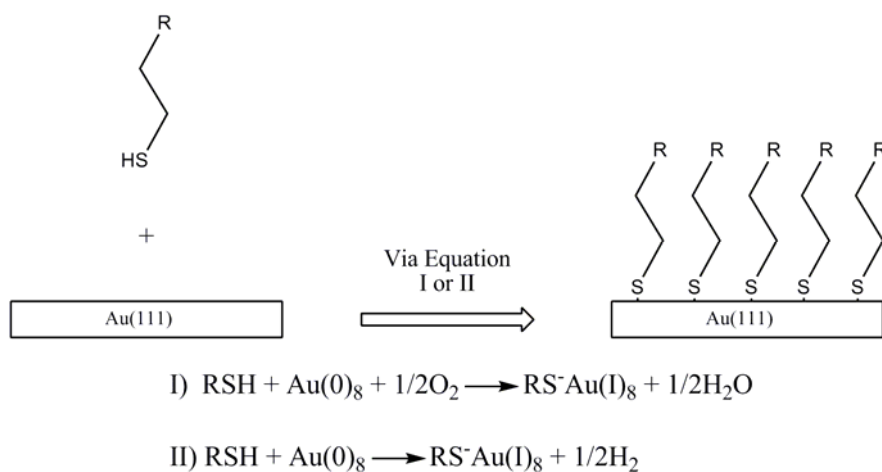


Figure 1.2 Space filling projection of a Au(111) crystal lattice with example binding sites (areas in gray, $\sim 21.6 \text{ \AA}^2$) centered between 3 Au atoms.¹⁰

In solution phase, the same results can be said for organic disulfides. The molecules tend to have a strong adsorbate-substrate interaction with gold having high surface coverages, depending on the functionality, almost reaching those of condensed crystalline bulk phases. Desorption data suggested that the adsorption bond energy still resides $\sim 30 - 35$ kcal/mol, which does not vary much from the values calculated from previous experiments under UHV.¹¹ However, this is not the case for single sulfur bearing thiols. In a study by George Whitesides et al.,¹² based on the theory disulfides adsorb as thiolate (RS^-), it was proposed that the same must occur for thiols. Looking at the adsorption of mixed thiols and analogous disulfides, the competitive nature of the self assembly process was investigated between the two types of sulfur bearing molecules in hopes of defining a mechanism. It was shown that in solution, thiols have a strong preference towards binding to gold (75:1) compared to disulfides, while XPS data showed that the mixed adsorbates yield the same species on the gold surface (RS^-).¹² Furthermore, advancing contact angle measurements of the mixed monolayers were not sensitive to the monolayers components, suggesting that the monolayers produced by the two types of molecules are structurally similar, verifying the notion the two adsorb as the same species.¹² However, this study still does not answer how thiols ($RS-H$) lose a proton to become thiolate. Therefore, it was suggested that the formation of thiolate may be the result of either oxidation by O_2 or the catalytic loss of $H_{2(g)}$ as depicted in Scheme 1.3 where $Au(0)_8$ and $Au(I)_8$ represent the 0 and +1 oxidation states of gold.¹²



Scheme 1.3 The formation of a monolayer via conversion of thiol to thiolate.¹²

Whitesides' theory as how the sulfur in organomercaptans binds to gold has become generally accepted amongst those in the self-assembled monolayer (SAM) research community.⁸ This theory was only further strengthened upon the transition from investigating SAM formation on flat gold surfaces to the 3-D surfaces of gold colloids. However, some have argued that the method in which thiol-based monolayers are produced on the surfaces of gold colloids dictates the path of the sulfur gold bond formation.¹³ As for the nature of the bond itself, modern day computing has helped to produce models using *ab initio* calculations. Based on the models, regardless of the surface or method used to produce thiol-based monolayers, the nature of the sulfur bond fits that described by inorganic chemistry where a σ bond is the result of the hybridization of p orbitals which combine with gold's states of proper symmetry.¹³ The result is the bridging of the sulfur atom between two gold atoms, which is in agreement with the previously mentioned (Figure 1.2) predicted space-filling models by Nuzzo and Dubois.¹⁰

1.1.2 Technological Applications

The early work investigating the thio-induced self-assembly process of organic monolayers has helped build an understanding of how to create ordered thin films on gold surfaces. However, the first thin films were found of little use, being simple alkyl thiols and alkyl thiolates.¹⁴ These initial films were subject to a variety of tests such as the addition of secondary adsorbates for applications in corrosion and lubrication.¹⁴ However, these films failed to display even coverage exposing the fact that secondary adsorbates can disrupt the surface coverage of the initial adsorbates. In terms of corrosion, any defects in the surface would be detrimental.¹⁴ Based on scratch tests performed in previous studies, single monolayers of alkyl thiols and alkyl thiolates failed to show any lubricating properties.¹⁵ Though these simple alkyl-based monolayers do not prove useful for any practical applications, they still remain the simplest for studying the self assembly process.

Functionalization of organomercaptans and manipulation of the self-assembly of these ligands has led to the development of a variety of technologies. These technologies often encompass the area of nanotechnology and are implemented in electronics, optics, catalysis, diagnostic sensors, imaging, and therapeutics.¹⁶ The basis for the design of such ligands can be seen in Figure 1.3 each containing the sulfur based anchor, a linker group, and the respective functional group for the desired application. The nanotechnology created based on these synthetic ligands has an impact in the development of many analytical applications, especially point-of-care (POC) devices.¹⁶ In the last decade, the functionalization of organomercaptans with biomolecules and their

immobilization on gold chips or colloids has been the main focus of researchers for the development of new analytical tools. Using functionalized gold has become the premier choice due to gold's unique properties, specifically those dealing with its optical and electronic properties that do not warrant the use of secondary detection reagents.¹⁷

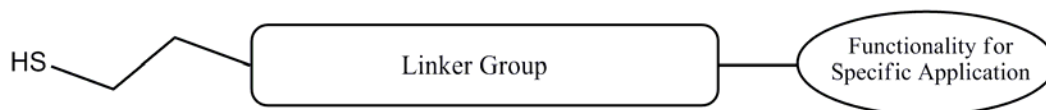
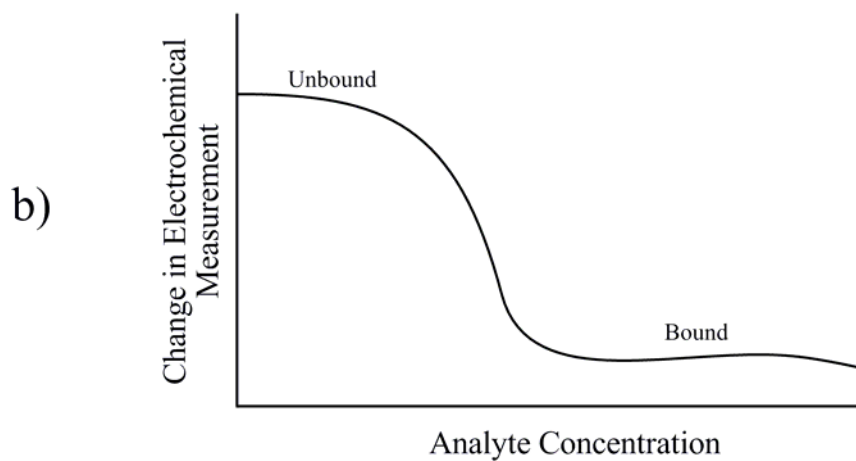
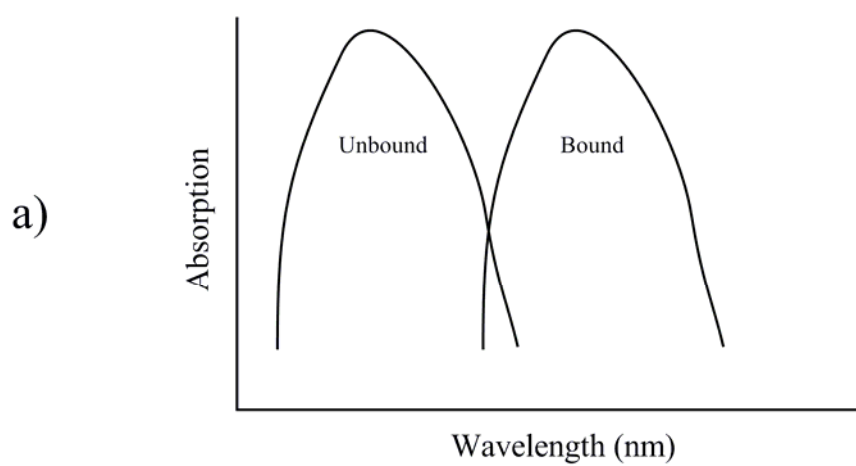
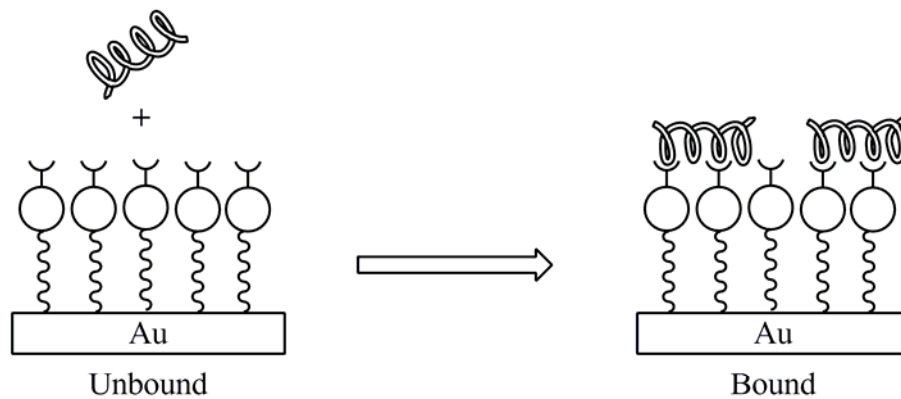


Figure 1.3 Typical design of an organomercaptan ligand for nanotechnology applications.

The unique optical behavior of gold is very sensitive to quantum effects, allowing for a unique phenomena called surface plasmon resonance (SPR).¹⁷ This is a phenomena in which electromagnetic waves propagate parallel to the gold/dielectric surface interface. These oscillations are defined by the electronic density of states of the gold structure, whether 1-D, 2-D, or 3-D, and are very sensitive to changes at the gold/dielectric interface.¹⁷ This can be visibly seen in gold colloids. In colloidal gold particles there exists the presence of a strong band in the visible region of light which is attributed to the SPR oscillation modes of the conduction electrons coupled through their surfaces to the applied electromagnetic field, in this instance light itself. This gives rise to plasmon absorption bands that appear around 520 nm, dependent upon the diameter of the particle size and distance between the particles, which produces red to purple wine-like colors in solution.¹⁸ When the distance is diminished between two functionalized gold particles upon binding of a target analyte, this color shift from red to purple is visibly notable and

represents just one of the many ways this type of system is implemented in the development of new analytical and diagnostic technologies. Flat gold and gold colloids alike, can both be used to detect analytes based on the same principles. However, one must use laser spectroscopy to detect the changes in the localized surface plasmon resonance (LSPR) on the surface of the gold/dielectric interface as depicted in Scheme 1.4a.¹⁹

Gold as a noble transition metal is a great conductor and implements itself in the development of electrical biosensor technologies. These electrical biosensors are attractive for the fact that, if properly designed, they allow for the multiplexed detection of a wide range of biomarkers with selectivity and sensitivity comparable to standard immunoassay methods.²⁰ This is done via the functionalization of flat gold surfaces with synthetically designed organomercaptans hosting a specific targeting groups that bind particular analytes. Upon binding of the analytes, electrochemical changes occur and are measured via electrochemical impedance spectroscopy (EIS) methods as represented in Scheme 1.4b. Changes can be measured via electrochemical conductance, capacitance or, the most difficult to implement, field effect transistor (FET) based transconductance.²¹ Charles Lieber of Harvard and his associates are in the forefront in developing biosensing technologies based on such measurements. They have demonstrated the detection of DNA within 10 femtomolar sensitivity as well as a number of other biological agents.²² Others following suite have designed a variety of biosensors. Some go beyond simple measurements, but instead are designed to mimic actual physical senses, specifically animal olfactory sensing.²³ Then there are those who, instead of detecting simple



Scheme 1.4 Representations of (a) spectroscopic and (b) electrochemical detection of targeted analyte binding.

biomarkers, have aimed at the detection of macromolecular proteins and even whole bacterial cells in an attempt to develop systems for the rapid identification of disease states.²⁴ The potential for development of such devices for electrochemical sensing of analytes as POC devices, far exceeds laser spectroscopy-dependent methods. This is because even the smallest laser set-up is still fairly large and requires more energy than the typical sensing set-up based on EIS methods.^{21,22}

1.2 Objectives and Approach

Self assembly of organic molecules on gold surfaces is dominated by the use of monodentate organomercaptans.⁸ However, there still exists many limitations surrounding the use of such ligands, especially in the development of new materials for analytical purposes. Monodentate ligands are unstable being susceptible to oxidation and are therefore often times difficult to deal with, requiring them to be synthesized and manipulated in a nearly oxygen free environment.⁸ There also exists issues of phase segregation.²⁵ As previously mentioned in the preceding sections of this dissertation, the use of a single type of organomercaptan ligand, even when functionalized with a targeting moiety, will assemble to form a nearly uniform, condensed crystalline bulk phase.²⁵ For applications, particularly those analytical in nature, this highly dense packing restricts the freedom of motion of the targeting moiety.²⁵ This restriction hinders the ability of the targeting moiety to assume the favored conformation to participate in multivalent interactions that are often times required for a successful binding event, particularly those of biological molecules.²⁶ In the past it was assumed that to overcome this problem, the use of mixed monolayers could be used. However, this is not the case

due to phase segregation into separate domains of the two molecules upon assembly on the gold surface. Like any other organic molecule, when assembling on a gold surface or any other interface, sulfur ligands of similar structure will favor assembling with each other rather than mixing with those of a completely different structure. The limitations caused by the issues of high density packing and phase segregation can be diluted via the use of sterically irregular linkers or mixing of short chain alkyl thiolates into the self assembled monolayer.²⁷

In 2002, the potential application of a previously synthesized, tridentate sulfur ligand to overcome the limitations of high density packing was recognized by Fox and Whitesell.²⁸ This tridentate sulfur ligand, 2,4,9-Trithiatricyclo[3.3.1.1^{3,7}]decane-7-substituent depicted in Figure 1.4, was reportedly synthesized by Lindgren in 1976.²⁹ It was purposed that this molecule could overcome the limitations of high density packing and provide a new organomercaptan ligand less susceptible to oxidation. With an adamantane-like cage, this ligand is a rigid and symmetrical structure having a large footprint and should be easy to characterize spectroscopically.²⁸ Due to the fact this ligand is functionalized at a single carbon, this large footprint should create a 1 to 3 dilution effect reducing the effect of high density packing allowing for an enhanced range of motion for any targeting moieties attached.²⁸ The base of the ligand also proves valuable in the sense that the three sulfurs are part of a more stable thioether moiety and provide a large area of surface coverage. However, the yield of this ligand was too low to elicit further pursuit. Thus, little progress was made to study this molecule as it proved difficult to acquire synthetically.²⁹

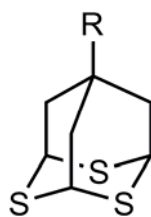
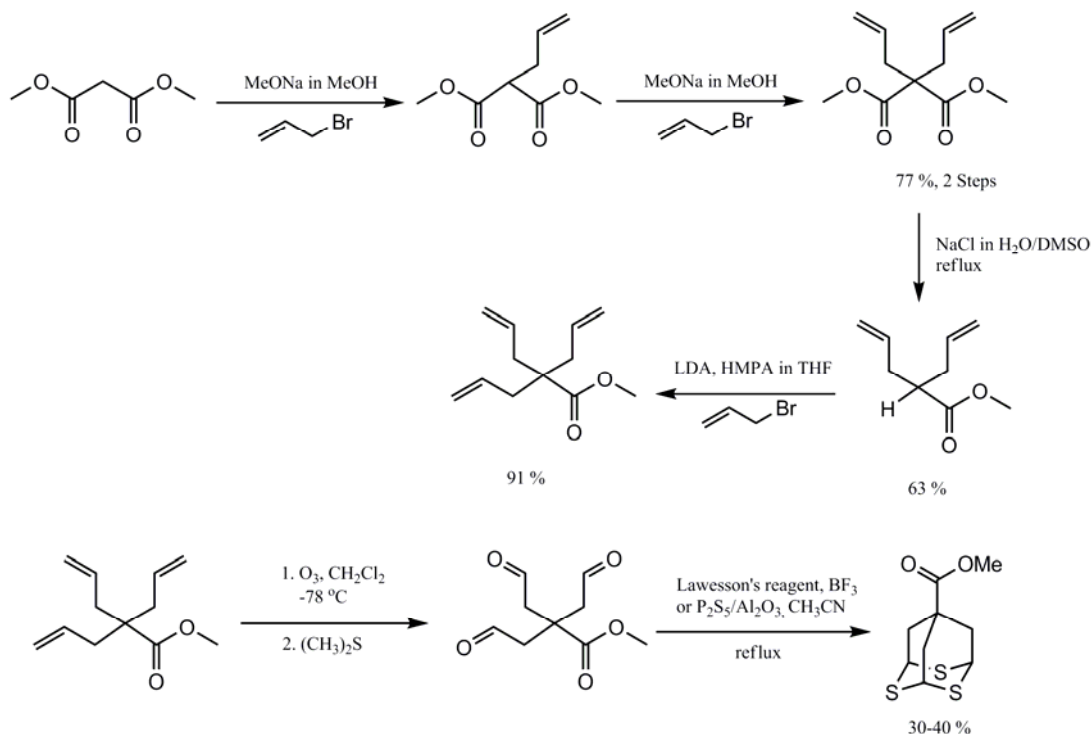


Figure 1.4 Random substituent (R) in the 7 position of the tridentate sulfur ligand 2,4,9-Trithiatricyclo[3.3.1.1^{3,7}]decane.

In 2005, the potential of this molecule was unlocked with the development of a new synthetic method produced by Jun Hu and Chalermchai Khemtong.³⁰ This synthetic method, illustrated in Scheme 1.5, allows for the production of the methyl ester derivative of the tridentate ligand, 7-methylester-2,4,9-trithiaadamantane or Tripod for short, in yields of 30-40%. With the capability of synthesizing this ligand in usable quantities, a variety of derivatives have been synthesized leading to investigative studies characterizing a number of physical properties of the molecule, including the formation of inclusion complexes in β -cyclodextrin and its use in photochemical patterning on gold surfaces.^{27,30,31}

Due to the uniqueness of the ligand, 7-substituted-2,4,9-trithiaadamantane, the number of potential applications seems limitless. Therefore, it is the aim of this dissertation to design, synthesize, characterize, and apply derivatives of the surface anchor as key building blocks in the self-assembly of supramolecular structures on gold surfaces. With the ability to be functionalized at the 7 position and the presence of three sulfurs at the 2, 4, and 9 positions of the adamantane cage, a variety of functionalities will be introduced effectively mimicking other assemblies produced using thiols. These assemblies and their interfacial chemistries will then be characterized, investigating their

potential for the development of new applications surrounding the use of 7-substituted-2,4,9-trithiaadamantane. The knowledge and understanding of such surface chemistries can then be applied to other supramolecular systems, in this dissertation specifically polymer nanocapsules.



Scheme 1.5 Synthesis of 7-methylester-2,4,9-trithiaadamantane developed by Hu and Khemtong.³⁰

1.3 Layout of Dissertation

The following chapters each discuss design, synthesis, assembly, and characterization of derivatives of 7-substituted-2,4,9-trithiaadamantane for specific applications. Chapter II shall discuss the electrochemical investigation of mixed 2,4,9-trithiaadamantane monolayers on gold surfaces using a ferrocene-based derivative. The study of such a system has been aimed towards investigating monolayer influences in

terms of sulfur base ligand mixing and phase segregation. Chapter III investigates the assembly and synthesis of macromolecular polymeric structures extending from gold surfaces using a 2,4,9-trithiaadamantane derivative as a immobilized initiator for Atom Transfer Radical Polymerization (ATRP). Chapter IV investigates the synthesis and characterization of monolayer protected gold nanoparticles as potential mimics of small cellular vesicles. Chapter V investigates the post-synthetic surface functionalization, encapsulation and the releasing studies of guest molecules from novel polymer nanocapsules.

CHAPTER II

ELECTROCHEMICAL INVESTIGATION OF MIXED 2,4,6-TRITHIAADAMANTANE (TRIPOD) MONOLAYERS ON GOLD SURFACES USING A FERROCENE-BASED DERIVATIVE

2.1 Introduction

As previously mentioned, the functionalization of gold with modified thiols has become the most prevalent and pivotal metal-molecule binding motif in the ongoing development of electrical sensor technologies.¹⁶ This in part, is owed to the past systematic investigations of alkanethiol self-assembled monolayers and their respective properties.³² Initially, the recognition of the ability of organomercaptans to bind to transition metals such as gold led to further investigations of SAM formation on other transition metal surfaces within the d^9 block. The d^9 block metals Cu, Ag, and Au are electronically important metals often times implemented in the circuit boards of devices. However, with the exception of Au, these metals are highly susceptible to oxidation. For this reason, alkanethiol SAM formation on these metals were first sought as a means to prevent oxidation, which results in corrosion, of these surfaces. However, this proved dire, the SAM quality being directly linked to the reactivity of the metal surface resulting in poor monolayer coverage when prepared in an aerobic environment.³³

By process of elimination, gold was recognized as the premier choice for not only studying the self assembly process of thiol monolayers but also their electrochemical properties as well, due to the metal's conductivity. Thus, using SAMs on gold became a convenient and versatile method, with much structural information already available, for producing models for electrochemical studies. Initial studies were aimed towards defining the electrochemical properties of thiols containing a variety of functionalities proving that those with carbon chains of 10 or longer packed into crystalline-like film create dielectrics of expected thicknesses and dielectric constants.³⁴ Further studies using mixed thiol systems in the self assembly process proved that perturbation of the underlying phase of the monolayer directly affects the properties of the dielectric monolayer.³⁴ This has led to two important observations that have had an impact on the current methods of electrical sensor design using such SAM systems on gold. One, ligands must be designed with built in phases using phase segregation as a method to prevent the active targeting moiety from penetrating back into the monolayer disrupting the crystalline nature of the monolayer, yet still must be flexible enough to bind the appropriate analyte.³⁴ The second observation, is the fact that a perturbation in the monolayer itself can be used as a detection method based on monitoring the electrochemical changes within the dielectric itself. These findings have been implemented in a variety of electrochemical-based sensor technologies.^{35,36}

Other uses for designing SAMs on gold for electrochemical investigations have a more fundamental approach. One example is the investigation of long-distance, interfacial electron transfer. This phenomena is central to a number of diverse processes ranging from those that are biological in nature, such as photosynthesis and respiration, to

man-made applied materials, such as dye sensitization of photographic materials and amperometric detection with enzyme-modified electrodes.³⁷ However, in the past experimental systems designed to investigate such events were far and few in between.³⁷ In 1984, Li and Weaver attempted such a study using an electroactive head group tethered to an electrode surface showing that rate of electron transfer is inversely related to carbon chain length, the longer the chain the slower the rate.³⁸ However, this system was limited to a few key observations for the structure of the interface was unknown.³⁸ For nearly a decade, after the accumulation of the structural information of various SAMs, would the notion of using an electroactive head group be explored.

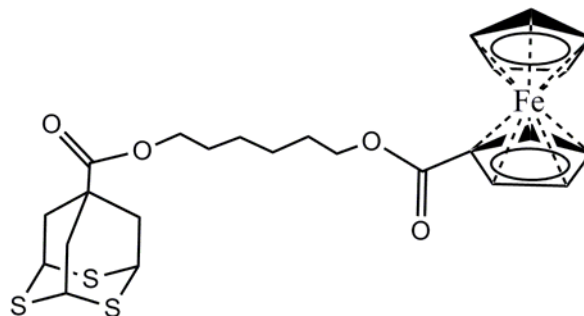
These electroactive head groups essentially act as redox centers and are typically composed of a transition metal coordinated to some organic ligand or ligands. Incorporated into a ligand for self-assembly, these reversible redox centers not only function as tools to investigate rates of electron transfer and tunneling,³⁹ but also help to explore the structure of the interface. This has proved quite valuable due to the fact that little was known about the structure of the SAM interfaces except for the bond connectivities.⁴⁰ By using a redox center at a known distance from an electrode, one can probe the surface of the monolayer for defects. The flexibility of the linker groups allow for the redox center to tilt or bend inward into a defect, thus decreasing the distance of the redox center from the electrode.⁴⁰ This produces a different electrochemical signature than if the monolayer were perfectly assembled in one continuous crystalline phase.⁴⁰ A key method in the investigation of the interfacial structure of mixed monolayer systems where ligands of different structure may not assembly in the predicted manner forming non-uniform SAMs, this technique is readily implemented.

2.1.1 Design and Approach

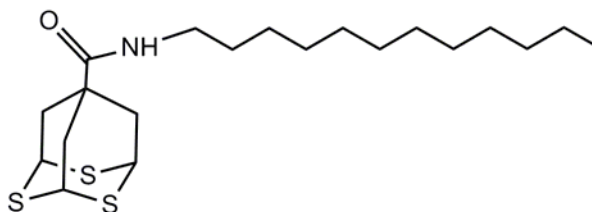
As the push to develop new monolayer systems for electro-sensing systems increases, the use of new functionalized ligands must be properly investigated, structurally and electrochemically. This is especially true for those which are sterically irregular and bulky in nature due to either the targeting moiety or the linker and adsorbing base. One such ligand is the novel tridentate surface ligand 2,4,9-trithiatricyclo[3.3.1.1^{3,7}]decane.

This Tripod ligand has been implemented in a number of studies regarding its supramolecular chemistry, especially in regards to its ability to self assemble on gold surfaces.^{27,30,31} However, little has been done, outside of knowing the bond connectivities, to characterize the interface of monolayers formed by the molecule. As previously mentioned, it was hypothesized that with a large cage-like structure as the base and a single point of attachment for tethering functionalities creating a 1:3 dilution effect, this ligand would provide adequate surface coverage yet still allow some freedom of motion for attached moieties.²⁸

To investigate this, one must implement the use of a redox probe in a mixed monolayer system. For the purpose of this study the redox probe chosen was ferrocene. Readily used in a number of other electrochemical studies of thiol-based SAMs, it was reasonable to chose ferrocene due to the wealth of information already available in terms of the characterization of monolayer interfaces.^{37,40} As the ferrocene-based ligand's counterpart, a simple alkyl derivative was designed similar in size to employ in the formation of a mixed monolayer system. Both derivatives are pictured in Figure 2.1.



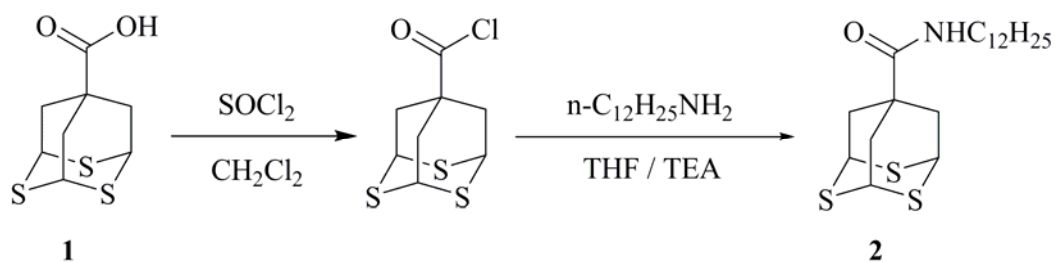
Ferrocene-based Tripod Ligand



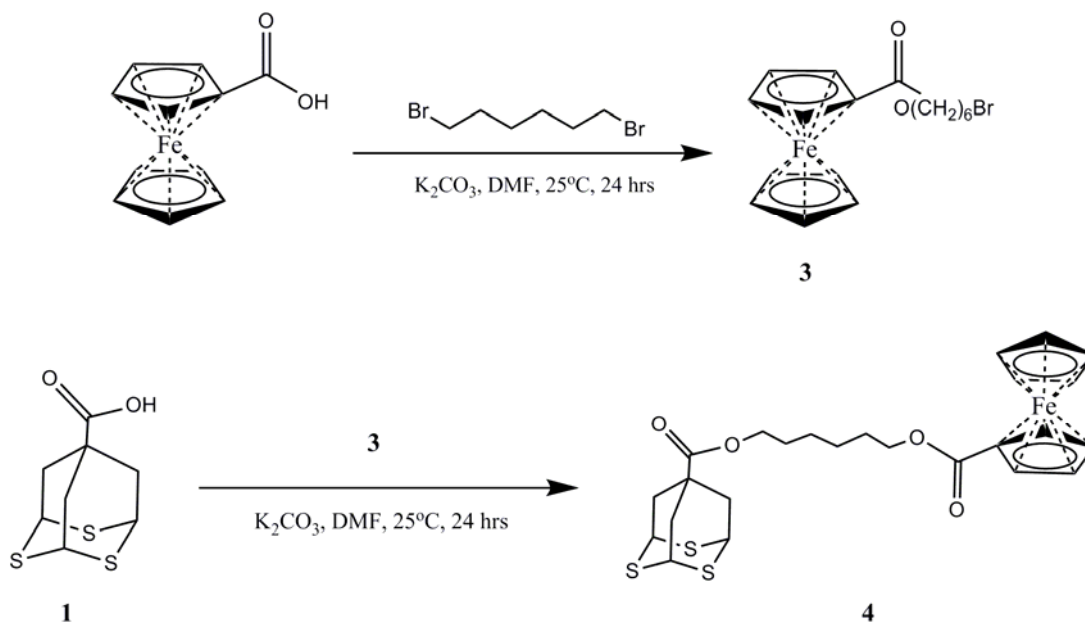
Alkyl-based Tripod Ligand

Figure 2.1 Designed derivatives for the electrochemical investigation of Tripod-based self-assembled monolayers.

The designed derivatives were both synthesized according to Schemes 2.1 and 2.2. These molecules were then used to create self-assembled mixed monolayers of varying composition in terms of mole ratio. The composition and interfacial properties of these mixed monolayers were then investigated and characterized via polarization modulation infrared reflectance absorption spectroscopy (PM-IRRAS), water contact angle (WCA) measurements, and cyclic voltammetry (Cv).



Scheme 2.1 The synthesis of 7-dodecylamide-2,4,9-trithiaadamantane as an alkyl derivative.



Scheme 2.2 The synthesis of the 2,4,9-trithiaadamantane derivative with a ferrocene redox probe attached.

2.1.2 Polarization Modulation Infrared Reflectance Absorption Spectroscopy (PM-IRRAS)

Infrared reflection absorptions spectroscopy (IRRAS) is a technique widely used to study self assembled monolayers (SAMs) on a variety of substrates. Pioneered by Greenler, this IR technique uses linear polarized light that reflects off the surface of a sample at a grazing angle of incidence to achieve a signal.⁴¹ However, the degree of sensitivity is limited and proves insufficient in the measuring of ultra-thin films often producing artifacts.⁴²

To solve this problem and improve the technique, polarization modulation was added. This technique developed by Pritchard in 1971, involves the fast modulation and circular polarization of the beam produced by the photoelastic modulator.⁴³ Effectively, this converts a single beam instrument into double beam instrument with the synchronous data acquisition. The electric vector of the incident and the reflected light are resolved in two components. The component that is parallel to the polarized radiation is known as the *p* component while the component that is perpendicular to the polarized radiation is the *s* component.^{41,42} The phase change of the *s*-polarized component is nearly 180° after reflection causing the net intensity of the IR signal for this component to be zero. The *p*-polarized component undergoes a phase change and represents the component that is responsible for a majority of the resolved signal. Based on the signal achieved through the *p*-polarized component, a differential reflectance spectrum can be obtained of the adsorbed surface species, $\Delta R/R$, which is shown by the following equation:

$$\Delta R/R = (I_p - I_s)/(I_p + I_s)$$

Where R is the absolute reflectivity, and I_p and I_s are the intensity of the p and s-polarized component of the irradiation.⁴¹ This measurement obtained by the FTIR exhibits sensitivity to the substrate surface in regards to the presence of thin films. This is typically performed using a synchronous sampling demodulator (SSD) 100 which, through signal filtering and demodulation and mathematical treatment of the signals, allows for the synchronous sampling requiring no background measurement and improved sensitivity. The background and theory behind this technique has been described in detail and used in a number of studies investigating organic molecules adsorbed as SAMs on substrates.^{42,43,44}

2.2 Experimental Section

The experimental details of the investigation of the mixed monolayer systems of alkyl and ferrocene terminated 2,4,9-trithiaadamantane derivatives are described in this section.

2.2.1 Materials and Methods

2,4,9-Trithia-tricyclo[3.3.1.1^{3,7}] decane-7-carboxylic acid (**1**), or 7-carboxylic acid-2,4,9-trithiaadamantane, was synthesized according to a previous procedure.³⁰ Ferrocene monocarboxylic acid (97%), 1,6-dibromohexane (96%), and thionyl chloride ($\geq 99\%$) were purchased from Aldrich and used as received. Dodecylamine (98%), sodium hydride (NaH, 60% in mineral oil), tetrahydrofuran (THF, 99.9%), and dimethylformamide (DMF, 99.8%) were purchased from Acros and used as received. Pyridine (99%) was purchased from EMD Chemicals Inc and distilled prior to

use. All other materials were purchased from commercial sources and used without further purification unless otherwise noted.

All ^1H NMR (330 MHz) and ^{13}C NMR (75 MHz) spectra were recorded using a Varian Gemini-300 spectrometer unless noted. NMR spectra recorded are reported in parts per million (ppm) relative to the chosen deuterated solvent's reference peak. ^1H NMR multiplicity was noted as follows: s, singlet; d, doublet; t, triplet; q, quartet; m, multiplet. IR spectra were recorded on a Nicolet Nexus 870 FT-IR spectrometer equipped with a Thunderdome Attenuated Reflectance (ATR) accessory and recorded in wavenumbers (cm^{-1}).

Prior to use, all glassware was flame or oven dried and then allowed to cool in desiccators. Air- and moisture-sensitive reactions were performed under argon gas (99.99%). Synthetic products were purified via flash chromatography and recrystallization. Thin-layer chromatography (TLC) was performed on Whatman silica gel glass backed plates of 250 μm thickness on which spots were visualized using UV light or iodine. EM Science silica gel 60 \AA (particle size 35-75 μm) was used for flash chromatography.

2.2.2 Derivative Synthesis

In this section the syntheses of 2,4,9-Trithia-tricyclo[3.3.1.1^{3,7}]decane-7-dodecylamide as the alkyl Tripod derivative and 2,4,9-Trithia-tricyclo[3.3.1.1^{3,7}]decane-7-carboxylic acid 6-ferrocenoyl-hexanoate as the ferrocene terminated derivative are described in detail.

2.2.2.1 Synthesis of 2,4,9-Trithia-tricyclo[3.3.1.1^{3,7}]decane-7-dodecylamide (TpC₁₂, **2**)

Unpurified compound **1** (0.0687 g, 0.293 mmol) was placed under vacuum in a flame dried round bottom flask with a stir bar overnight. The vessel was flushed with argon, then the sample was dissolved in 3 mL of dry dichloromethane and placed on an ice bath to stir for five minutes. While stirring on the ice bath, SOCl₂ (0.05 mL, 0.688 mmol) was slowly added dropwise along with 2-3 drops of pyridine. Then the ice bath was removed and the reaction vessel was allowed to come to room temperature before refluxing at 50°C. The reaction was monitored via FTIR. Upon completion the reaction vessel, the solvent was removed under reduced pressure and excess SOCl₂ was removed via vacuum pump into a liquid nitrogen vacuum trap. The sample was then redissolved in dry THF (2 mL) and then cooled on a water bath. To the stirring vessel containing the acid halide, undecylamine (0.07 g, 0.377 mmol) dissolved in dry THF (1.5 mL) was added dropwise and the reaction was brought to room temperature and then heated on an oil bath at 40°C until completion was indicated via TLC. The reaction was stopped, adding 5 mL of distilled H₂O and extracting with 3 x 5 mL portions of diethyl ether and then washed with 5 mL of a saturated solution of NaHCO₃. The organic layer was then separated, dried over Na₂SO₄ and purified via flash column chromatography using a mixture of ethyl acetate/hexanes (3:10) to give the product (0.0641 g, 66%). ¹H NMR δ (300 MHz, CDCl₃): 0.88 (t, 3H, CH₃), 1.26 (m, 21H, (CH₂)₁₀), 1.51 (d, 2H, CH₂CH₃), 2.87 (d, 6H, CH₂CHS), 3.27 (t, 2H, CH₂NH), 4.35s (s, 3H, SCHS), 5.62 (s, 1H, NH). ¹³C NMR δ (75 MHz, CDCl₃): 14.3, 22.9, 27.1, 29.5, 29.5, 29.8, 32.1, 38.2, 39.9, 40.28, 41.9, 175. FTIR (cm⁻¹): 3305 (-NH), 2918 (-CH), 2851 (-CH), 1632 (-C=O), 1549 (-CH₃).

2.2.2.2 Synthesis of Ferrocenoyl-6-bromohexanoate (**3**)

In a round bottom flask flushed with argon, anhydrous K_2CO_3 (0.270 g, 1.17 mmols) was dissolved in a 5 mL mixture of anhydrous DMF and 1,6-dibromohexane (1 mL, 6.56 mmols) under stirring. To the stirring solution, ferrocene monocarboxylic acid (0.150 g, 0.652 mmols) dissolved in 1.5 mL of anhydrous DMF was slowly added dropwise. Under stirring, the reaction was then gently heated at 40°C and monitored via TLC. Upon completion, 15 mL of diethyl ether was added to the reaction mixture and then it was washed with 3 x 5 mL portions of distilled H_2O . The organic layer was separated, dried over anhydrous Na_2SO_4 and then purified via flash column chromatography using a mixture ethyl acetate:hexanes (3:20) giving the desired product (256 mg, 91%). 1H NMR δ (300 MHz, $CDCl_3$): 1.5 (m, 6H, CH_2), 1.75t (t, 2H, CH_2), 1.91 (t, 2H, CH_2CH_2Br), 3.44 (t, 2H, CH_2Br), 4.21 (s, 8H, CCH), 4.24(t, 2H, $COOCH_2$), 4.39 (s, 2H, CCH), 4.81 (s, 2H, $CHCCOO$). ^{13}C NMR δ (75 MHz, $CDCl_3$): 19.2, 22.5, 25.4, 25.52, 28.1, 29.0, 64.2, 69.3, 69.9, 70.3, 71.5, 107, 154, 174 (C=O). FTIR (cm^{-1}): 3094 (=CH), 2937 (-CH), 2858 (-CH), 1711 (-C=O), 1460 (- CH_2 -), 1276 (-C-O-C-), 1137 (-C-O-C-).

2.2.2.3 Synthesis of 2,4,9-Trithia-tricyclo[3.3.1.1^{3,7}]decane-7-carboxylic acid 6-ferrocenoyl-hexanoate (TpFc, **4**)

To a round bottom flask compound **1** (0.078 g, 0.333 mmols) and anhydrous K_2CO_3 (0.135 g, 0.977 mmols) were added and then put under vacuum for 5 min. The flask was then filled with argon and the solids were dissolved in 2 mL of anhydrous DMF while stirring. While under argon the vessel was allowed to stir for 15 min, then the

stirring reaction solution was charged with 1 mL of a 0.1 M solution of compound **3** and gently heated at 40°C. The reaction was monitored via TLC. Upon completion, 10 mL of distilled H₂O was added and then the reaction products were extracted into 3 x 10 mL portions of diethyl ether. The organic layer was separated, dried over Na₂SO₄ and purified via flash column chromatography using a mixture of ethyl acetate:hexanes (1:4) giving the desired product (0.093 g, 58%). ¹H NMR δ: 1.48 (d, 4H, CH₂), 1.72 (p, 4H, CH₂CH₂COO), 2.89 (d, 6H, CH₂CHS), 4.15 (t, 2H, COOCH₂), 4.2 (s, 8H, CCH), 4.22 (t, 2H, CH₂OOCFc), 4.32 (s, 3H, SCHS), 4.39 (s, 2H, CCH), 4.81 (t, 2H, CHCCOO). ¹³C NMR δ: 25.8, 25.9, 28.7, 29.0, 38.6, 40.0, 41.4, 64.2, 65.3, 69.9, 70.3, 71.4, 172 and 175 (2 x C=O). FTIR (cm⁻¹): 3094 (=CH), 2937 (-CH), 2859 (-CH), 1709 (-C=O), 1459 (-CH₂-), 1274 (-C-O-C-), 1138 (-C-O-C-).

2.2.3 Self Assembled Mixed Monolayer Preparation and Characterization

In this section the preparation of self assembled mixed monolayers on gold substrates and subsequent characterizations via PM-IRRAS, WCA, and cyclic voltametry are described.

2.2.3.1 Self Assembled Mixed Monolayer Preparation on Au(111)

Gold coated slides purchased from EMF, were cut into square centimeter pieces. The substrate consisted of a 50 Å Ti layer which was overlaid with a 1000 Å film of Au(111). Gold thin film substrates were cleaned by soaking in piranha solution (7:3 concentrated H₂SO₄/30% H₂O₂) for 2 h and thoroughly washed with ethanol, and then were immersed in 10 mL dichloromethane/ethanol/acetonitrile (1:2:2) solutions with

varying mole fractions of compounds **2** and **4** for 24 hr at room temperature. These fractions of compounds **2:4** with 1.0×10^{-5} mols set as 1, were as follows: 1:0, 1:0.25, 1:0.5, 1:0.75, 1:1, 0.75:1, 0.5:1, 0.25:1 and 0:1. The substrates were rinsed sequentially with ethanol and dried under a stream of N_2 prior to characterization and further use.

2.2.3.2 Surface Characterization of Mixed SAMs on Au(111)

PM-FTIRRAS was performed using a Nicolet Nexus 870 Fourier transform infrared spectrometer with a liquid nitrogen cooled MCT detector and a Hinds Instruments PEM-90 photoelastic modulator operating at 100 kHz. The incoming infrared radiation was reflected from the sample at an angle of incidence of 80° . The spectra were usually collected in 1200 scans at a spectral resolution of 4 cm^{-1} . Water contact angle (WCA) of samples was measured using a 318CU 3.2M CMOS MicrometricsTM camera along with MicrometricsTM BE software package. Each datum is an average of three individual points with an accuracy of $\pm 2^\circ$.

2.2.3.3 Electrochemical Characterization of Mixed SAMs on Au(111)

Cyclic voltammograms (Cv) were recorded using a CHI 660B electrochemical workstation, which included the use of a Gamry potentiostat and software, and the use of a standard 3-electrode chemical cell as depicted in Figure 2.3.

The gold slides act as the working electrode, while the counter electrode was a platinum wire and the reference was a Ag:AgCl electrode within a 2 mm bore, two compartment Luggin capillary containing saturated KCl and a platinum junction between the capillary and the working electrolyte solution. The measurements were performed at

room temperature using a working electrode (the prepared gold slides) with an immersed surface area of 19.6 mm^2 . Prior to use, the electrochemical set-up was calibrated using a bare gold slide and two degassed electrolyte solutions. One comprised of 0.1 M KCl and 0.5 mM of $\text{K}_3\text{Fe}(\text{CN})_6$ and $\text{K}_4\text{Fe}(\text{CN})_6$ as redox probes, while the other was 0.1 M KCl and 0.5 mM of ferrocenecarboxylic acid. Cyclic voltammetry measurements of the mixed monolayer prepared gold slides were performed using a degassed 0.1 M KCl electrolyte solution with a max current of 0.3 mA and a scanning limit between -0.3 and 0.7 V with a scanning rate of 100 mV/s . Data was processed and analyzed using Microcal Origin version 6 software.

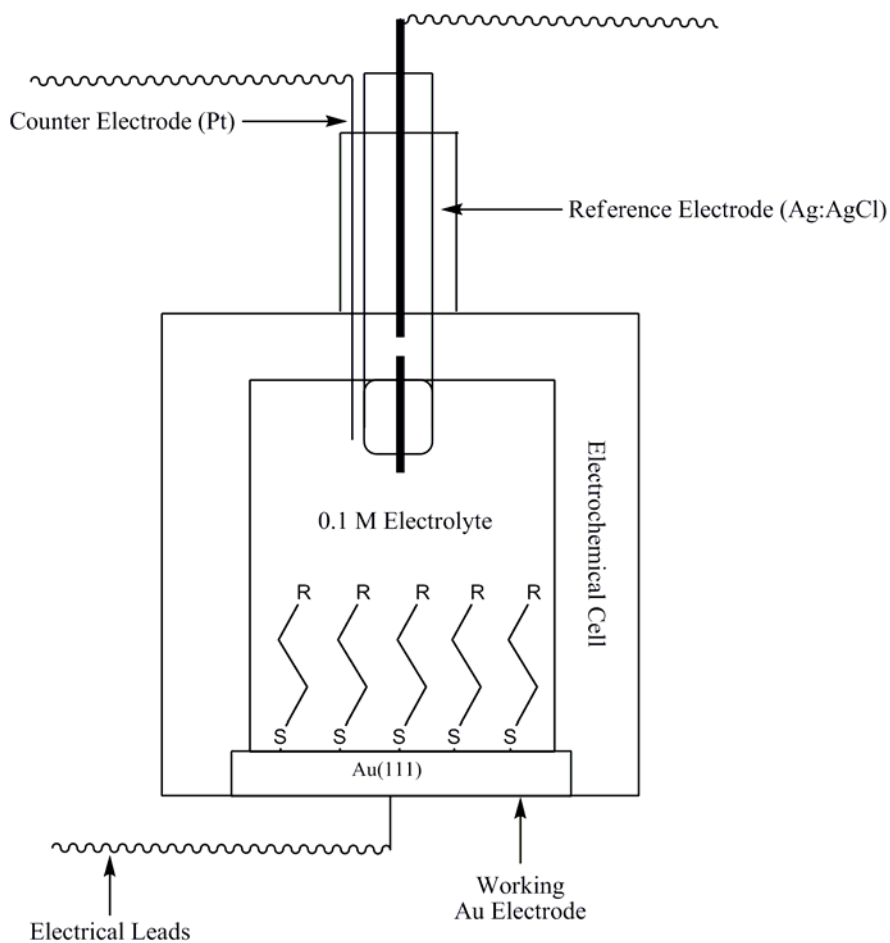


Figure 2.2 A representation of the electrochemical cell used in the experiment.

2.3 Results and Discussion

The synthesis of the derivatized 2,4,9-trithiaadamantane ligands according to Schemes 2.1 and 2.2 proved successful. Both ligands were synthesized in moderate yields, TpC₁₂ (**2**) at 66% and TpFc (**4**) at 58%, and their structure confirmed spectroscopically. Self-assembled monolayers were formed using dilute ethanol solutions containing varying mole fractions of the two ligands were used to dope freshly cleaned polycrystalline Au(111) slides. After 24 h of immersion in the doping solutions, the slides were removed, washed with ethanol to remove any excess ligands, and dried with a steady stream of N₂ gas. Successful immobilization of the ligands on the gold surface in the formation of self-assembled monolayers was confirmed by PM-FTIRRAS. The presence of the ligands exhibited various modes of C-H stretching in the 2900–2800 cm⁻¹ region of the IR spectra (Figures 2.4 and 2.5). The stretching modes within this region correspond to the long 12 carbon, alkane chain of the TpC₁₂ ligand (**2**) as well as the aliphatic carbon chain present in the diester linkage of the TpFc ligand (**4**).

The PM-IRRAS spectral data, Table 2.1, was not only effective in confirming the presence of the monolayers, but also provided structural information as well. Specifically looking at the methylene symmetric and anti-symmetric stretching modes, CH_{2sym} and CH_{2asym} respectively, of the monolayers neither ligand by itself exhibits the same signature as that of its bulk material. The signatures for a monolayer consisting of 100% of either TpC₁₂ or TpFc ligand show a significant decrease in the wavenumbers of the CH_{2sym} and CH_{2asym} modes by nearly 10–20 cm⁻¹. This decrease indicates that assembly of uniform semi-crystalline materials with limited degrees of freedom for the attached functionalities. This is in agreement with previous studies performed in the

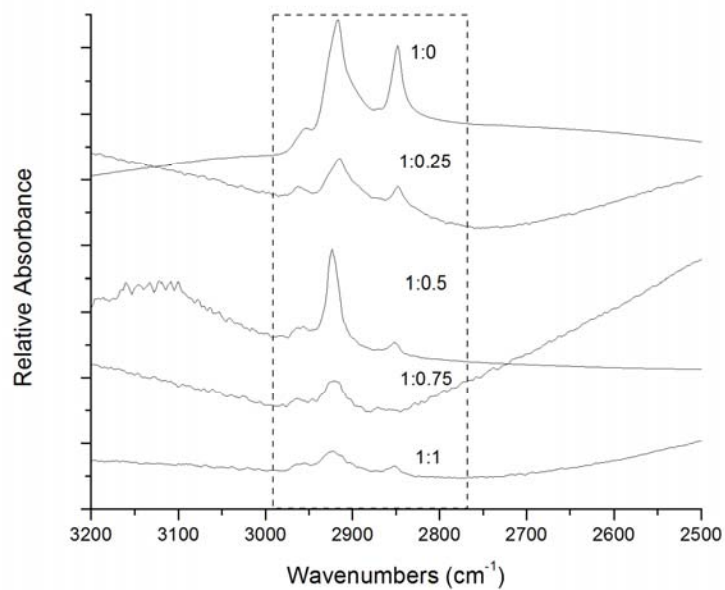


Figure 2.3 PM-FTIRRAS spectra of the mixed monolayers (TpC₁₂:TpFc) with increasing mole ratio of the ferrocene derivatized 2,4,9-trithiaadamantane.

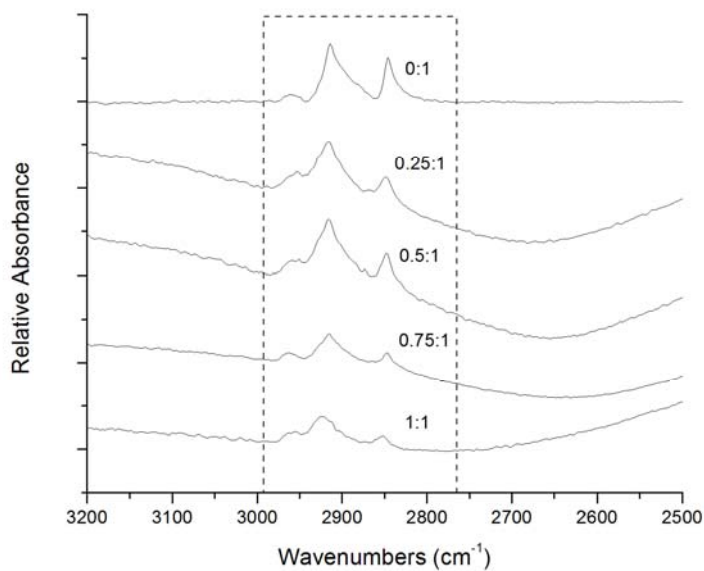
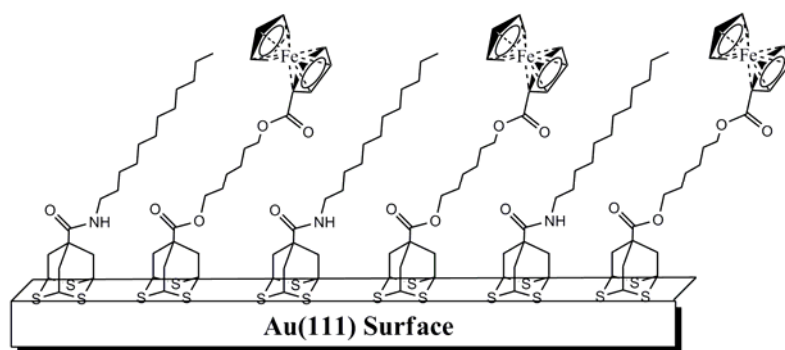


Figure 2.4 PM-FTIRRAS spectra of the mixed monolayers (TpC₁₂:TpFc) with increasing mole ratio of the alkyl derivatized 2,4,9-trithiaadamantane.

assembly of monolayers consisting of one ligand as the sole adsorbate.³³ Upon introduction of increasing mole fractions of the ligands approaching a 1:1 ratio in forming the mixed monolayers, whether starting from either purely TpC₁₂ or TpFc, a slight increase in the wavenumbers of the CH_{2sym} and CH_{2asym} stretching modes occurs as well as a decrease in the absorbance of the peaks, Figures 2.3 and 2.4. This is indicative of a perturbation in the uniformity of the assembled monolayers due to the presence of the bulky ferrocene groups causing the monolayers to stray from existing in a semi-crystalline state.³⁴ With the introduction of this ligand of different structure, with a bulky head group such as ferrocene as well as the presence of hydrophilic diester linkages, it is reasonable to believe that there is some type of increase in the degrees of freedom for the attached functionalities. This presents one of two scenarios, either there is an even distribution of the ligands at a set distance from each other, as depicted in Scheme 2.3, or with the introduction of different ligands defects are created in the monolayers in the form of tilt domain boundaries. These tilt domain boundaries are representative of various issues. They could be the product of accumulated impurities or grain boundaries on the gold slide surface. One other feasible explanation exists is the variations in the exchange process for the ligands, where one ligand may occupy a site first and effectively block the adjacent binding site on the gold surface via the tilting of its attached functionality, whether it is the alkyl chain of TpC₁₂ or the ferrocene of TpFc.⁴⁰ If this is the case, issues of phase segregation may be present within the mixed monolayer systems.



Scheme 2.3 Representation of a mixed monolayer using the designed derivatives.

Table 2.1 PM-FTIRRAS data for methylene stretching modes compared to varying mole fractions (based on 1×10^{-5} mols) and bulk material

Mole Fractions (TpC ₁₂ :TpFc)	IR Stretching Modes (cm ⁻¹)	
	CH ₂ antisymmetric	CH ₂ symmetric
Bulk TpC ₁₂	2918	2851
1:0	2917	2848
1:0.25	2913	2843
1:0.5	2922	2850
1:0.75	2917	2868
1:1	2921	2848
0.75:1	2909	2844
0.5:1	2913	2843
0.25:1	2913	2843
0:1	2908	2839
Bulk TpFc	2937	2859

The data from the water contact angle measurements (WCA) depicted in Figure 2.5 were the result of averaging three consecutive measurements to three significant digits. For WCA of gold, a freshly cleaned gold slide, using piranha solution, was used obtaining a contact angle of $\sim 70.7^\circ$. For the WCA measurements it would be expected that with an increase in the mole ratio of diester linkage containing TpFc ligand,

hydrophilicity of the surface would slightly increase thus decreasing the contact angle.³³ For the increase of the mole ratio of TpC₁₂ compared to TpFc, the opposite effect should present itself with an increasing contact angle with the increase in hydrophobicity of the monolayer. However, this is not the cause for the data attained which strays from fitting any discernable pattern. This discredits the plausibility of the scenario where the ligands are evenly distributed through the monolayer independent of the varying mole ratios. A reasonable explanation for this is that the variations in the exchange process could lead to the formation of tilt domain boundaries which are a result of islets of phase segregation. The formation of these domain boundaries leading to defects in the monolayer would lead to a higher degree of water penetration into the monolayer.³⁴ This higher degree of penetration would thus result in a smaller contact angle than would be expected. To further explore the possibility of the existence of such phenomena resulting in tilt boundary domains and the presence of phase segregation, cyclic voltametry was performed on the monolayers to investigate the presence of such defect sites.

Cyclic voltammograms (Cv) of the mixed monolayer prepared gold slides were acquired using 0.1 M KCl electrolyte solution with a max current of 0.3 mA and a scanning limit between -0.3 and 0.7 V with a scanning rate of 100 mV/s. At an initial glance of Figures 2.6 and 2.7, the information gathered can be used qualitatively assess the mixed monolayers used in the measurements. Hypothetically, if the monolayers have no defects, the Cv's should be smooth and nearly symmetric. However, if the monolayer, the dielectric, is disrupted in any manner whether from a scratch or impurity on the surface, it should be easily seen as a distinct, sharp peak representative of a sudden increase in current, the rate of electron transfer.²⁵ Such is the case in Figure 2.6, Cv's

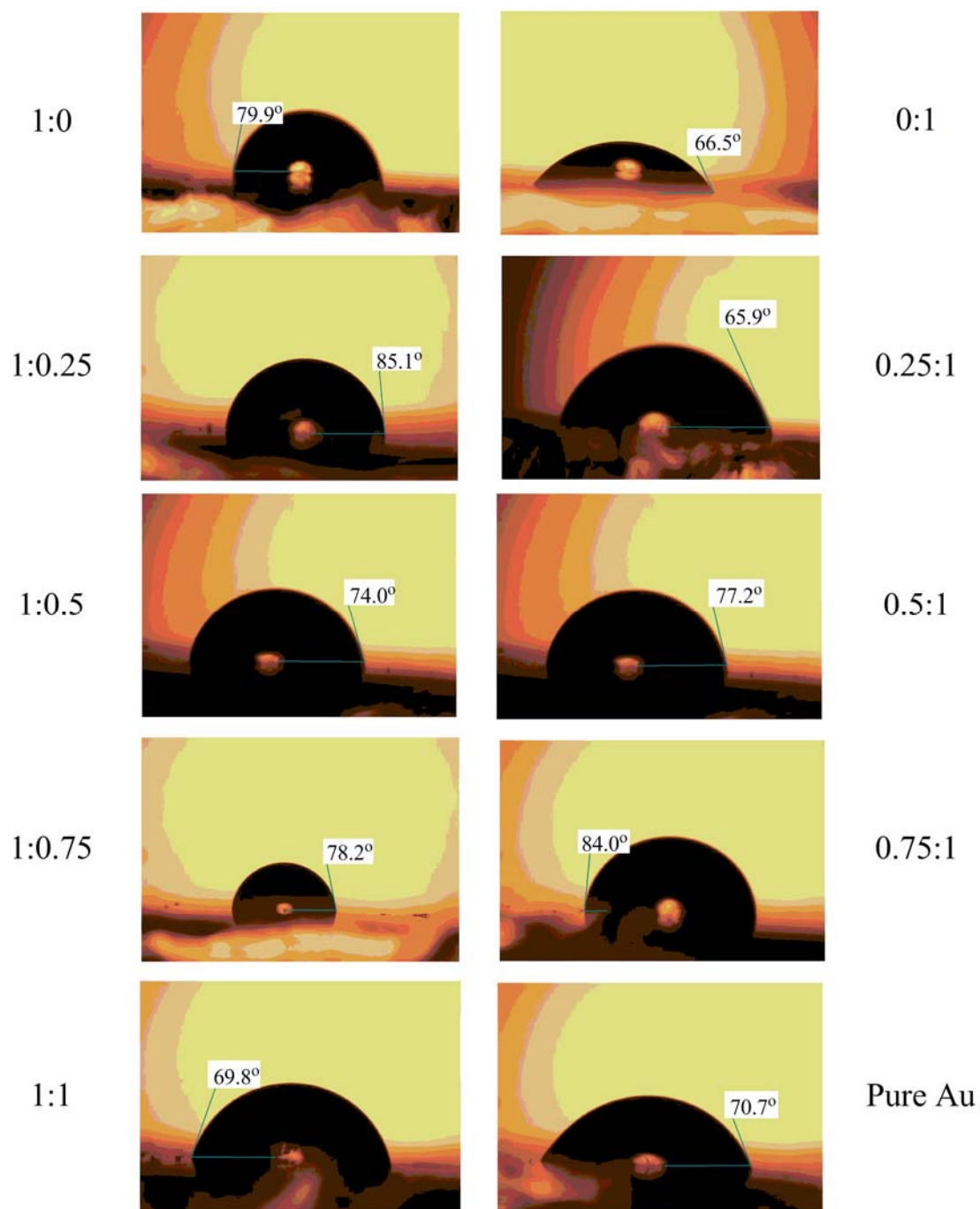


Figure 2.5 Water contact angle measurements with noted mole ratios (TpC₁₂:TpFc).

increasing in mole ratio from 1:0 to 1:1 TpC₁₂:TpFc, for the mole ratios 1:0.5 and 1:0.75. For the Cv's increasing in mole ratio from 1:1 to 0:1 TpC₁₂:TpFc, Figure 2.7, no such phenomena was present.

Based on previous studies performed on mixed monolayer systems using ferrocene terminated thiols as redox probes, as the mole fraction of the designed probe increases the Cv's of the monolayers should exhibit broadening, develop an asymmetry and eventually an additional set of peaks as the amount of ferrocene is increased across the surface of the monolayers.^{37,40} With the exception of three measurements due to damaging of the slides in the handling process, the Cv's pertaining to the monolayers of mole fractions 1:0.25, 1:0.5 and 0.75:1, fit this trend. As the mole fraction of TpFc increases in monolayers, the Cv's in Figures 2.6 and 2.7 do exhibit a broadening and eventually develop asymmetry as well as a defined set of peaks at 80 mV for the cathodic peak and 245 mV for the anodic peak. The full width at half maximum (fwhm) for the cathodic and anodic peaks is about 82.5 ± 10 mV which roughly corresponds to the reduction and oxidation, respectively, of the ferrocene redox center as reported in the literature.⁴⁰

Cyclic voltammetry can not only be used to qualitatively assess the integrity of a monolayer but can also be used to attain information pertaining to ion permeation. In these mixed monolayer systems, ideally ion permeation should be severely hampered essentially allowing the monolayers to act as simple dielectrics.³⁴ Hence ion permeation into the monolayers is oftentimes the result of defects at the surface. For the Cv's recorded, the current is much lower being within the microampere range compared to that

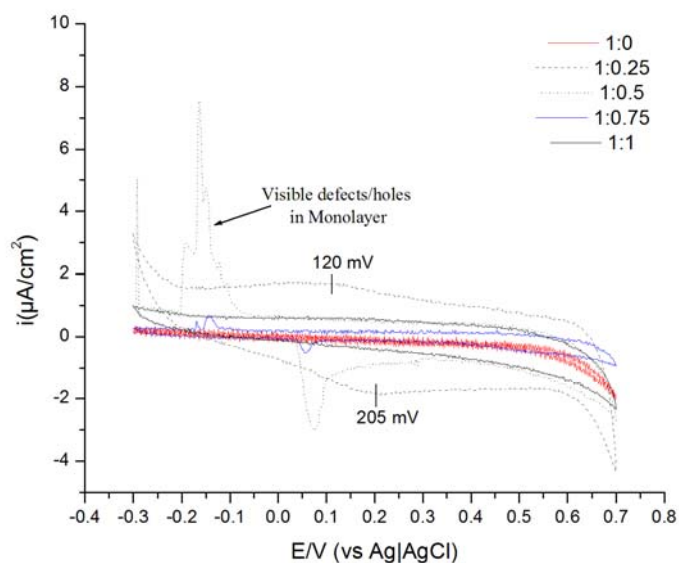


Figure 2.6 Cyclic voltammograms of mixed monolayers with increasing mole ratio of TpC12:TpFc from 1:0 to 1:1 (1.0×10^{-5} mols set as 1).

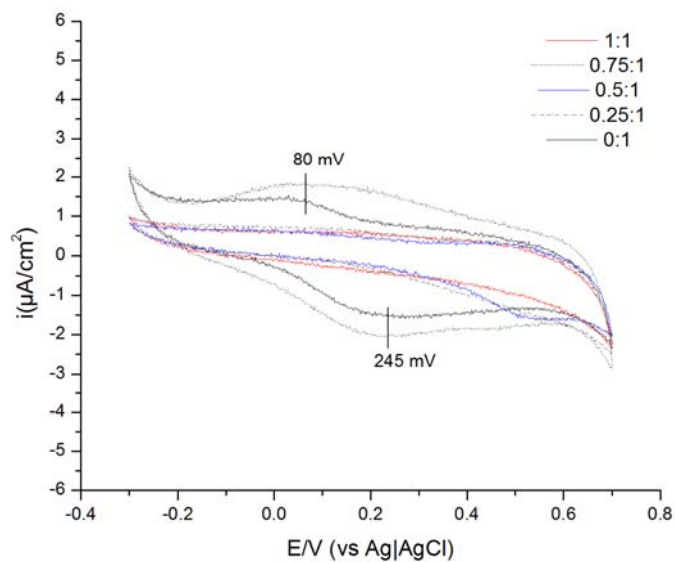


Figure 2.7 Cyclic voltammograms of mixed monolayers with increasing mole ratio of TpC12:TpFc from 1:1 to 0:1 (1.0×10^{-5} mols set as 1).

of the reference sample, using ferrocene carboxylic acid as a probe on bare gold, which was a of 10^6 higher thus the current for these monolayers is capacitive. Based on the notion that these monolayers act as capacitors, the surface charge densities (Table 2.2) of the monolayers were attained by integrating the area under the Cv peaks using Microcal Origin version 6 software and then dividing by the scan rate.

Table 2.2 The data obtained from calculating surface charge densities of the mixed monolayers.

Mole Fraction (TpC₁₂:TpFc)	Integration Values	Capacitance ($\mu\text{C}/\text{cm}^2$)
1:0	0.01885	0.1885
1:0.25	2.35104	23.5104
1:0.5	1.43696	14.3696
1:0.75	0.33456	3.3456
1:1	0.84935	8.4935
0.75:1	2.3811	23.811
0.5:1	0.89696	8.9696
0.25:1	0.95274	9.5274
0:1	1.65211	16.5211

Plotting the surface charge density, capacitance, versus the mole percent of TpFc a trend is observed (Figure 2.7). With increasing mole percent of TpFc, capacitance in the monolayer is also increased. This is expected as the increase in the presence of ferrocene, a redox center, across the monolayer should increase the ability of charge to be held across the surface of the monolayer at the interface of the monolayer and the electrolyte solution.^{39,40} Based on the fact that these monolayers should act as capacitors, using the equation (2.1) from the linear fit obtained from Figure 2.7 is used in the application of the Helmholtz theory model (2.2) of the electrical double layer as an ideal capacitor,

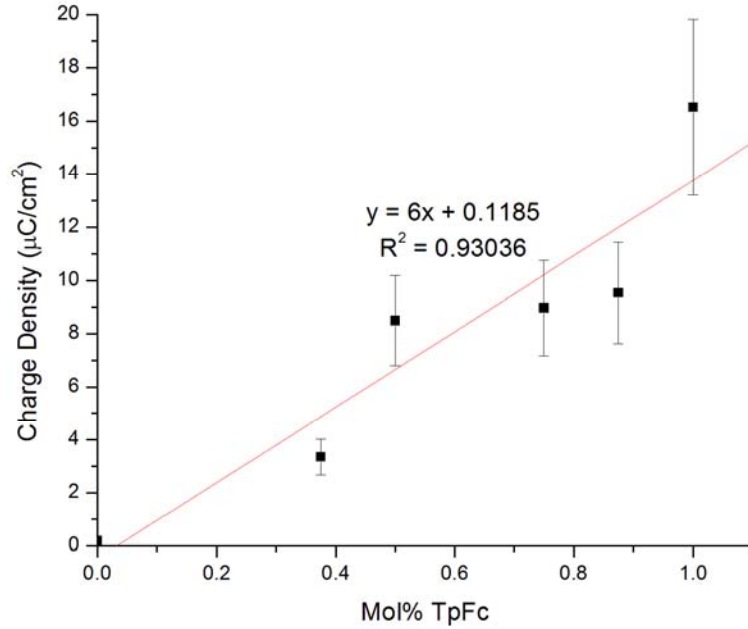


Figure 2.8 A plot of charge density versus mole percent TpFc with a linear fit (standard error of data points $\pm 20\%$, data from mole ratios 1:0.25, 1:0.5 and 0.75:1 removed due to slide damage).

the following equation (2.3) is derived stepwise to calculate the dielectric constant of the monolayers of pure TpC₁₂ and TpFc.²⁵

$$C = 6x + 0.1185 \quad (2.1)$$

$$C = \epsilon\epsilon_0/d_{\text{eff}} \quad (2.2)$$

$$\epsilon = d_{\text{eff}}(6x + 0.1185)/\epsilon_0 \quad (2.3)$$

For equation 2.3, ϵ is the dielectric constant of the monolayer, ϵ_0 is the permeativity of free space, x is the mole percent of TpFc and d_{eff} is the thickness of the dielectric medium, in this case the monolayer. The thickness of the monolayers was

roughly estimated using bond lengths attained from literature.^{30,45} Based on the model (Scheme 2.3) previously described, if the molecules are packed and extend perpendicular to the gold surface the corresponding film thickness would be $\sim 25.3 \text{ \AA}$ for pure monolayers of TpC12 and $\sim 30.1 \text{ \AA}$ for that of TpFc. Based on this, the following dielectric constants were calculated as 3.511×10^{-6} and 2.157×10^{-4} far exceeding the lower limits of dielectrics with that of vacuum being 1. Thus, application of the Helmholtz theory model proves inaccurate and not appropriate to properly access the dielectric of the monolayer systems containing TpC₁₂ and TpFc.

2.4 Conclusions and Future Work

In summary, the synthesis of the designed ligands, 2,4,9-Trithia-tricyclo[3.3.1.1^{3,7}]decane-7-dodecylamide and 2,4,9-Trithia-tricyclo[3.3.1.1^{3,7}]decane-7-carboxylic acid 6-ferrocenoyl-hexanoate, proved successful and in adequate yields. The use of these ligands in the self assembly of mixed monolayers from dilute ethanol solutions proved successful. The composition and interracial properties of the mixed monolayers were investigated via PM-FTIRRAS, WCA measurements, and cyclic voltammetry. As a result, it was noticed that monolayers of pure ligand, having a sterically large anchor that should entail a dilution effect, assemble in a nearly uniform semicrystalline material. However, upon mixing of the ligand in varying mole ratios perturbation in the monolayers occur increasing the degrees of freedom for the attached functionalities with the possibility of forming defects in the form of tilt domain boundaries. This notion was reverified, the monolayers exhibiting that as amount of the attached ferrocene at the interface of monolayer and electrolyte solution increased, the

surface charge increased which is in agreement with the notion that the electrolyte penetration increases with increasing mole ratio of the Tripod-ferrocene derivative. These monolayer systems should be subject to future investigations to more quantitatively access the electrochemical properties of the ligand system. Once a more in depth understanding is achieved, pursuit in the design of electrochemical biosensors based on this platform will become more feasible for the detection of specific analytes.

CHAPTER III

ATRP INITIATED POLYMERIZATION OF POLYMER BRUSHES FROM A SELF ASSEMBLED MONOLAYER OF TRITHIAADAMANTANE DERIVATIVE AS AN IMMOBILIZED INITIATOR ON GOLD SUBSTRATE

3.1 Introduction

The spontaneous self-assembly of organic molecules at solid surfaces provides a convenient technique by which compact monolayers with well-defined composition, structure and thickness can be obtained.⁴⁶⁻⁴⁹ In recent years, self-assembled monolayers (SAM) have focused on a number of systems, including activated *N*-hydroxysuccinimide ester on glass carbon electrode,⁵⁰ organosilicon derivatives on indium tin oxide (ITO), silicon or silica⁵¹ and organosulfur compounds on gold. Of these systems, SAMs on gold substrates have been widely investigated as organosulfur monolayers, which offer the best presently available combination of high structural order, ease in modification of the tail group and ease of preparation and analysis.^{49,52}

Growth of polymers from gold surfaces using controlled polymerization schemes, such as atom transfer radical polymerization (ATRP), has become a powerful strategy for anchoring well-defined polymers to gold substrates. The polymer brushes grown on gold have shown high technological potential for separation,⁵³ surface transport,⁵⁴ microfluidic

devices,⁵⁵ sensors,⁵⁶ responsive colloids,⁵⁷ and biomedical applications.⁵⁸ However, many polymer brushes are currently based on single-chain alkanethiols.

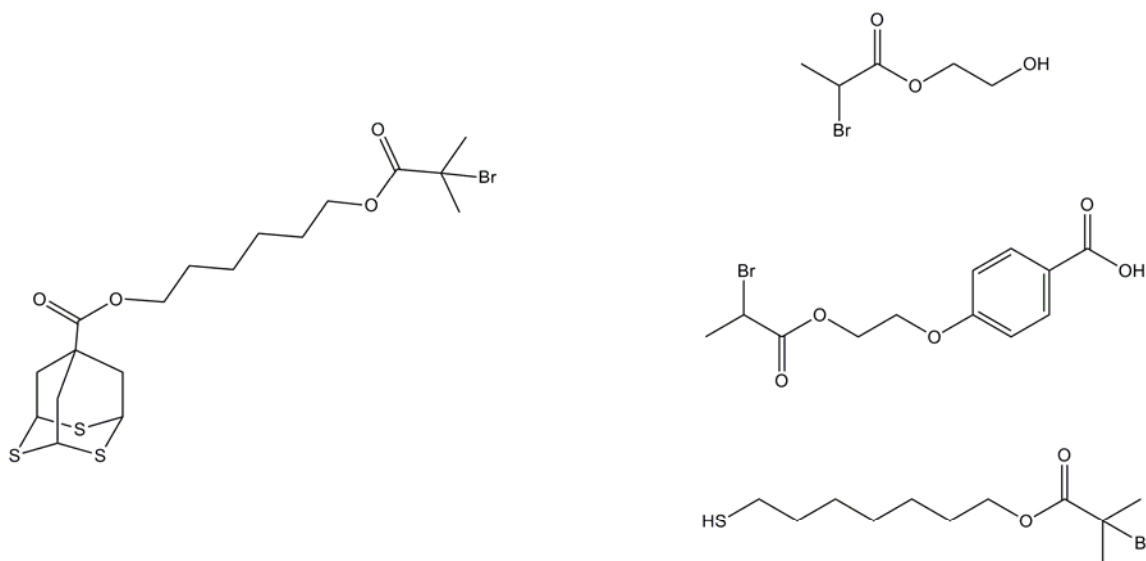
A major disadvantage of single-chain thiols is their thermal and air instability.⁵⁹ They are very susceptible to oxidative damage and difficult to handle requiring a nearly anaerobic environment.⁶⁰ This becomes a serious problem because the sulfur at the base of the thiol ligands oxidized or unoxidized can bind and potentially kill the metal catalyst, in most cases copper, used in the ATRP synthesis.⁶¹ Therefore, various sulfur-based functional groups less susceptible to oxidation, such as thioethers, thioacetate groups, and tetradentate thioether ligands, have been attempted as alternatives to single-chain thiols for the preparation of SAMs on gold surfaces.^{28,62}

As previously mentioned, one promising category of SAMs is based on the derivatives of 7-substituted-2,4,9-Trithiaadamantane, or Tripod, developed by Hu and Khemtong.³⁰ The three sulfur atoms residing on the base of trithiaadamantane molecule conveniently allows them to adsorb on metal or semiconductor surfaces. This adsorption mechanism was previously investigated using the Tripod derivative 7-ethynyl-2,4,9-trithia-tricyclo[3.3.1.1^{3,7}]decane, to produce ultra-thin CdS films monitoring the molecules interactions by multiple reflection absorption IR spectroscopy and inelastic electron tunneling spectroscopy.⁶³ This mechanism has been proposed to happen with similar or even stronger interactions as compared to that of single thiols and, because of their rigid and chemically stable molecular structure, are less susceptible to oxidation.⁵⁹ Recent studies demonstrated that the SAMs can be formed by spontaneous physical adsorption of 7-(diazomethylcarbonyl)-2,4,9-trithiaadamantane, a photoreactive

trithiaadamantane compound, on a gold surfaces. The α -diazo ketone moiety of the SAM was found to display the classical Wolff rearrangement reactivity to produce a ketene intermediate on the exposed area.²⁷ In contrast to single-chain thiols, the end group density of the resulting SAMs was remarkably decreased by using tripodal surface anchors so that solvation and reactions on the SAMs were strikingly accelerated by the reduction of the steric hindrance between end groups of the SAMs.²⁷ Because of these unique chemical advantages of tripodal surface anchors, they offer an optimal platform to pursue the design and development of a new ATRP surface initiator.

3.1.1 Design and Approach

Typically, for ATRP synthesis alkyl halides are used to achieve an accelerated rate of polymerization. This high rate, which is first order in respect to the initiator, allows for the growth of well-defined polymer chains. The highest rates of polymerization achieved are currently systems using alkyl halides where the halide is attached along with activating substituents to a secondary or tertiary α -carbon allowing for initiation to be fast and quantitative. This is important in the design of ATRP initiators for enhanced rates of polymerization limiting the chance of radical termination reactions to occur with typically no more than 5% of growing chains terminating during the initial polymerization stages.⁵⁷ Therefore in this work, 2,4,9-trithiatricyclo[3.3.1.1^{3,7}]decane-7-carboxylic acid 6-(2-bromo-2-methyl-propionyloxy)-hexyl ester was designed as the immobilized initiator. The initiator designed is depicted along with other initiators used in ATRP synthesis in Scheme 3.1.



Designed initiator based on
7-substituted-2,4,9-Trithiaadamantane

Typical initiators derived from
alpha-haloesters

Scheme 3.1 Comparison of the 7-substituted-2,4,9-trithiaadamantane initiator to other typically used ATRP initiators.

Using the designed and synthesized surface initiator 2,4,9-trithia-tricyclo[3.3.1.1^{3,7}] decane-7-carboxylic acid 6-(2-bromo-2-methyl-propionyloxy)-hexyl ester, surface-initiated atom transfer radical polymerizations (ATRP) of *tert*-butyl acrylate (*t*-BA) and (dimethylamino)ethyl methacrylate (DMAEMA) monomers from the initiator immobilized on gold substrate. Subsequently, the polymer brushes grown were then chemically converted to their polyelectrolyte forms and the stimuli-responsive natures of the brushes were characterized and studied by polarization modulation infrared reflectance absorption spectroscopy (PM-IRRAS), atomic force microscopy (AFM) and water contact angle (WCA) measurements.

3.2 Experimental Section

In this section the experimental procedures performed are described in detail in the design, synthesis, immobilization and growth of polymer chains from 7-substituted-2,4,9-Trithiaadamantane initiator on gold substrate.

3.2.1 Materials and Methods

tert-Butyl acrylate (Acros, 99%) was passed through a column of activated basic alumina and degassed with high-purity argon for 1 h prior to use. CuBr (99.999%), CuBr₂ (99.999%), *N,N*-dimethylformamide (DMF, 99.8%), 4,4'-dinonyl-2,2'-bipyridyl (dnNbpy, 97%), and 2,2'-bipyridyl (BiPy, 99%) were obtained from Aldrich and used as received. 1,4,8,11-Tetramethyl-1,4,8,11-tetraazacyclotetradecane (Me₄Cyclam) (98%) was purchased from Alfa Aesar and used without any purification. (Dimethylamino)ethyl methacrylate (DMAEMA) was obtained from Aldrich and redistilled in the presence of CuCl before use. Potassium chloride (KCl, Fisher), sodium dodecyl sulfate (SDS, 99%, Acros), and 1-butyl-3-methylimidazolium (bmimPF₆, ≥97%, Aldrich) were used as electrolytes without further purification. All other reagents were purchased from commercial sources and purified when needed.

All ¹H NMR (330 MHz) and ¹³C NMR (75 MHz) spectra were recorded using a Varian Gemini-300 spectrometer unless noted. NMR spectra recorded are reported in parts per million (ppm) relative to the chosen deuterated solvents reference peaks. ¹H NMR multiplicity was noted as follows: s, singlet; d, doublet; t, triplet; q, quartet; m, multiplet. IR spectra were recorded on a Nicolet Nexus 870 FT-IR spectrometer

equipped with a Thunderdome Attenuated Reflectance (ATR) accessory and recorded in wavenumbers (cm^{-1}).

Prior to use, all glassware was flame or oven dried and then allowed to cool in desiccators. Air- and moisture-sensitive reactions were performed under argon gas (99.99%). Synthetic products were purified via flash chromatography and recrystallization. Thin-layer chromatography (TLC) was performed on Whatman silica gel glass backed plates of 250 μm thickness on which spots were visualized using UV light or iodine. EM Science silica gel 60 Å (particle size 35-75 μm) was used for flash chromatography.

3.2.2 ATRP Initiator Synthesis

In this section the synthesis of the Tripod derivative 2,4,9-trithiatricyclo-[3.3.1.1^{3,7}]decane-7-carboxylic acid 6-(2-bromo-2-methyl-propionyloxy)-hexyl ester as an immobilized initiator is described for ATRP polymer synthesis.

3.2.2.1 Synthesis of 2,4,9-Trithia-tricyclo[3.3.1.1^{3,7}]decane-7-carboxylic acid 6-hydroxy-hexyl ester (**5**)

To a flame-dried 25 mL round bottom flask containing **1** (307 mg, 1.3 mmols) synthesized according to a previously published procedure,³⁰ anhydrous K_2CO_3 (543 mg, 3.9 mmols) and a stir bar under argon was added 5 mL of dimethylformamide, DMF. After stirring at room temperature for 1 h, 6-bromo-1-hexanol (0.25 mL, 1.9 mmols) was slowly added via syringe. The reaction was allowed to stir over a 24 hour period and monitored till completion via TLC. Upon completion the reaction was washed with 5 mL

distilled H₂O and the product extracted using 3 x 10 mL portions of diethyl ether. The ether layer was then separated, dried over anhydrous Na₂SO₄ and purified on silica gel via flash column chromatography using ethyl acetate:hexanes (2:5) giving the desired product **2** (320 mg, 73%). ¹H NMR δ: 1.36 (t, 4H, CH₂), 1.54 (t, 2H, CH₂), 1.63(t, 2H, CH₂), 2.0 (s, H, OH), 2.86 (d, 6H, CH₂), 3.6 (t, 2H, CH₂), 4.09 (t, 2H, CH₂), 4.3 (t, 3H, CH). ¹³C NMR δ: 25.6, 25.9, 28.7, 32.7, 38.6, 40.1, 41.4, 62.9, 65.4, 175. FTIR (cm⁻¹): 3339 (-OH), 2933 (-CH), 2858 (-CH), 1728 (-C=O), 1265 (-C-O-C-), 1044 (-C-O).

3.2.2.2 Synthesis of 2,4,9-Trithia-tricyclo[3.3.1.1^{3,7}]decane-7-carboxylic acid 6-(2-bromo-2- methyl-propionyloxy)-hexyl ester (**6**)

In a flame dried 10 mL round bottom flask purged with argon, compound **2** (135 mg, 0.4 mmols), K₂CO₃ (167 mg, 1.2 mmols) and 2-3 crystals of dimethylaminopyridine, DMAP, were dissolved in 2 mL of dry dichloromethane. After cooling the vessel under stirring on an ice bath, 2-bromoisobutyryl bromide (0.065 mL, 0.53 mmols) was added and the reaction was allowed to stir under argon on the ice bath. The reaction was monitored via TLC, and if needed, more 2-bromoisobutyryl bromide can be added until all of compound **2** is reacted away. Upon completion, the reaction was washed with 5 mL of brine solution and the reaction product was extracted into 3 x 10 mL portions of dichloromethane. The dichloromethane was then dried over anhydrous Na₂SO₄, then purified via thin layer chromatography using ethyl acetate:hexanes (1:4) giving the desired product **3** (98 mg, 50%). ¹H NMR δ: 1.25 (s, 4H, CH₂), 1.58 (s, 4H, CH₂), 1.94 (s, 6H, CH₃), 2.91 (s, 6H, CH₂), 4.13 (d, 4H, CH₂), 4.34 (s, 3H, CH₃). ¹³C NMR δ: 23.7, 25.9, 26.0, 28.7, 29.8, 32.5, 38.6, 40.1, 41.4, 65.4, 67.0, 65.3, 67.2, 171, 175. FTIR

(cm^{-1}): 2959 (-CH₃), 2930 (-CH), 2860 (-CH), 1731 (-C=O), 1274 (-C-O-C-), 1041 (-C-O).

3.2.3 Initiator Immobilization, Surface-Initiated ATRP, and Characterization

The following procedures described entail the self assembly of the initiator on gold substrates, ATRP polymerizations of *t*-BA and DMAEMA from gold substrate surfaces and their subsequent characterizations.

3.2.3.1 Preparation of Immobilized Initiators on Gold Substrates

Gold coated slides purchased from EMF, were cut into square centimeter pieces. The substrate consisted of a 50 Å Ti layer which was overlaid with a 1000 Å film of Au(111). Gold thin film substrates were cleaned by soaking in piranha solution (7:3 concentrated H₂SO₄/30% H₂O₂) for 2 h and thoroughly washed with ethanol, and then were immersed with ethanolic solution of compound **6** for 48 h at room temperature. The immobilized initiator layer was then formed. The substrates were rinsed sequentially with ethanol and dried under a stream of N₂ prior to characterization and further use.

3.2.3.2 Preparation of Polymer-Modified Gold Substrates

An initiator-modified Au substrate was sealed in a 100 mL Schlenk flask, and the flask was degassed by three vacuum purge/argon fill cycles. The polymerization of *t*-BA was carried out according to a rapid synthesis process.⁶⁴ Typically, 8.6 mg (0.06 mmol) of CuBr, 6.7 mg (0.03 mmol) of CuBr₂, 15.4 mg (0.06 mmol) of Me₄Cyclam, and 24.5 mg (0.06 mmol) of dnNbpy were added to a round-bottom flask with a magnetic stirrer

bar, which was also degassed by three vacuum purge/argon fill cycles. Then 30 mL of a degassed monomer in DMF/anisole solution (*t*-BA/DMF/anisole = 2:1:1 v:v:v, [*t*-BA] = 5.25 M, degassed for 1 h) was then transferred to the above round-bottom flask containing the Cu(I/II) with their corresponding amine containing ligands. The mixture was well-stirred and heated with an oil bath to 50 °C until a transparent, light green solution formed. The obtained solution was then transferred into the Schlenk flask containing an initiator-modified Au substrate to start the surface-initiated polymerization. After one hour at 50 °C, the polymer-modified substrate was removed from the Schlenk flask, washed with water, ethyl acetate and THF sequentially, and then was dried under a flow of argon. The hydrolysis of Poly-*t*-BA was carried out using 0.15 M methanesulfonic acid in CH₂Cl₂ for 10 min as previously reported⁶⁵ and poly(acrylic acid) (PAA) brushes were obtained. The PAA brushes were treated with a pH=10 NaOH solution, followed by rinsing with ethanol and water. The obtained carboxylate PAA polyelectrolyte brushes were then dried under a flow of argon. Polymer brushes of PDMAEMA were prepared according to a recipe of [DMAEMA]:[CuBr]:[Bipy]:[CuBr₂] = 100:2:5:0.2 in methanol/H₂O (1:1 v:v) at room temperature.⁶⁵ A typical polymerization solution is as follows: DMAEMA, 7.85g; CuBr, 0.144g; Bipy, 0.39g; CuBr₂, 0.0224g; solvent, 15mL. The solution was degassed with argon for 30 min, transferred to deoxygenated Schlenk flask containing an initiator-modified Au substrate, and allowed to polymerize for 12 h. After polymerization, the polymer-modified substrate was thoroughly rinsed with pure water and ethanol, and then was dried under a flow of argon. Quaternization was carried out in 2 mL of iodomethane/10 mL of CH₃NO₂ at room

temperature for 24 h. The quaternized PDMAEMA polyelectrolyte brushes were thoroughly rinsed with water and were then dried under a flow of argon.

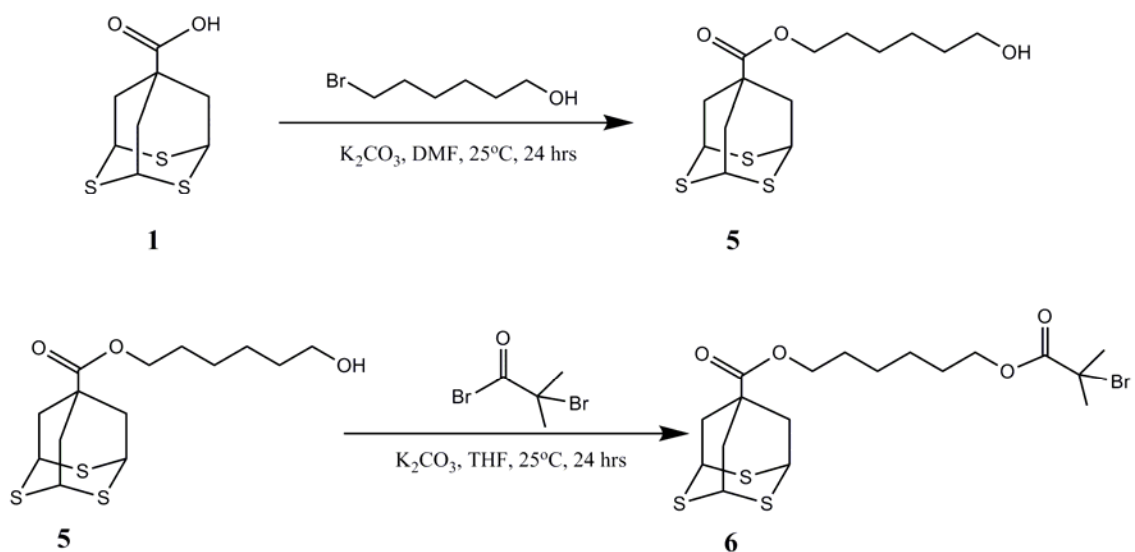
3.2.3.3 Characterization of Polymer Brushes

PM-IRRAS was performed using a Nicolet Nexus 870 Fourier transform infrared spectrometer with a liquid nitrogen cooled MCT detector and a Hinds Instruments PEM-90 photoelastic modulator operating at 100 kHz. The incoming infrared radiation was reflected from the sample at an angle of incidence of 80°. The spectra were usually collected in 4000 scans at a spectral resolution of 4 cm⁻¹. Atomic force microscopy (AFM) images were taken with a Digital Instruments multimode IIIa nanoscope SPM in the tapping mode. Water contact angle (WCA) of samples was measured using a 318CU 3.2M CMOS MicrometricsTM camera along with MicrometricsTM BE software package. Each datum is an average of five individual points with an accuracy of ±2 °. The thicknesses of polymer brushes were measured using an ellipsometer (model 439, Rudolph Instruments) with a helium-neon laser ($\lambda = 632.8$ nm). The angle of incidence was 70° normal to the surface. The compensator was set at +45°. The accuracy of the film measured with this ellipsometer is ±2 Å. A minimum of four spots were measured on each sample.

3.3 Results and Discussion

The synthesis of an attachable initiator for self-assembly to a gold surface is illustrated in Scheme 3.2. The hydroxyl groups of the 2,4,9-trithiatricyclo[3.3.1.1^{3,7}]-

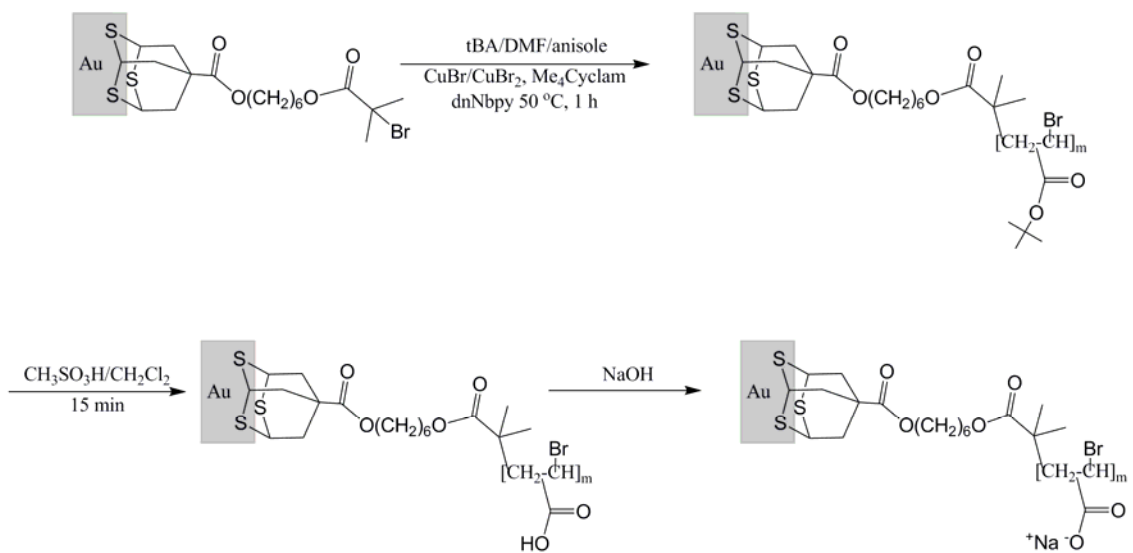
decane-7-carboxylic acid 6-hydroxy-hexyl ester (**5**) were esterified by reaction with 2-bromoisobutyryl bromide, yielding bromo-ester end-groups, which was later used to initiate the ATRP of both *t*-BA and DMAEMA monomers. Formations of densely covered monolayers of initiator (**6**) on gold surface were created by immersing surface-cleaned gold slides in a dilute solution of the trithiaadamantane initiator in ethanol. Any of the excess initiator was removed from the monolayer by completely rinsing gold slides with absolute ethanol and blow drying with nitrogen. The successful immobilization of the designed Tripod-based ATRP initiator (**6**) on gold substrate was confirmed by PM-IRRAS spectrum (Figure 3.1a). As expected, a strong peak at 1740 cm^{-1} due to the carbonyl group of ester was observed. The asymmetric CH_3 stretching vibration (2960 cm^{-1}), C-O vibration of ester (1280 cm^{-1}) and CH_2 stretching vibration (2870 cm^{-1}) of the 6-carbon alkyl linker group and the methyls of the bromoisobutyryl head group were also detected. This indicated that the trithiaadamantane initiator was successfully immobilized on the gold surface. The thickness of the initiator based SAM was estimated to be 12.9 \AA by ellipsometry. The formation of thin SAM was further confirmed by WCA measurements (Table 3.1). After the gold surface was covered by trithiaadamantane initiator, the SAM exhibited a relatively hydrophobic behavior and the WCA was increased to 57.1° from that of 36.4° (bare gold slide). This increase can be attributed to the methyl groups on the end of each initiator that reside across the top of the SAM on the gold surface.



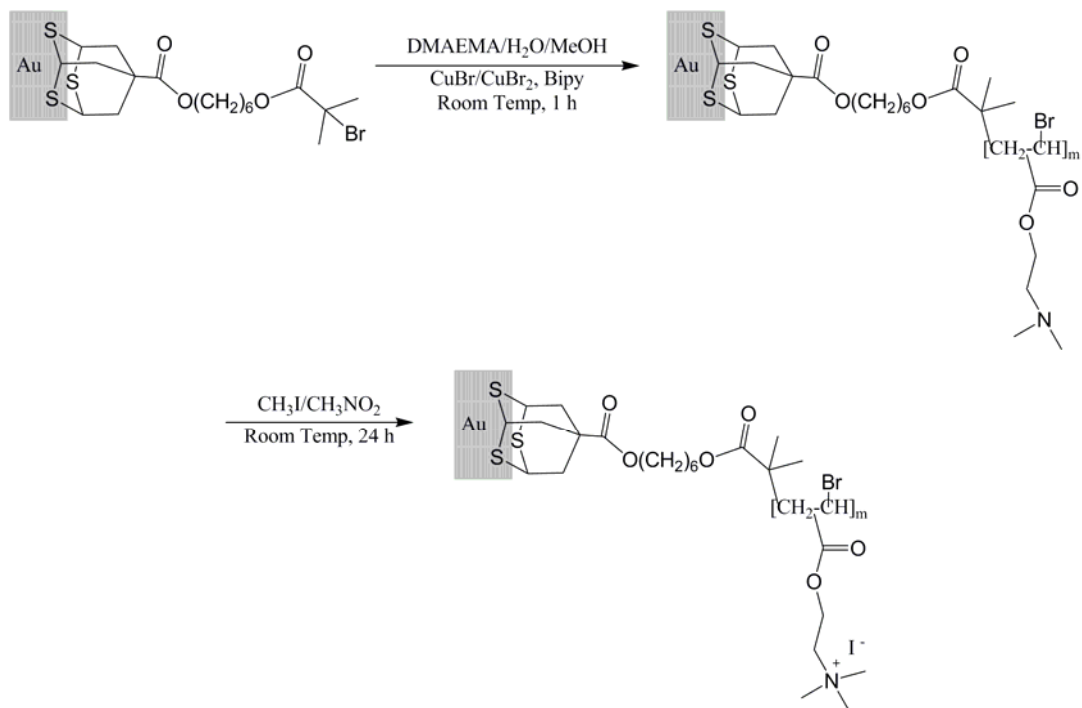
Scheme 3.2 Synthesis of the 2,4,9-trithiaadamantane ATRP surface initiator group.

The total experimental procedure for the synthesis of Poly-*t*-BA and PDMAEMA is outlined in Schemes 3.3 and 3.4, respectively. The ATRP of *t*-BA and DMAEMA from the modified gold substrates were performed with a rapid and controlled polymerization process without added free initiator.^{64,66,67} Therefore the polymerizations of both *t*-BA and DMAEMA do not take place in solution, but instead should occur with polymerization extending from the surface of the SAM thus limiting the chances that bulk polymer, if any in solution from detached initiator, does not stick to the gold surface disrupting the monolayer. To confirm that the prepared trithiaadamantane compound (**6**) can induce the surface-initiated polymerizations of the surface-grafted polymers, a trace amount of compound (**6**) as free initiator in a polymerization solution of *t*-BA. The rapid polymerization of Poly-*t*-BA was observed with the formation of polymer in 5 minutes as indicated by an increase in the viscosity of the reaction solution. The formed polymer was analyzed by FTIR spectroscopy (not shown here) and it was confirmed that Poly-*t*-

BA was formed. This result indicates that with the use of the designed immobilized initiator, the ability of ATRP to grow well-defined polymer chains is feasible.



Scheme 3.3 The synthesis of the poly-*t*-BA brushes.



Scheme 3.4 The synthesis of the PDMAEMA brushes.

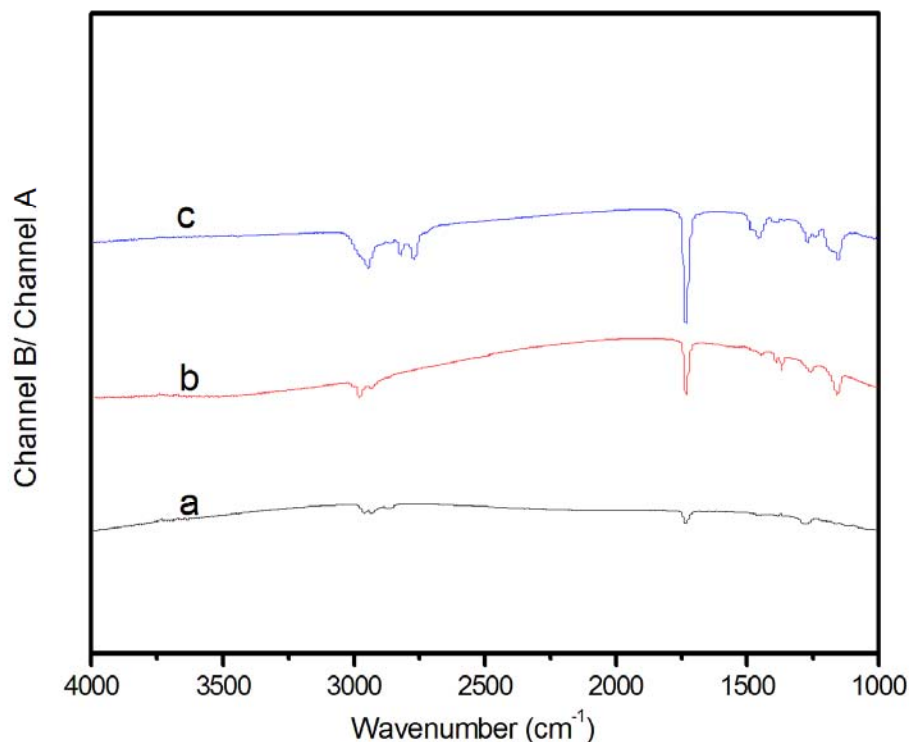


Figure 3.1 Polarization modulation infrared reflectance absorption spectroscopic data for (a) 2,4,9-trithiaadamantane polymer brush initiator, (b) poly-*t*-BA brushes, and (c) PDMAEMA brushes on a Au slide surface.

The WCA of the Poly-*t*-BA-tethered gold surface increased significantly to 65.6° compared to that of unreacted initiator. This resulted from the more hydrophobic *tert*-butyl groups of the Poly-*t*-BA. In contrast to the Poly-*t*-BA-tethered gold substrate, the wettability of the PDMAEMA brushes was not found to change significantly, Table 3.1 shows that wettability changes only slightly in comparison with that of initiator-modified gold surface. In other words, the surfaces of PDMAEMA brushes have similar wetting

properties with that of initiator-modified SAM. This is due to the weak hydrophobicity of PDMAEMA brushes that have been considered as weak polyelectrolytes with properties that are pH dependent in other studies.^{64,67,68} The WCA of Poly-*t*-BA brushes was decreased from 65.6° to 43.2° after the Poly-*t*-BA chains were converted to poly(acrylic acid) (PAA) via hydrolysis. Following hydrolysis, the polymer brush thickness decreased to from 135.6 nm to 111.8 nm most likely due to relaxation of the chains upon removal of the bulky *tert*-butyl groups.^{69,70} A similar result that was also observed by Bruening et al.⁶⁴ The WCA was further decreased to about 38.3° upon treating PAA brushes with a NaOH solution (pH = 10) as the formation of carboxylate PAA polyelectrolyte brushes renders the surface anionically charged and more hydrophilic. Similarly, the quaternized PDMAEMA brushes, as cationic polyelectrolytes, exhibited a relatively hydrophilic behavior compared to their neutral counterpart. The thickness of the PDMAEMA brushes was slightly increased from 101.5 nm to 111.9 nm after quaternization. This is expected due to the electrostatic repulsion force of the charged side chains as well as the increase in the bulkiness of the groups. For better comparison, all WCA data are summarized in Table 3.1.

Table 3.1 Water contact angle (WCA) and ellipsometry measurements.

	Au Slide	SAM	PtBA	PAA	Carboxy-late PAA	PDMAE MA	Quarter-nized PDMAEMA
WCA	36.4°	57.1°	65.6°	43.2°	38.3 °	55.7 °	39.1 °
Thick-ness		12.9Å	135.6 nm		111.8 nm	101.5 nm	111.9 nm

The surface morphology of Poly-*t*-BA and PDMAEMA brushes and their corresponding polyelectrolyte brushes were visualized via atomic force microscopy (AFM). Figures 3.2 and 3.3 show the microscopic morphology of various polymer brushes grafted to the gold slides. The film of Poly-*t*-BA appears as a macroscopically, homogeneous flat thin film with segregated nanodomains (clusters with a 40 ± 5 nm diameter). These domains indicate the dimple (pinned micelles) regime of the polymer brush as described in previous studies and can be seen in Figure 3.2.⁷¹ Such micellar structures are believed to form when the polymer brushes grow to a point that they are no longer soluble in the solvent system. At points of solvent penetration, the brushes aggregate forming the visible micellar nanodomains to avoid unfavorable interaction with the solvent.^{72,73} After the Poly-*t*-BA brushes were converted into carboxylate PAA polyelectrolyte, similar to the Poly-*t*-BA brushes, the latter adopts a similar type of morphology in air, but the surface roughness was slightly decreased (rms roughness decreases from 1.47 to 1.005 nm). This is likely due to the removal of the bulky *tert*-butyl groups (Figure 3.2). In Figure 3.3, PDMAEMA brushes were found to have a different surface morphology compared to Poly-*t*-BA brushes. As mentioned above that PDMAEMA is a weak polyelectrolyte and the wettability measurements revealed that the PDMAEMA brushes have weak hydrophobic properties. As a result, AFM revealed that the surface morphology was not similar to that of the Poly-*t*-BA brushes, exhibiting no signs of homogeneously segregated micellar nanodomains but instead a quite heterogeneous surface (Figure 3.3). After quaternization of PDMAEMA, the surface roughness rms decreases from 2.25 to 1.80 nm as a more uniform surface is created most likely due to the electrostatic repulsion force of the charged side chains as well as the

increase in the bulkiness of the groups which decrease the chance of polymer chain entanglement (Figure 3.3).

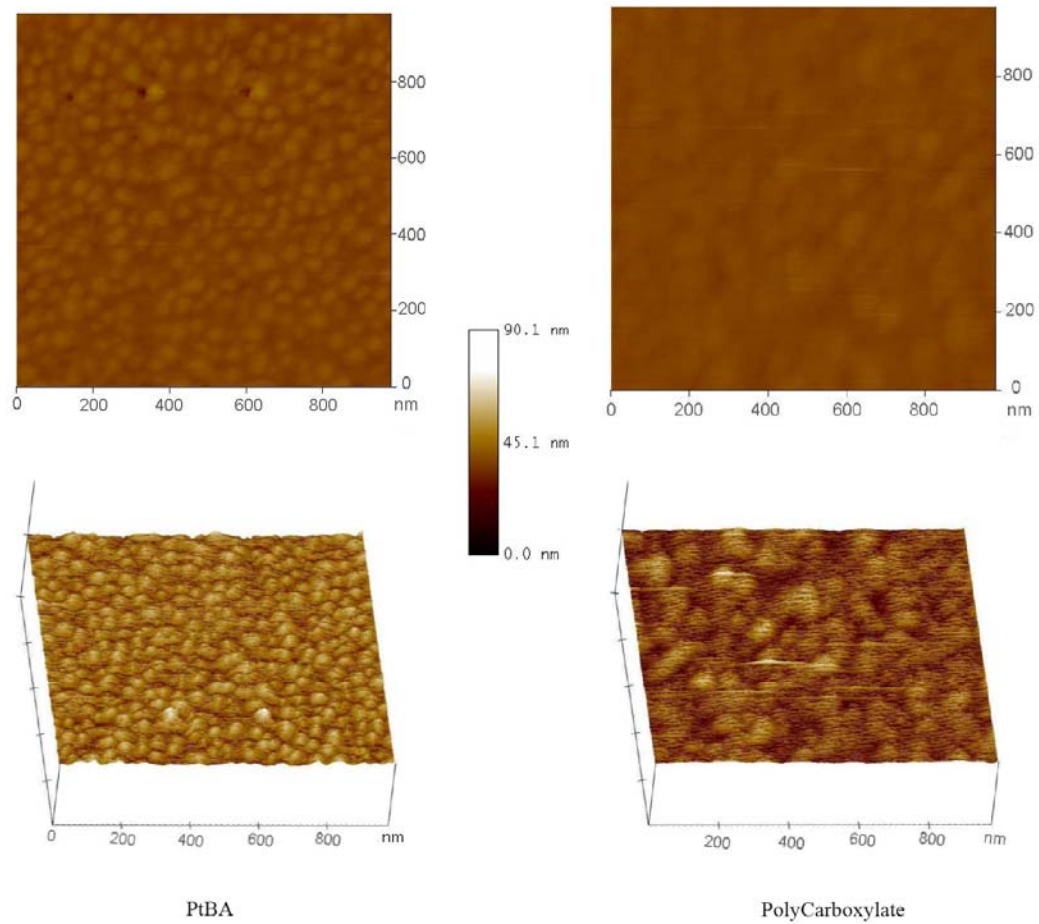


Figure 3.2 The AFM profiles of Poly-*t*-BA and PAA carboxylate polymer brushes.

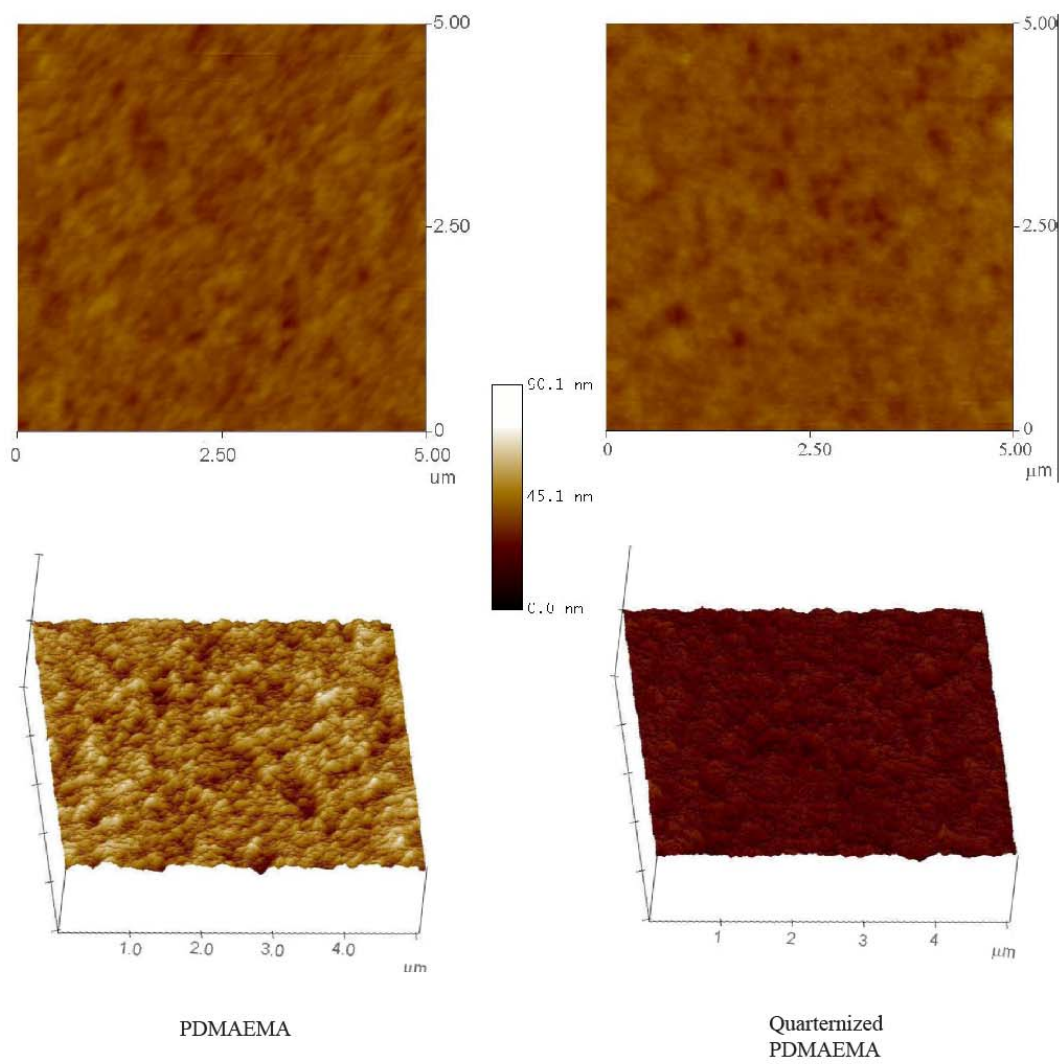


Figure 3.3 The AFM profiles of PDMAEMA and quaternized PDMAEMA polymer brushes.

3.4 Conclusions and Future Work

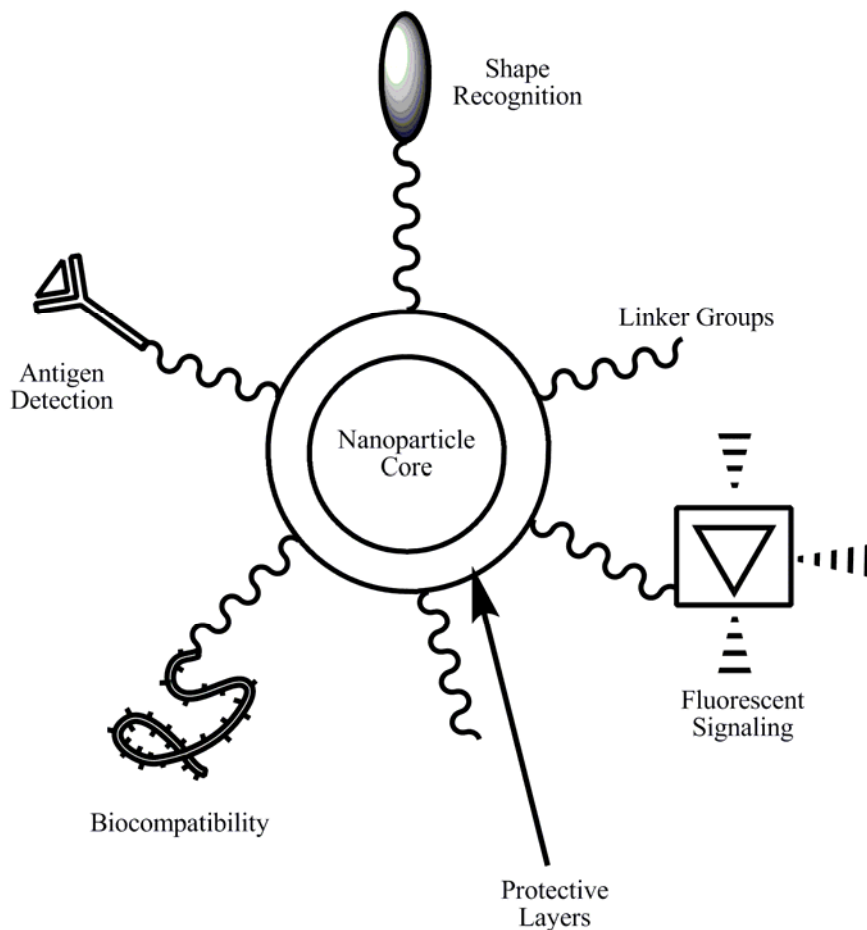
In summary, the trithiaadamantane, 2,4,9-trithia-tricyclo[3.3.1.1^{3,7}]decane-7-carboxylic acid 6-(2-bromo-2-methyl-propionyloxy)-hexyl ester, was designed and synthesized as a unique tridentate surface anchor for ATRP surface-initiated polymerization. The prepared initiator was proven effective in forming self-assembled monolayers (SAMs) on gold substrates from which surface-initiated atom transfer radical polymerization (ATRP) of *tert*-butyl acrylate (*t*-BA) and dimethylamino)ethyl methacrylate (DMAEMA) were successfully performed. Polarization modulation infrared reflectance absorption spectroscopy (PM-IRRAS), atomic force microscopy (AFM), and water contact angle (WCA) measurements were used to confirm that the polymer brushes and their corresponding polyelectrolyte brushes were present on the gold slide surfaces. As previously mentioned, this new type of surface initiator, having enhanced stability, may prove more effective in the grafting of polymer chains, synthesized via ATRP, to gold for various nanotechnology applications.

CHAPTER IV

SYNTHESIS AND CHARACTERIZATION OF MONOLAYER PROTECTED AU NANOPARTICLES AS FUNCTIONAL MIMICS OF SMALL CELLULAR VESICLES.

4.1 Introduction

The development of nanotechnology offers new tools to investigate biomacromolecular interactions at the molecular/cellular level. Nanoparticles of many compositions can be tailored and synthesized to mimic the sizes of various viruses and pathogens with various cores ranging from polymers to that of inorganic metals.⁷⁰ These cores often provide a support onto which varying functionalities can be attached that offer the particle protection while providing it the ability to target and detect specific receptors as depicted by Scheme 4.1. For this reason, nanoparticles have found uses as fluorescent biological labels, MRI contrast agents and as therapeutic delivery and bio-detection devices. The ultimate goal of this field of research is to develop a system that will be able to diagnose accurately and early, treat without side effects, and evaluate the efficiency of its specific treatment noninvasively.⁷⁴ One group of nanoparticles that have been continuously investigated as such devices are gold nanoparticles, the focus of this chapter.



Scheme 4.1 A representation of a general nanoparticle with varying functionalities.

Gold metal issues unique spectroscopic signatures to these nanoparticles, allowing them to be quantitated through a variety of techniques such as UVVis and Raman spectroscopy.^{76,77} These nanoparticles can range from sizes of 2–100 nm in size and are readily endocytosed into human cells exhibiting little to no toxicity making them an optimal platform for designing bioanalytical devices.⁷⁸ As previously mentioned, the development of functionalized gold nanoparticles owes its existence to the work of Nuzzo and Allara who pioneered studying the growth of self assembled monolayers (SAMs) of thiols on gold surfaces.⁸ Thiols, which readily bind to gold surfaces, have

proven valuable in the stabilization of gold nanoparticles with highly functionalized surfaces.⁷⁹ For this reason, monofunctionalized gold nanoparticles have found uses as imaging agents, bio-detection and drug delivery devices employing a number of targeting ligands such as DNA and sugar moieties.^{80,81} Though these systems are unique and show potential, there always exist limitations. Most monodentate sulfur ligands, dependent on the attached targeting moiety, are often subject to phase segregation across the gold nanoparticle surface. Therefore, mixed monolayers of different thiol ligands are not guaranteed to be evenly distributed across the surface of the particle. Another issue arising from the use of monodentate thiols is the immobility of the targeting ligands due to high density interchain packing. Alkane SAMs often display a high packing order when the alkyl chains are longer than C6 restricting their freedom of motion.²⁵

Restricting the freedom of motion of the linker group with a targeting moiety attached is severely detrimental to the effectiveness of the particle's ability to bind to its target. This is especially true when the target is biological in nature. Many surface binding interactions at the cellular and molecular level take place through multivalent interactions. Multivalency addresses the binding events at cellular surfaces that fail to be explained by the conventional lock and key understanding of how binding occurs. Typically, these binding events are the result of multiple binding interactions enhancing the avidity, overall association constant, of one entity for another.⁸² One example of this is the targeting and binding of antibodies. Antibodies are composed of three fragments, two that are responsible for the binding event. Binding of one fragment, only loosely holds the antibody to its target but it allows for the positioning of the antibody in a manner in which the second fragment can bind enhancing the avidity between it and its

target. To address multivalency and make sure that multiple targeting groups are binding, linkers on the surface of these nanoparticles must serve multiple functions of physically connecting, spatially separating and allowing the targeting moiety to assume the favored conformation to that of the target.⁸³ This is not the case for systems where the movement of the targeting ligand is severely restricted and the point of attachment not conformationally favorable to that of the target. However, it is possible that the limitations caused by high density packing can be diluted through the use of sterically irregular linkers or mixing of short chain alkyl thiolates into the self assembled monolayer.²⁷

As previously mentioned, the potential application of 7-substituted-2,4,9-trithiaadamantane to overcome the effects of high density packing was reported by Fox and Whitesell.²⁸ Yet, little progress was made until a new synthetic method was developed.³⁰ So far, a number of investigative studies have led to the characterization of a number of physical properties of the molecule, including the formation of inclusion complexes in β -cyclodextrin and its use in photochemical patterning on gold surfaces.^{27,31} Previous studies have proven that this tridentate, or tripod, molecule can be used to bind to and stabilize the surface of gold nanoparticles through direct reduction methods or ligand exchange reactions.⁸⁴ The use of this molecule on the gold nanoparticle surface should dilute the effects of interchain packing, making this particular sulfur ligand an invaluable tool for designing probes with functional targeting moieties exhibiting the appropriate free range of motion for multivalent binding.

The best examples of entities that are capable targeting and binding to others in a multivalent fashion are pathogenic in nature. These interactions heavily rely

on carbohydrates or protein-based ligands that bind in a multivalent fashion. These two types of ligands are readily involved in a number of specific molecular and cellular recognition events such as cell-cell recognition, adhesion, and pathogenesis.^{85,86} For example, it is well known that amongst malignant cancers often an alteration of cellular glycosylation occurs on the surface of the cell. This imparts two key survival abilities to the cancer cell; invisibility to immune recognition and the ability to cellularly adhere to endothelial cells.⁸⁷ Viruses and other pathogens acquire these abilities in a similar way which dictates their virulence.⁸⁸

4.1.1 Objectives

More emphasis is being placed on probing and understanding these particular events in hopes of developing new treatments and preventative measures surrounding these particular disease states. Currently, most analytical methods that have been developed rely heavily on the binding of a single ligand, for example a protein, to a particular receptor, or vice versa within a prepared sample. However, as mentioned *in vivo* interactions of this nature rarely occur and require some form of multidentate binding. Therefore, it is reasonable to mimic the components of a virus based on gold nanoparticles stabilized by functionalized 2,4,9-trithiaadamantane as a platform to develop some type of probe as a tool to investigate and build a better understanding of these complex interactions at the molecular/cellular level.

4.1.1.1 Design and Approach

Unlike systems involving mono- or bidentate sulfur ligands, the tridentate ligand, 2,4,9-trithiaadamantane, minimizes Van der Waals interchain packing creating a self assembled monolayer (SAM) that provides enough space for the intercalation of other hydrophobic alkyl chains. This phenomena was first noticed upon the exposure of gold nanoparticles (GNPs) stabilized by alkyl functionalized 2,4,9-trithiaadamantane to polar solvents. Upon exposure, the GNPs became aggregated. A closer look via TEM microscopy shows that alkyl chains extending from the nanoparticles are intercalated as shown in Figure 4.1.⁸⁰

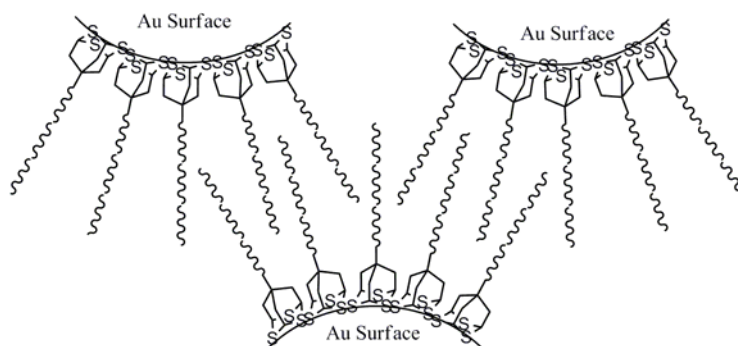
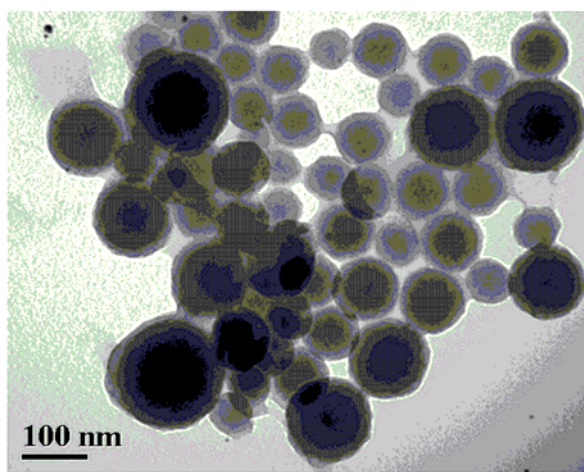
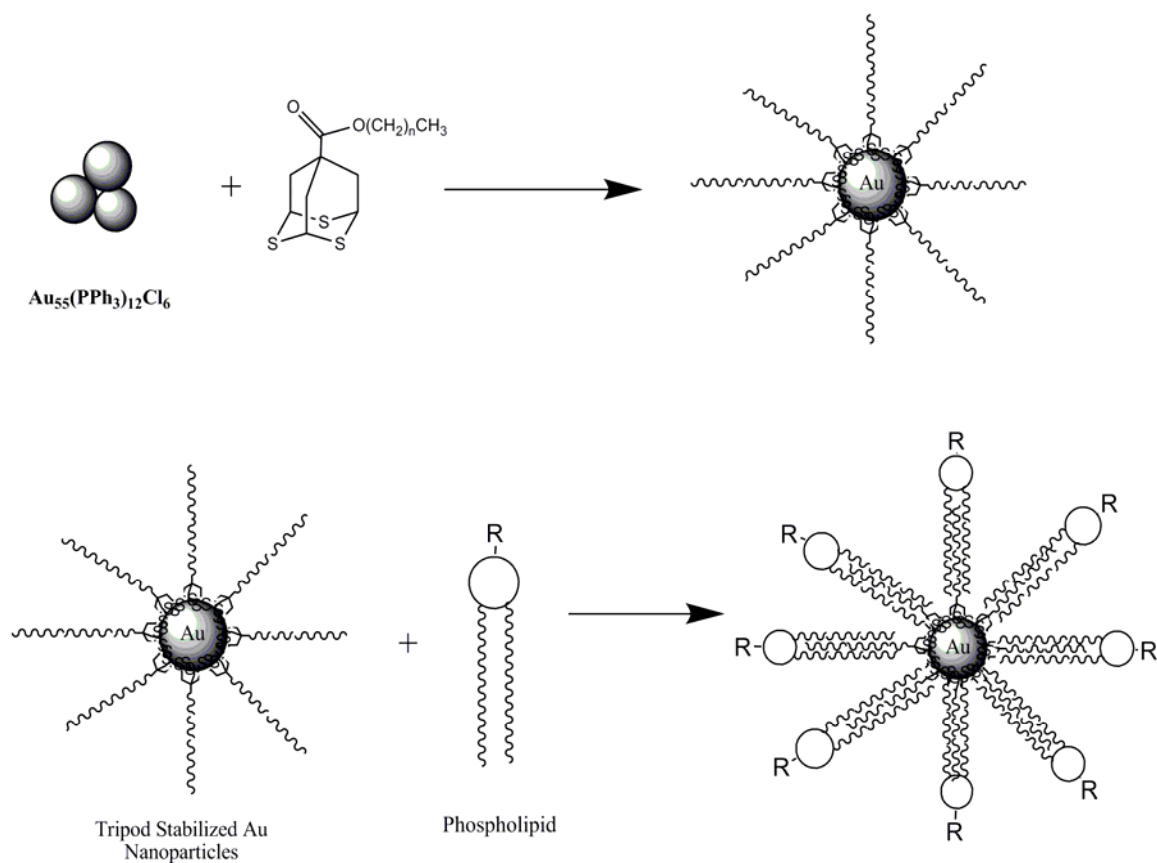


Figure 4.1 A TEM image of GNPs exposed to polar solvent and a depiction of alkyl chain intercalation on the Au nanoparticle surfaces.⁸⁰

Typically, a viral nanoparticle is composed of 3 parts: nucleic acid, protein capsid, and lipid membrane. In terms of multivalent binding, the lipid membrane of the viral particle constitutes the most important part. Based on this, using the tridentate sulfur ligand 2,4,9-trithiaadamantane functionalized with alkyl chains to stabilize and protect Au nanoparticles, the intercalation of a lipid layer across the surface should be induced to form a small liponanovesicle mimicking a viral particle as depicted in Scheme 4.2.



Scheme 4.2 A schematic representation of gold nanoparticle stabilization and protection by an alkyl derivative of 2,4,9-trithiaadamantane and subsequent lipid intercalation.

The research presented uses a tridentate sulfur ligand based on 2,4,9-Trithia-tricyclo[3.3.1.1^{3,7}]decane in the stabilization and protection of Au nanoparticles. The ligand was functionalized with an alkyl chain and assembled on the surface of the gold nanoparticles via a ligand exchange reaction monitored via NMR spectroscopy. The ability of the GNPs to effectively intercalate lipids was tested in the solid state via Thermogravimetric analysis (TGA) and Differential scanning calorimetry (DSC). For solution studies, a series dispersion tests were performed to find the most stable composition of the liponanovesicles followed by subsequent NMR study.

4.2 Experimental Section

In this section, the methods and procedures regarding the synthesis of the alkyl Tripod ligand, its exchange with triphenyl phosphine on the surface of gold nanoparticles, and the intercalation of lipids across the surface are described.

4.2.1 Materials and Methods

All solvents and reagents were purchased from commercial sources and purified when needed. 1,2-Didecanoyl-*sn*-glycerol 3 phosphate sodium salt and 1,2-dipalmitoyl-*rac*-glycero-3-phosphocholine hydrate were purchased from Sigma Aldrich and used as received. Chicken egg L- α -phosphatidylcholine was purchased from Avanti Polar Lipids Inc. and hydrogenated when needed. Compound **1**, 2,4,9-Trithia-tricyclo[3.3.1.1^{3,7}]decane-7-carboxylic acid, and Ph₃P-stabilized gold nanoparticles (GNPs) were synthesized according to a previously cited procedures.^{30,84}

All ^1H NMR (330 MHz) and ^{13}C (77 MHz) NMR spectra were recorded using a Varian Gemini-300 spectrometer unless noted. NMR spectra recorded are reported in parts per million (ppm) relative to the chosen deuterated solvent's reference peak. ^1H NMR multiplicity was noted as follows: s, singlet; d, doublet; t, triplet; q, quartet; m, multiplet. IR spectra were recorded on a Nicolet Nexus 870 FT-IR spectrometer equipped with a Thunderdome Attenuated Reflectance (ATR) accessory and recorded in wavenumbers (cm^{-1}). Thermogravimetric analysis (TGA) was performed with a TGA Q500 (Q Advantage 2.8 TA) instrument. Differential scanning calorimetry (DSC) was performed with a DSA Q2000 (Q Advantage 2.8 TA) instrument.

Prior to use, all glassware was flame or oven dried and then allowed to cool in desiccators. Air- and moisture-sensitive reactions were performed under argon gas (99.99%). Synthetic products were purified via flash chromatography and recrystallization. Thin-layer chromatography (TLC) was performed on Whatman silica gel glass backed plates of 250 μm thickness on which spots were visualized using UV light or iodine. EM Science silica gel 60 \AA (particle size 35-75 μm) was used for flash chromatography.

4.2.2 Synthesis of Ligands and Ligand-stabilized GNPs

In this section the synthesis of the alkyl Tripod derivative is described as well as its use in the stabilization of gold nanoparticles via ligand exchange with triphenyl phosphine.

4.2.2.1 Synthesis of 2,4,9-Trithia-tricyclo[3.3.1.1^{3,7}]decane-7-octadecylamide

(TpCONC₁₈, 7)

Unpurified compound **1** (1.86 g, 7.97 mmol) was vacuum pumped dry in a round bottom flask with a stir bar overnight. The vessel was flushed with argon, then the sample was dissolved in dry dichloromethane (20 mL) and placed on an ice bath to stir for five minutes. While stirring on the ice bath, SOCl₂ (3 mL, 41.3 mmol) was slowly added dropwise, then the ice bath was removed and the reaction vessel was allowed to come to room temperature prior to refluxing at 60°C. The reaction was monitored via I.R. Upon completion the solvent in the reaction vessel was reduced under pressure and excess SOCl₂ was removed via vacuum pump into a liquid nitrogen vacuum trap. The sample was then redissolved in dry THF (20 mL). To the stirring vessel containing the acid halide, octadecylamine (2.59 g, 9.56 mmols), along with 2-3 drops tetraethylamine, dissolved and transferred in dry THF (35 mL). The reaction was stopped and then dry Na₂CO₃ was added to the reaction to quench any excess acid. The reaction was then filtered and rinsed with CH₂Cl₂. Then an extraction was performed using water and CH₂Cl₂. The organic layer was dried over Na₂SO₄ and flash column chromatography was performed using a 1:4 mixture of ethyl acetate/hexanes to obtain the product (0.998 g, 26%). ¹H NMR δ: 0.88 (t, 3H, CH₃), 1.26 (m, 30H, (CH₂)₁₅), 1.51 (d, 2H, CH₂CH₃), 2.88 (d, 6H, CH₂CHS), 3.29 (t, 2H, CH₂NH), 4.36s (s, 3H, SCHS), 5.60 (s, 1H, NH). ¹³C NMR δ: 14.3, 22.8, 27.0, 29.0, 32.0, 38.2, 40.0, 41.0, 175. FTIR (cm⁻¹): 3299 (-NH-), 2916 (-CH₃), 2849 (-CH₂-), 1634 (-C=O), 1548 (-NH-).

4.2.2.2 Preparation of TpCONC₁₈ Monolayer Protected Gold Nanoparticles (Au MPNs)

The following ligand exchange was performed using triphenylphosphine-stabilized gold nanoparticles (Au₅₅(PPh₃)₁₂Cl₆) synthesized according to a reported procedure. To approximately 100 mg of Au₅₅(PPh₃)₁₂Cl₆ nanoparticles dissolved in CD₂Cl₂ (1.5 mL) in a 8", 5 mm O.D. NMR tube, was added compound **7** (20 mg). The exchange reaction was then monitored via ¹H NMR over a 24 hour period. Upon the exchange reactions completion, the nanoparticles were removed from the tube rinsing with dichloromethane into a round bottom flask and dried. To remove traces of triphenylphosphine oxide, the dry particles were suspended in an 2:1 ethanol:water (5 mL) mixture to induce aggregation. The aggregated nanoparticles were then filtered from the solution onto a hydrophilic polypropylene membrane (0.2 μm pore size, PALL Life Sciences) and rinsed using the 2:1 ethanol:water mixture (10 mL) then dried. The aggregated particles were then resuspended from the membrane into a dry round bottom flask using chloroform and a fraction was removed and prepared for spectroscopic characterization. ¹H NMR δ: 0.85 (t, 3H, CH₃), 1.26 (m, 30H, (CH₂)₁₅), 1.55 (s, 2H, CH₂CH₃), 2.82 (d, 6H, CH₂CHS), 3.22 (dd, 2H, CH₂NH), 4.34s (s, 3H, SCHS), 5.61 (s, 1H, NH), 7.52 (m, 15H, CCH). ¹³C NMR δ: 14.4, 23.3, 27.4, 30.3, 32.5, 40.1, 40.8, 42.4. FTIR (cm⁻¹): 3294 (-NH-), 2917 (-CH₃), 2850 (-CH₂-), 1632 (-C=O), 1549 (-NH-), 1468, 1377 (-CH₃), 1103 (-CH).

4.2.3 Lipid Interdigitation into the Monolayer of the Au MPNs

The following experiments were used to investigate the ability of the alkyl Tripod stabilized gold nanoparticles to intercalate lipids across the particle surface.

4.2.3.1 Thermogravimetric and Differential Scanning Calorimetry Analyses of Lipid Interdigitation in the Solid State

Thermo-gravimetric analysis (TGA) was performed on the TpCONC₁₈ ligand protected nanoparticles with a TGA Q500 (Q Advantage 2.8 TA) instrument with a scan rate of 10°C/min from 25–300°C. Scans were run at Differential scanning calorimetry (DSC) was performed with a DSA Q2000 (Q Advantage 2.8 TA) instrument with a scan rate of 10°C/min from 0–200°C for pure tripod-capped nanoparticles and 0–170 °C for the nanoparticle lipid mixtures. Prior to DSC analysis, lipid-nanoparticles mixes were prepared by mixing TpCONC₁₈ Au MPCs in approximately 1:1 weight ratios with L- α -phosphatidylcholine and 1,2-dipalmitoyl-*rac*-glycero-3-phosphocholine hydrate.

4.2.3.2 Forced Lipid Interdigitation via Induced Solvent Effects

Pursuing further testing of the alkyl derivative protected Au nanoparticules, TpCONC₁₈ GNPs in 90 μ g portions were mixed in a varying w/w ratios of three different lipids, 1,2-didecanoyl-*sn*-glycerol 3 phosphate sodium salt, 1,2-dipalmitoyl-*rac*-glycero-3-phosphocholine hydrate and chicken egg L- α -phosphatidylcholine, in chloroform (Chl) as listed in Table 4.1. The solvent of the sample mixtures was then slowly evaporated under a stream of N₂ gas over 24 h. After complete evaporation, the samples in the solid state were heated to ~65 °C for 15 min then 1 mL of phosphate buffer (pH 7.4) was slowly added as not to disturb of GNP/Lipid films. In buffer, the samples were reheated to ~65 °C for an additional 15 min and then sonicated to disperse the nanoparticles. The dispersions were then allowed to sit for 72 h at room temperature monitoring dispersion stability.

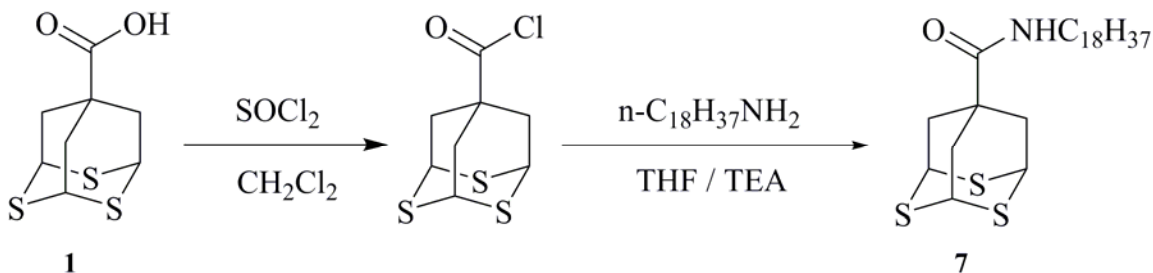
4.2.3.3 Interdigitation of TpCONC₁₈ Au MPNs with the Alkyl Chains of 1,2-Didecanoyl-*sn*-glycerol 3-phosphate sodium salt and Extraction from CDCl₃ to D₂O

To a conical flask containing 1,2-didecanoyl-*sn*-glycerol 3-phosphate sodium salt (24.6 mg, 0.032 mmols) was added TpCONC₁₈ (16 mg, 0.033 mmols). The solids were dissolved in deuterated methanol (0.1 mL) creating a viscous slurry and then heated to ~ 80 °C on a hot water bath and then sonicated, repeating the process 3–5 times. After repeated heating and sonication, triphenylphosphine-stabilized gold nanoparticles (16.4 mg) were added and the vessel was again heated and sonicated repeatedly. A sample of the slurry was taken for ¹H NMR. The vessel was then set in the refrigerator for 15 min to solidify the slurry. After solidification, any excess supernatant was poured off and D₂O (3 mL) was added. The vessel was again heated at ~ 80 °C without any further sonication for ~5 min and then a sample was removed for ¹H NMR.

4.3 Results and Discussion

The 2,4,9-trithia-tricyclo[3.3.1.1^{3,7}]decane-7-octadecylamide derivative (**2**) was synthesized according to Scheme 4.3. As previously mentioned, to form the TpCONC₁₈ stabilized GNPs, TpCONC₁₈ was mixed with Au₅₅(PPh₃)₁₂Cl₆ nanoparticles and dissolved in CDCl₃ within an NMR tube. The ligand exchange reaction was monitored via NMR over a 24 h period (Figure 4.2). Prior to exchange (noted as 0 hrs), PPh₃ can be seen on the gold cluster (broad peak, 6-9 ppm) and in excess in solution (narrow peak at 7.6 ppm). As the reaction proceeded, PPh₃ on the surface is gradually converted into the free ligand as the broad peak diminishes and the narrow peak intensifies. After 16 h, the

spectra of the exchange reaction exhibited no change and the reaction was noted as complete.



Scheme 4.3 The synthesis of 2,4,9-trithia-tricyclo[3.3.1.1^{3,7}]decane-7-octadecylamide.

The Au MPNs formed by the ligand exchange reaction were very large (ca. 50-70 nm) and formed aggregates in polar solvent as revealed by past TEM analysis. In contrast to Au MPNs formed in ligand exchange reactions with thiols, these nanoparticles exhibited a significant increase in size.⁸⁹ However, the nanoparticles seemed to be round, the shape suggesting the MPNs to be a single crystalline truncated octahedron. It is likely that the 2,4,9-trithiaadamantane derivative prefers to bind to the Au(111) surface with all three sulfur atoms explaining the structure the nanoparticles. To accurately look at any remaining PPh₃ bound to the surface, the nanoparticles were exposed to polar solvent to induce aggregation. These aggregates (ranging from 0.1 – 0.2 μm) were large enough to be filtered from the ligand exchange mixture removing any excess PPh₃ and TpCONC₁₈ ligands. Resuspension and characterization via NMR indicated that a small amount of PPh₃ remained (7.52 ppm). The intermediate peak width observed suggested that the remaining PPh₃ had a higher degree of free motion compared to that of the highly packed PPh₃ prior to ligand exchange suggesting that the remaining PPh₃ is at the edges of the truncated octahedron where the sulfurs of the tridentate ligand cannot be bonded. Poor

binding on the edges maybe be the factor allowing for continued growth of the cluster during the exchange reaction which leads to the formation of a larger Au nanoparticle than those using common alkyl thiols.

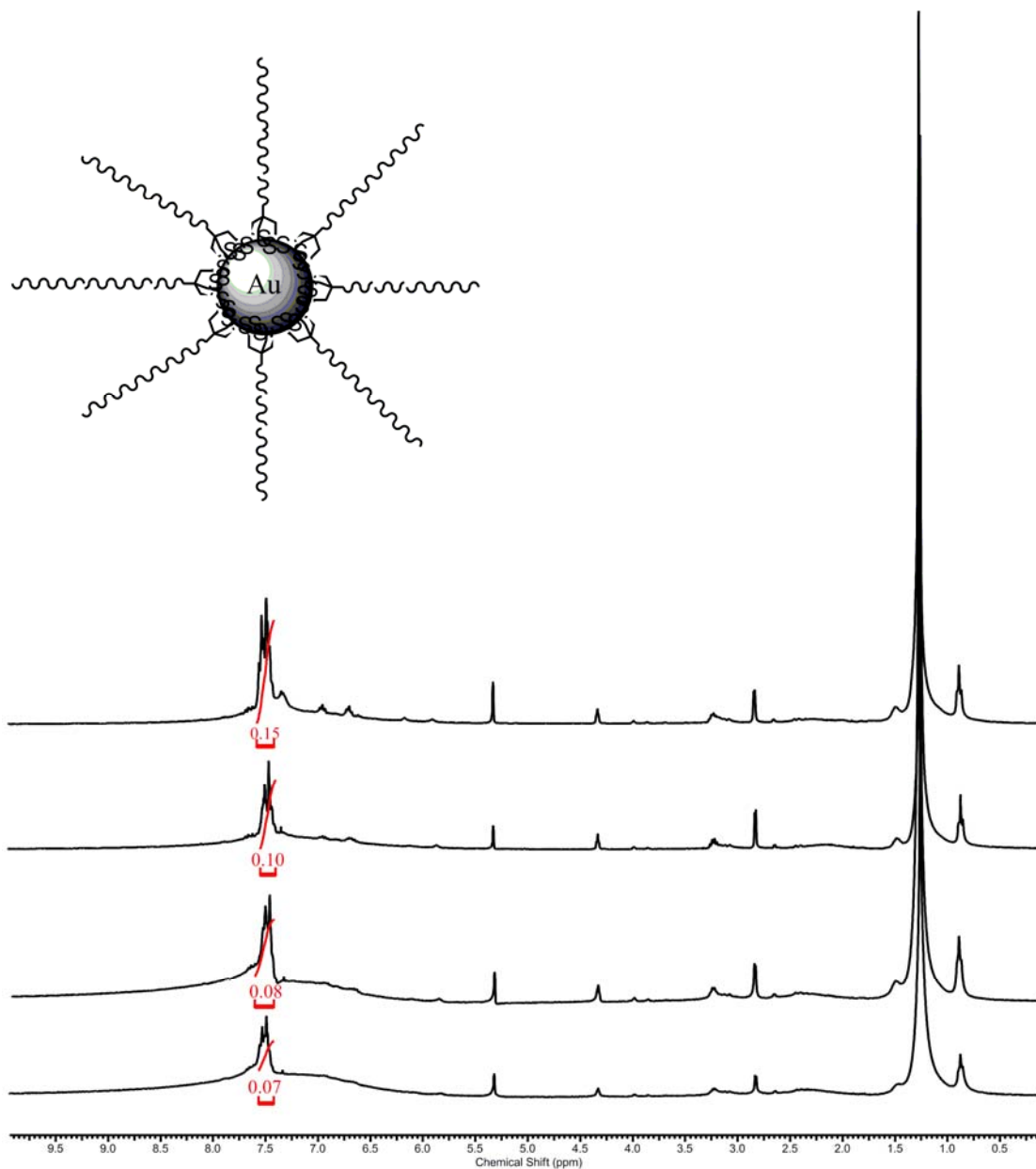


Figure 4.2 The ligand exchange reaction of TpCONC₁₈ with Ph₃P, starting from the bottom recorded at 0 h, 1 h, 4 h, and 16 h (intergration values noted in red), on GNP surface monitored via ¹H NMR spectroscopy.

Prior to investigating of lipid interdigitation on the surface of the TpCONC₁₈ Au MPNs in solution, solid state thermoanalysis was performed on lipid/TpCONC₁₈ Au MPN mixtures. TGA of the TpCONC₁₈ ligand (Figure 4.3) shows remarkable stability up to ~280 °C before degradation. Thus, if this ligand is used as a component of Au MPNs it should allow them to withstand a wide range of temperatures for surface reaction chemistry and is well within the temperature range of reactions that occur within most biological systems.

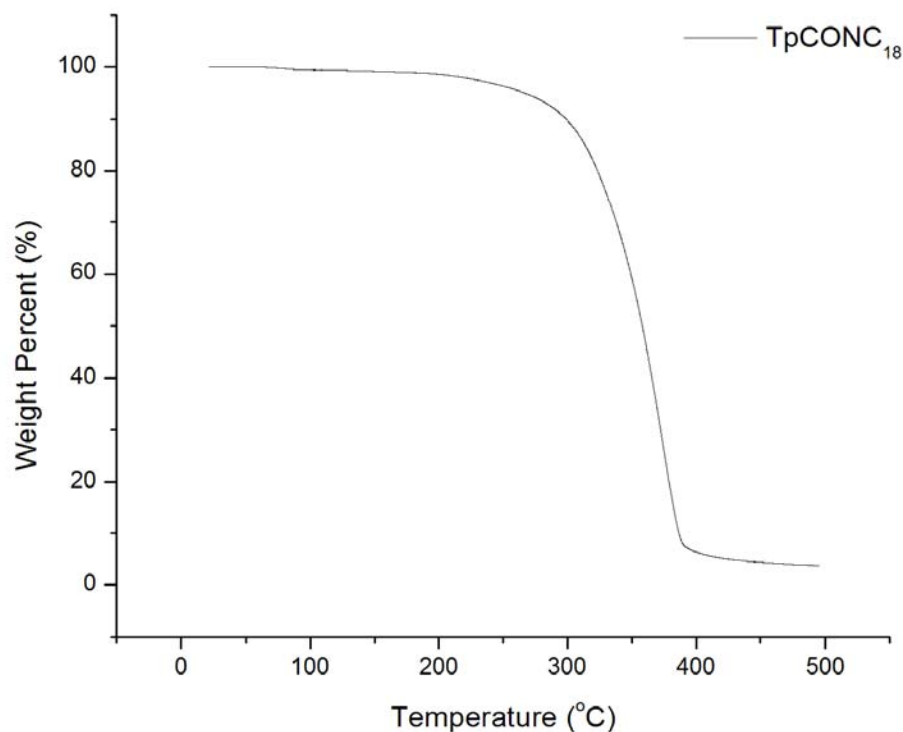


Figure 4.3 The thermo-gravimetric analysis (TGA) of TpCONC₁₈.

DSC was performed on three samples, TpCONC₁₈ Au MPNs themselves and the nanoparticles mixed in a 1:1 weight ratio with chicken egg L- α -phosphatidylcholine and 1,2-dipalmitoyl-*rac*-glycero-3-phosphocholine hydrate. DSC of the TpCONC₁₈ Au MPNs themselves (Figure 4.4) initially shows three significant glass transition states (T_g 's) at 98.9, 128.5 and 180 °C. It is reasonable to suggest that the three T_g 's represent the two molecules on the nanoparticle surface. The two T_g 's at 128.5 and 180 °C most likely represent long alkyl chains and the trithiaadamantane base of the TpCONC₁₈ respectively, while the T_g at 98.9 °C is representative of triphenyl rotation from the PPh₃ residing along the edges of the particle surface. When sample was cycled and allowed to cool and Ramp 2 was recorded, there appeared a new T_g occurring at 38 °C as well as a temperature shift increasing two of the previous T_g 's from 98.9 and 128.5 °C to 102.0 and 130.5 °C, a difference of ~ 3 and 2 °C. The T_g at 180 °C displayed no significant shifts. The shifts in the two T_g 's to higher temperatures maybe accounted for as the result of the reordering of the molecules during the cooling process on the nanoparticle into a more uniform crystalline surface. The appearance of the new T_g occurring at 38 °C is close to 40 °C and indicative of interdigitation that seen amongst the alkyl chains of various lipid bilayer systems.⁹⁰ This is of great importance considering that under physiological conditions lipids exist in a liquid-crystalline state in biomembranes, which accounts for the membrane fluidity, at these temperatures.⁹⁰

To ensure that this was a valid result, chicken egg L- α -phosphatidylcholine, which contains a *cis*-double bond on one of the alkyl chains, was added to a mixture of the TpCONC₁₈ Au MPNs in a 1:1 weight ratio to see if the reorganization and

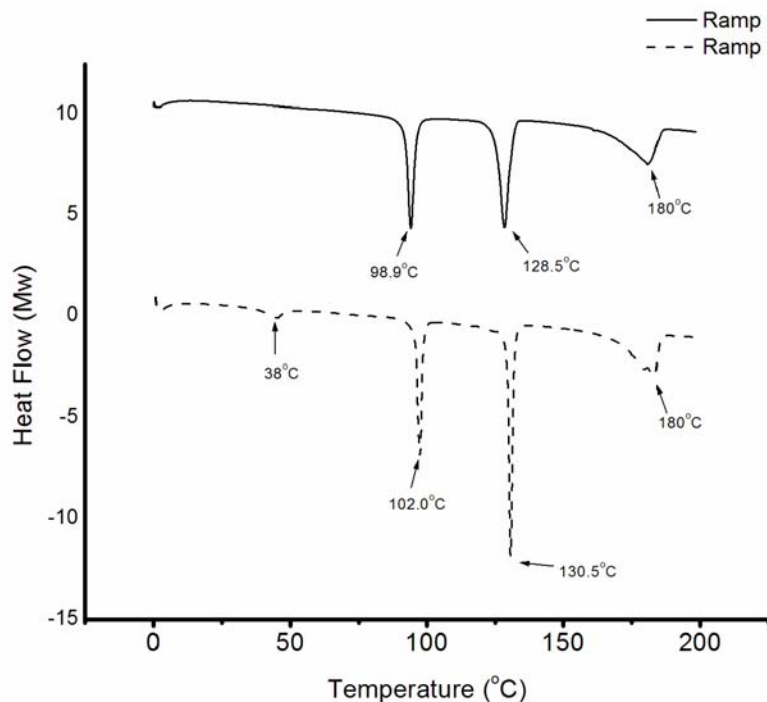


Figure 4.4 The DSC thermogram of TpCONC₁₈ Au MPNs (data offset by 10 mW).

interdigitation of the alkyl chains on the nanoparticle surface can be interrupted resulting in a decrease in the temperature for the observed T_g 's. The DSC thermogram (Figure 4.5) shows the disappearance of one T_g at 25.1 °C and a decrease in temperature of the two T_g 's 102.2 and 133 °C from Ramp 1 to 98.2 and 131 °C in Ramp 2, differences of ~ 4 and 2 °C. The disappearance of the T_g at 25.1 °C can be explained by the fact that the chicken egg L- α -phosphatidylcholine begins to melt and reorganize itself into the alkyl chains of the TpCONC₁₈ Au MPNs. The decrease in the two T_g 's 102.2 and 133 °C from Ramp 1 to 98.2 and 131 °C in Ramp 2, can be attributed to the kink, the *cis* double bond, in one of the alkyl chains of the lipid disrupting the packing with the alkyl chains of the

TpCONC₁₈ Au MPNs. This in turn disrupts the uniformity of the liquid-crystalline surface by introducing more disorder creating lower T_g 's.

The results from the DSC experiments using 1,2-dipalmitoyl-*rac*-glycero-3-phosphocholine hydrate, which is similar in structure to chicken egg L- α -phosphatidylcholine with two saturated alkyl chains, exhibited a slightly different trend (Figure 4.6). Though there is recognizable interdigitation of the alkyl chains on the nanoparticle surface resulting in interruption of the alkyl monolayer and a decrease in the temperature for the observed T_g 's, this is only represented by the decrease in a single T_g from 102 °C in Ramp 1 to 99 °C in Ramp 2. The lowering of this T_g is an indication that remaining Ph₃P along the edges of the nanoparticle packing is interrupted. Surprisingly, there are two T_g 's that most likely represent the long alkyl chains of the TpCONC₁₈ Au MPNs interdigitating in varying degrees with the saturated alkyl chains of 1,2-dipalmitoyl-*rac*-glycero-3-phosphocholine hydrate. One is the increase of the T_g at 131 °C in Ramp 1, which is associated with the long alkyl chains long alkyl chains of the TpCONC₁₈ Au MPNs, to 132 °C in Ramp 2. This increase is due to the increased packing of alkyl chains leading to a more uniform crystalline structure. The second T_g appears at 119 °C in Ramp 2. The appearance of this peak can be explained as possible partial interdigitation of the lipid alkyl chains into the alkyl chains of the monolayer.

To investigate lipid interdigitation on the surface of the TpCONC₁₈ Au MPNs induced by a polar solvent, varying w/w/w ratios of three different lipids, 1,2-didecanoyl-*sn*-glycerol 3 phosphate sodium salt, 1,2-dipalmitoyl-*rac*-glycero-3-phosphocholine hydrate and chicken egg L- α -phosphatidylcholine, were mixed 90 μ g portions of TpCONC₁₈ Au MPNs in chloroform (Chl) and evaporated to create thin films as listed in Table 4.1.

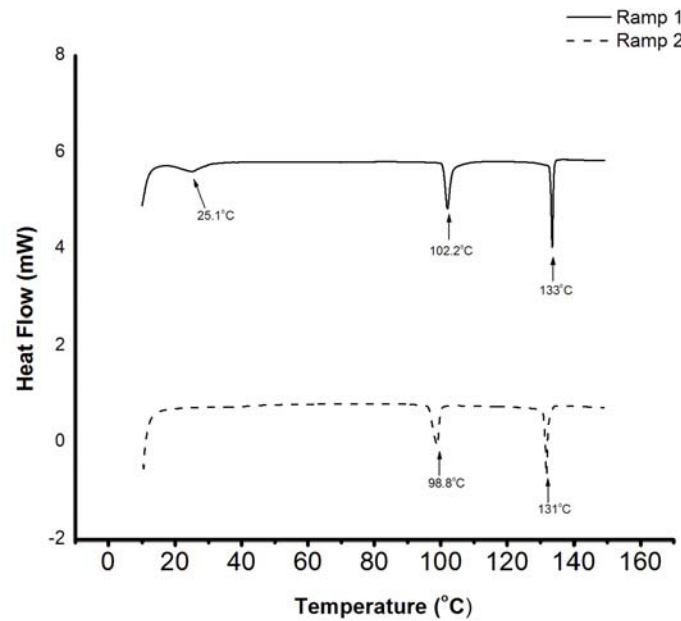


Figure 4.5 The DSC thermogram of TpCONC₁₈ Au MPCs mixed with chicken egg L- α -phosphatidylcholine (data offset by 5 mW).

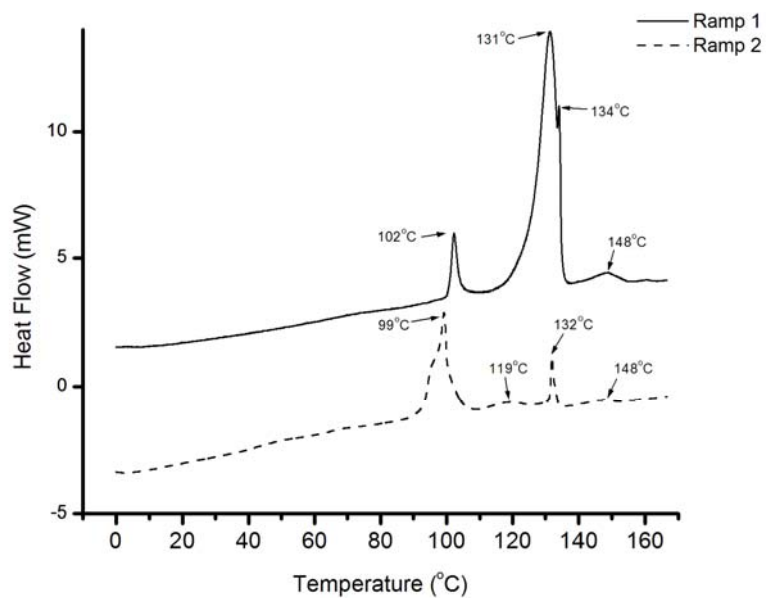


Figure 4.6 The DSC thermogram of TpCONC₁₈ Au MPCs mixed with 1,2-dipalmitoyl-*rac*-glycero-3-phosphocholine hydrate (data offset by 5 mW).

These thin lipid/MPN thin films were then heated and sonicated in the presence of phosphate buffer (pH 7.4) solution.

Table 4.1 A list of lipid mixture weight ratios mixed with TpCONC₁₈ Au MPNs and observations upon 72 h exposure to phosphate buffer (pH 7.4).

Sample	Lipid Weight Ratios (mg)			Observations (72 hrs)
	A	B	C	
1	6.0	-	-	slight pink color, minimal ppt
2	-	6.4	-	cloudy, large ppt
3	-	-	5.7	purple/pink color, barely visible ppt
4	5.3	1.6	-	pink color, no ppt
5	3.9	-	1.8	pink color, no ppt
6	2.0	4.4	-	pink color, no ppt
7	-	4.1	2.5	cloudy, large ppt
8	2.3	-	5	cloudy, large ppt
9	-	6.2	13.4	cloudy purple, visible ppt
10	-	-	-	clear colorless solution, large black ppt

*1,2-didecanoyl-sn-glycerol 3 phosphate sodium salt (A), chicken egg L- α -phosphatidylcholine (B), and 1,2-dipalmitoyl-rac-glycero-3-phosphocholine hydrate (C) are the lipids represented.

Though the weight ratios of the three lipids varied, the overall effective concentration was 100x or greater than the concentration of TpCONC₁₈ Au MPNs in solution. Of the three lipids, depicted in Figure 4.7, the most effective in stabilizing the nanoparticles in buffer solution, over 72 hours, was the 1,2-didecanoyl-sn-glycerol 3 phosphate sodium salt. This lipid is anionically charged allowing a clathrate of water to surround the head group of the lipid, driving the hydrophobic portion of the molecule into the alkyl chains of the monolayer across the surface of the gold nanoparticle. This is not the case for the other two lipids, which have a zwitterionic head groups containing

opposing charges that essentially neutralize each other. This neutralization effect seemingly limits the ability of the water in the buffer solution to surround that lipid head group and provide an effective driving force for the interdigitation of the lipids alkyl chains into those of the monolayer on the gold nanoparticles.

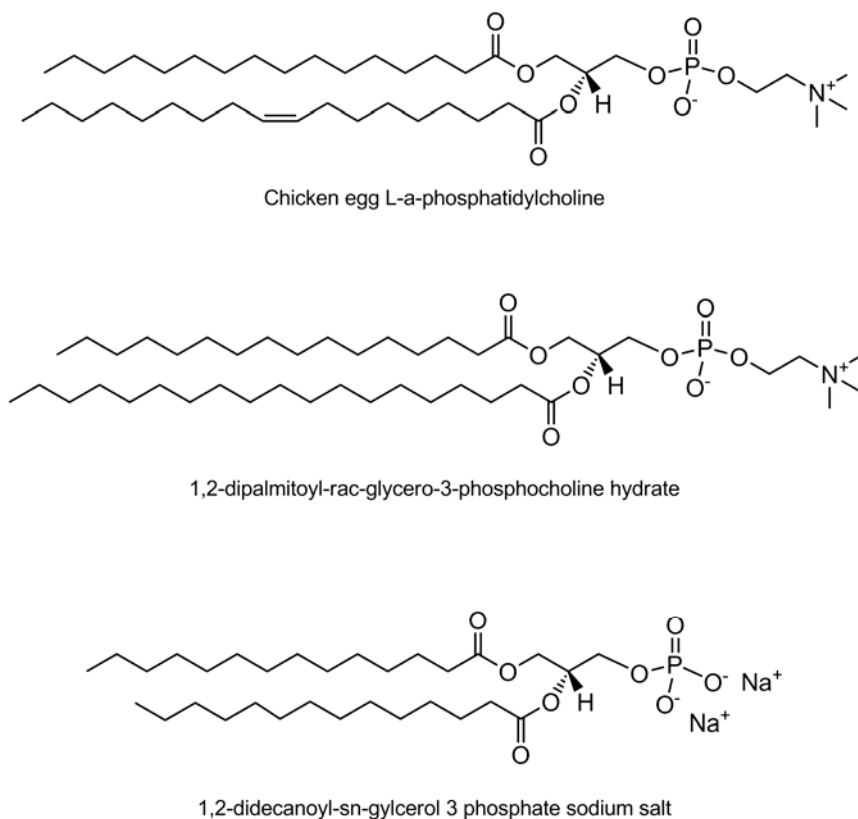


Figure 4.7 The chemical structures of the three lipids tested.

Prior to the intermixing of the 1,2-didecanoyl-sn-glycerol 3 phosphate sodium salt lipid with TpCONC₁₈ Au MPNs, the most dominant ¹H NMR resonance peak across the particle surface is at 1.26 ppm representing the CH₂ groups of the long alkyl chains. If the two mix and interdigitate, this peak should disappear due to the fact that the deuterated solvent only resides on the surface of the lipid head group. With this in mind,

the lipid and TpCONC₁₈ Au MPNs were mixed in a thick slurry, the solvent being deuterated methanol, and heated to induce a chain melting amongst the long alkyl chains of the two. A sample was pulled for spectral analysis. As it turns out, heat with a minimal amount of CD₃OD was not able to induce any type of interdigitation. Resonances of the alkyl chains of the lipid and the TpCONC₁₈ residing on the nanoparticle surface were prevalent indicating that they exist freely moving and exposed to deuterated solvent (highlighted, Figure 4.8). CD₃OD was removed by setting the sample in the refrigerator, allowing the sample to solidify with the solvent residing on top of the mass. In this manner the CD₃OD was simply decanted or poured off and D₂O was added to the sample and heated to ~ 80 °C. At this temperature the alkyl chains should achieve a melt transition and reorder themselves while any residual CD₃OD is slowly evaporated. Monitoring the system over time, there appeared to be some pink color transfer to the D₂O solution. A portion of this D₂O solution was pulled for spectral analysis (Figure 4.8). The only peaks visible in the spectrum, exhibiting minimal intensity, were those at 1.11, 3.24 and 3.6 ppm. These peaks respectively represent the CH₃ group of the long alkyl chains of the TpCONC₁₈, and the CH₂ groups of the glycerol backbone and those residing next to the carbonyl of the attached fatty acids. A majority of the peaks, representing the CH₂ groups of the alkyl chains of both the TpCONC₁₈ and the lipid, highlighted prior to D₂O extraction have dissipated suggesting that interdigitation may have occurred helping stabilize the nanoparticle in solution. The peaks that do show in the D₂O ¹H NMR spectra can be explained as spaces or gaps in between the lipids interdigitated on the edges of the nanoparticle where PPh₃ still resides instead of the TpCONC₁₈ trithiaadamantane derivative. These gaps allow for enough

penetration by the D₂O solvent deep enough to detect a minimal signal from the alkyl chains of the TpCONC₁₈ monolayer.

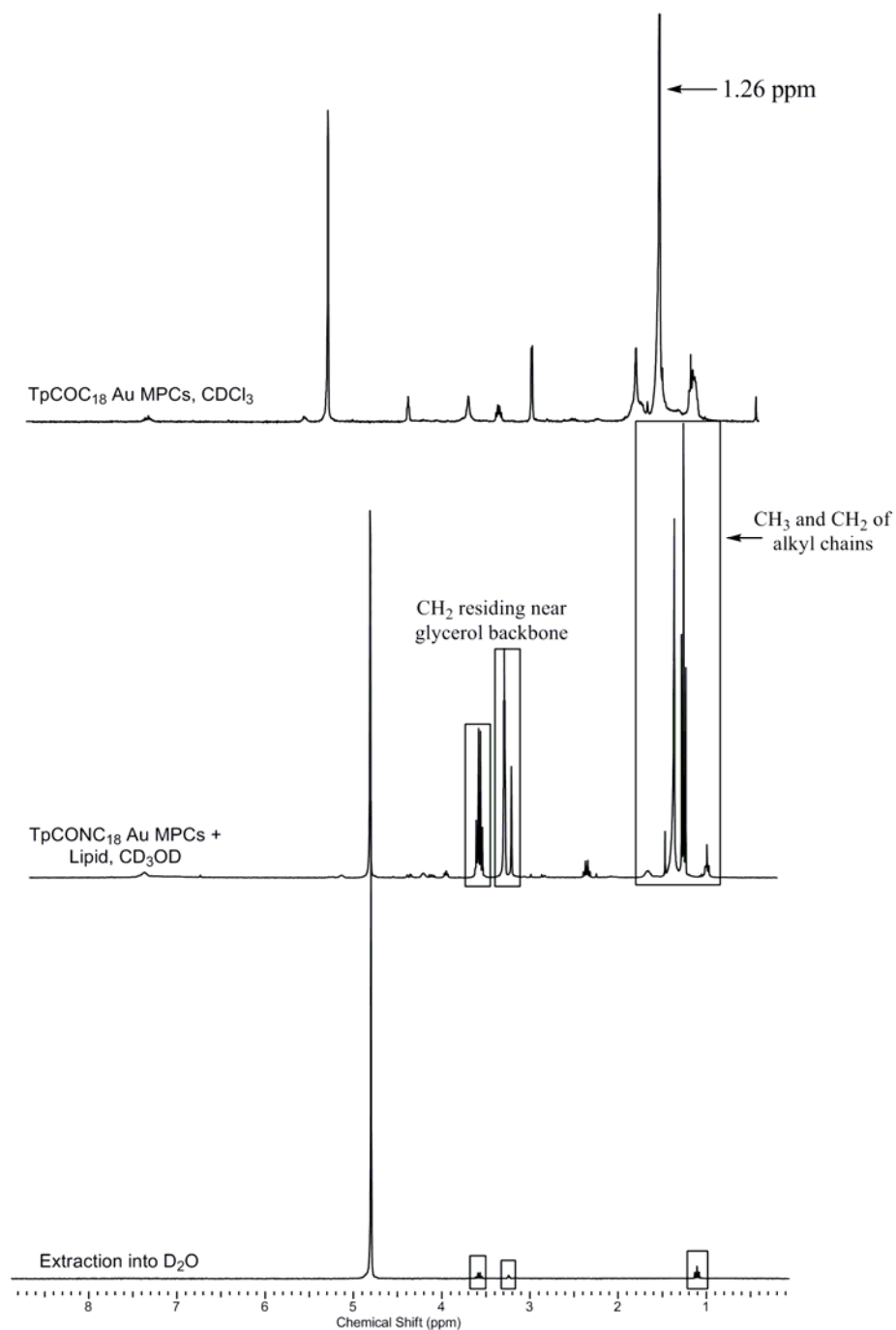


Figure 4.8 The induced lipid interdigitation into TpCONC₁₈ Au MPNs and transfer to D₂O monitored via ¹H NMR.

4.4 Conclusions and Future Work

Based on the thermometric analyses of lipid interdigitation into the TpCONC₁₈ monolayer of the gold nanoparticles in the solid state, it is reasonable to believe that the low packing density of the alkyl derivatized 2,4,9-trithiadamantane is capable of intercalating the alkyl chains of other molecules. This ability was further tested in an attempt to assemble a lipid layer around the TpCONC₁₈ Au MPNs providing stabilization in polar solvent, mainly water or buffer solution. Based on simple qualitative solubility tests, anionically charged lipids proved the best in terms of stabilizing the nanoparticles in a buffer/water solution. Using the anionic lipid 1,2-didecanoyl-sn-glycerol 3 phosphate sodium salt, this was investigated via ¹H NMR spectroscopy and exhibited characteristics as if a lipid monolayer surrounded the gold nanoparticles. Though this study's evidence suggests lipids can intercalate across the surface of gold nanoparticles stabilized with alkyl derivatized 2,4,9-trithiaadamantane, further more detailed testing must be performed to resolve the structure and rheology of the assembled liponanovesicle.

CHAPTER V

POST-SYNTHETIC SURFACE FUNCTIONALIZATION, ENCAPSULATION, AND RELEASING STUDIES OF A NOVEL POLYMER NANOCAPSULE

5.1 Introduction

Nanotechnology focusing on the understanding and application of supramacromolecular structures has led to implementation of various materials within the field of medicine. One emerging area of interest is the use of nanoparticles for targeted therapeutic delivery due to the favorable size and surface functionalities of various synthetic nanomaterials.⁹² Whether the reagent is one used for imaging, chemotherapy, or both, the use of nanoparticles for targeted reagent delivery offers a series of advantages over the traditional small molecular medicines. These carriers are advantageous in the fact that they are similar in size to lipoproteins, and a number of other naturally occurring transport systems, as well as biocompatible through synthetic manipulation of the outer shell, aiding in the stability of otherwise sensitive or insoluble reagents.⁹³ In addition, the potential of incorporating targeting ligands on the outer surfaces of the nanocapsules can not only offer directed delivery reducing overall body distribution, but can also provide sustained release within the targeted tissues specific to the actions of the chemotherapeutic reagents.^{92,93} This maximizes the dose of the reagent

at the target site while minimizing side effects that are often caused by a broad biodistribution as seen in individuals treated by means of conventional chemotherapy.⁹⁴ Typically, these nanocarriers are produced from smaller building blocks or even small molecular monomers by molecular recognition and self-assembling similar to the packaging of biological particles such as viral particles and small membrane vesicles. The use of synthetic building blocks is preferred to reduce the potential of rapid bioabsorption and immunosensitization of the nanoparticles. For example, the use of amphiphilic block copolymers as the building blocks has received much attention.⁹⁵ Well-defined nano-sized micelles can form spontaneously in water from polymers with well-controlled segments and molecular architectures. Nanocapsules arise from the subsequent covalent cross-linking of the building blocks followed by selective chemical degradations of the hydrophobic core segments.⁹⁶⁻⁹⁸ With such nanocapsules, the type of monomers as well as length of the crosslinkers used in the polymerization process allow for manipulation of properties in terms of biodegradability, swelling kinetics, and release rates. This also allows for the construction of nanocarriers that can incorporate both hydrophilic and hydrophobic drugs with adjustable release rates. In typical cases, diblock and triblock copolymers allow the most precise control of forming nanocapsule structures for these purposes. However, the synthesis of well-defined block copolymers, the self-assembling, cross-linking and chemical formations of such nanocapsules remain daunting tasks in terms of scaling-up for practical uses.

One such copolymer that has been widely investigated as an alternative in a variety of nanocapsule formulations is the amphiphilic block copolymer poly(allylamine), PAA, and its derivatives. Considering its structure, the free amines of PAA allow for the

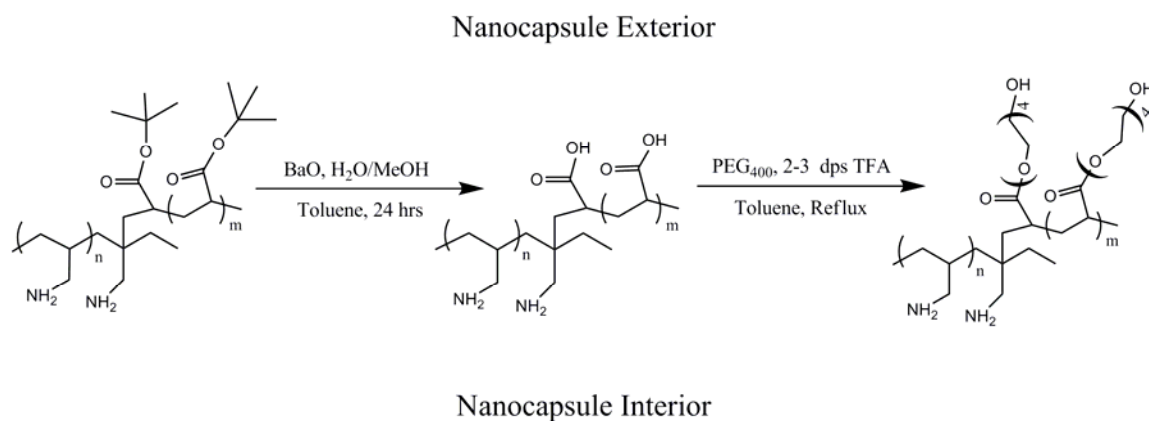
ionic complexation of the copolymer onto oppositely charged macromolecules as well as the formation of a variety of self-assembled polymer architectures dependent upon the moieties attached to the chain.^{99,100} This method though proven to stabilize such charged biomacromolecules as lipids and DNA in nanocapsule-like structures, is quite demanding requiring the rigorous changing of environmental conditions, such as salt concentration, to induce such formations.^{101,102} However, PAA has still remained attractive due to the fact that upon the formation of such aggregates, one can choose to polymerize it covalently attaching the polymer chain to the enwrapped structure or crosslink the polymer to ensure structural stability of the nanocapsule architecture.¹⁰³⁻¹⁰⁵

5.1.1 Objectives

In this research, the development of alternative methods that combine the supramolecular architectures of block copolymers and the efficiency of controlled radical polymerizations for polymer nanocapsules are sought. A method for producing amphiphilic comb-polymer materials, favorable towards large scale synthesis using inverse microemulsion radical polymerization with a novel waterborne radical initiation system is reported.¹⁰² In this method, the self-assembled comb polymer architecture, formed during the inverse micro emulsion radical polymerization of t-butyl acrylate grafted to the waterborne macromolecular radical initiator containing poly(allylamine), was cross-linked in situ at the water/oil interface of the inverse micro emulsions to form the desired polymer nanocapsules.

For the intended uses in biological applications, it is necessary to test the surface chemistry of this new type of materials for further functionalization. In this report, we

demonstrate the post-synthetic surface functionalization strategy with two types of surface modifications. At first, the surface layer of the nanoparticles were found to be



Scheme 5.1 The chemical modifications of the poly(allylamine)-g-poly(*t*-butylacrylate) nanocapsules.

readily hydrolyzed to polycarboxylates under acid or basic conditions, and second, the surface layer can also be easily PEGylated using acid catalyzed esterification reaction with excess of oligo(ethylene glycol). Both surface functionalized nanocapsules were investigated for their water dispersibility, encapsulation and controlled releasing properties with fluorescein, an anionic fluorescence probe, and 5-fluorouacil, an anticancer drug as the model compounds. Through two simple synthetic steps (Scheme 5.1) the material was functionalized with oligo(ethylene glycol). PEGylation was chosen because of its use in various biomedical applications and as a surface coat in many nanoencapsulate systems.¹⁰⁷ Though PEG is not biodegradable, it is nontoxic, nonantigenic and soluble in water with molecule weights up to 4000 being easily excreted in humans.¹⁰⁸ The hydrophilic nature of this material, when attached to a

surface of a nanomaterial, inhibits protein adsorption increasing overall blood retention.¹⁰⁸ The additional PEG layer coating of the nanoencapsulate system may create three distinct phases in which a variety of drugs or imaging agents maybe loaded into. The interior of the nanocapsule containing basic amine groups should be positively charged in neutral pH, capable of loading more anionic species such as DNA and RNA. The cross-linked polymer backbone shell and PEG layers are more hydrophobic, provides a sink for hydrophobic guest molecules. To test this idea, the nanocapsules were loaded with the anionic imaging reagent, fluorescein, and the anti-cancer drug, 5-fluorouracil.

Post-synthetic surface functionalizations of the amphiphilic poly(allyamine)-g-poly(t-butylacrylate) nanocapsule of 50-100 nm diameters were investigated. The hydrophobic poly(t-butylacrylate) surface of the polymer nanocapsules were functionalized with poly(acrylate) and poly(ethylene glycol) and characterized via NMR and FTIR spectroscopies. These new nanocapsules were then investigated for their water dispersibility, encapsulation and controlled releasing properties with fluorescein, an anionic fluorescence probe, and 5-fluorouracil, an anticancer drug as the model compounds using UVVis spectroscopy.

5.2 Experimental Section

In this section the methods and procedures used to synthesize the polymer nanocapsules, modify their surface and investigate their releasing properties are described as follows. This also includes a brief list of the materials and a detailed descriptions of the instruments used in the investigation of the nanocapsules.

5.2.1 Materials and Methods

t-Butyl acrylate (t-BA, Aldrich, 98%) and ethylene diacrylate (ED, Acros, 70%) were washed with NaOH (MERCK, 97%) 5% aqueous solutions to remove the radical polymerization inhibitors, and dried over anhydrous MgSO₄ (Fischer, 99%) overnight and stored at 12 °C prior to uses. Poly(allylamine) (PAA, 20 wt % solution in water, M_w 17,000, Aldrich), H₂O₂ (30 wt % solution in H₂O, Aldrich), toluene (Fischer, 99.9%), buffer solution pH 7.40 (PBS, Fischer), poly(ethylene glycol) (PEG, M_w 400, Acros), trifluoroacetic acid (TFA, Acros, 99%), 5-fluorouracil (5-FU, Acros, 99%) , fluorescein (Acros, 99%), and sorbitan monooleate (Span[®] 80, Aldrich) were used as received.

5.2.1.1 Methods for Spectral and Thermometric Analyses

All ¹H NMR (330 MHz) spectra were recorded using a Varian Gemini-300 spectrometer unless noted. NMR spectra recorded are reported in parts per million (ppm) relative to CDCl₃, reference peak 7,27 ppm. ¹H NMR multiplicity was noted as follows: s, singlet; d, doublet; t, triplet; q, quartet; m, multiplet. IR spectra were recorded on a Nicolet Nexus 870 FT-IR spectrometer equipped with a Thunderdome Attenuated Reflectance (ATR) accessory and recorded in wavenumbers (cm⁻¹). Thermogravimetric analysis (TGA) was performed with a TGA Q500 (Q Advantage 2.8 TA) instrument. Differential scanning calorimetry (DSC) was performed with a DSA Q2000 (Q Advantage 2.8 TA) instrument. UV-Vis spectra were recorded on an Oceanoptics USB4000 UV-Vis spectrometer. All data was processed using Microcals Origin version 6 software.

5.2.2 Polymer Nanocapsule Synthesis and Functionalization

The detailed synthesis of the polymer nanocapsules and subsequent surface modifications are described in detail as follows. The process used to synthesize the polymer nanocapsules was inverse-emulsion polymerization followed by hydrolyzation of the surface and subsequent esterification of the surface via the attachment of poly(ethylene glycol).

5.2.2.1 Synthesis of the Polymer Nanocapsules

The synthesis of the polymer nanocapsules was achieved using the previously reported procedure.^{106,110} Briefly, a three-necked round-bottomed flask was equipped with a thermometer, a condenser, an argon inlet, and a magnetic stir bar. The flask was charged with PAA (0.2 g in 5 mL of water), t-BA monomer (4.5 mL), ED (0.7 mL in 5 mL toluene), H₂O₂ (1.0 mL), and Span[®] 80 (0.17 g). The resulting mixture was sonicated (Fisher FS6) at room temperature for 30 min, resulting in an inverse emulsion that was at least stable for 20 min when sitting at room temperature. The round-bottomed flask was placed in an oil bath and was heated at 65°C ± 2°C for 4 h under constant argon purge and uniform stirring. After the reaction, 50% v/v of an ethanol/water solution (30 mL) was added to the reaction mixture to precipitate the polymer. A white/pale yellowish sticky solid was obtained after removing the solvents and drying under vacuum at room temperature (0.7 g). The sample displayed identical NMR and IR spectra as the previous reported samples. ¹H NMR: 0.89 (d, 2H, (CH₂)_n), 1.26 (d, 2H, (CH₂)_n), 1.5 (m, 9H, C(CH₃)₃), 1.57 (m, 2H, (CH₂)_n), 2.04 (t, 2H, CHCH₂NH₂), 2.18 (d, 2H, CH₂NH₂). FTIR (cm⁻¹): 2928 (-CH), 1727 (-C=O), 1407 (-CH₃), 1176 (-C-O-C-), 1077 (-C-O-C-).

5.2.2.2 Hydrolyzation of the *t*-Butyl Ester of the Polymer Nanocapsule

The use of *t*-butyl ester as the acrylic monomer for the polymer nanocapsule synthesis was intended for two purposes. At first, the *t*-butyl group is hydrophobic, which facilitates the formation of the reverse micro emulsions during the radical polymerization. Second, the *t*-butyl group is also well-known to be readily removed under basic or acidic conditions.¹¹¹ For example, hydrolysis of the *t*-butyl group was achieved by employing the following base catalyzed reaction: To a suspension of the polymer (100 mg) in toluene (10 mL) in a 50 mL round bottom flask equipped with a magnetic stirrer was added a solution of BaO (41 mg) in a mixed solvent of H₂O/MeOH (1.0 mL, 1:4). The reaction mixture was stir at ambient conditions overnight. Afterwards, the reaction mixture was washed with HCl (1 M) to precipitate the polymer. The resulting suspension was filtered and the polymer was collected. The solid polymer was washed with MeOH and then dried under vacuum. ¹H NMR: 0.89 (d, 2H, (CH₂)_n), 1.26 (d, 2H, (CH₂)_n), 1.64 (m, 2H, (CH₂)_n), 2.04 (t, 2H, CHCH₂NH₂), 2.9 (d, 2H, CH₂NH₂), 3.0 (d, 2H, CH₂COO). FTIR (cm⁻¹): 2900 (-CH), 1725 (-C=O), 1550 (-C=O), 1452 (-CH₃), 1407 (-CH₃), 1148 (-C-O-C-).

5.2.2.3 Surface Modification of Polymer Nanocapsules with Poly(ethylene glycol)

Into a two necked 50 mL round bottom flask equipped with a reflux condenser and a magnetic stirrer, was charged with the hydrolyzed polymer nanoparticle (36 mg), PEG (MW 400, 77 mg), TFA (1 drop), and toluene (anhydrous, 20 mL). The reaction mixture was refluxed under argon for 6 h. After refluxing the polymer was filtered, revealing a sticky yellowish solid mass of particles that were washed with MeOH and

then vacuum freeze dried. ^1H NMR: 0.88 (d, 2H, $(\text{CH}_2)_n$), 1.25 (d, 2H, $(\text{CH}_2)_n$), 2.4 (d, 2H, CH_2NH_2), 3.66 (t, 4H, $(\text{OCH}_2\text{CH}_2\text{O})_n$), 3.77 (t, 2H, COOCH_2). FTIR (cm^{-1}): 2874 (-CH), 1788 ($-\text{C}=\text{O}$), 1455 ($-\text{CH}_3$), 1220 ($-\text{C}-\text{O}-\text{C}-$), 1162 ($-\text{C}-\text{O}-\text{C}-$).

5.2.3 Encapsulation and Release Studies

In the following sections, the methods in which the guest molecules of fluorescein and 5-fluorouracil were encapsulated and their release studied are described.

5.2.3.1 Encapsulation of Fluorescein into the Polymer Nanocapsules and Release Studies

The fluorescein-loaded nanoparticles were produced using dialysis methods.^{112,113} A total of 5.0 mg and 45 mg of the capsule polymer were dissolved in 50 mL of MeOH and then vortexed for 6 h at room temperature. Then the fluorescein loaded nanoparticles were placed in a dialysis membrane (FisherBrand, cellulose) and soaked in water for 24 h. To determine the loading amount, 10 mg of the loaded nanoparticles were dispersed in 10 mL of phosphate buffer (1 mM, pH 7.4), and the mixture was shaken on a vortexer (Fisher) for 2 min. The formed emulsion was centrifuged and the aqueous phase was collected to determine the amount of fluorescein released via UV-Vis spectroscopy over time.

5.2.3.2 Encapsulation of 5-Fluorouracil into Surface Modified Polymer Nanocapsules and Release Studies

Similarly to the previously used methods above, the polymer nanocapsules were dispersed in 2 mL and a predetermined amount of 5-fluorouracil, an anticancer

therapeutic, was added to the solution. The nanoparticle-drug solution was stirred at room temperature for 6 h. The nanoparticles were then frozen by a freeze-dyer system to obtain the dried nanoparticles loaded with the drug. To determine the loading amount, 10 mg of 5-fluorouracil loaded nanoparticles were dispersed in 10 mL of phosphate buffer (1 mM, pH 7.4), and the mixture was shaken on a vortexer for 2 min. The formed emulsion was centrifuged and the aqueous phase was collected to determine the amount of 5-fluorouracil via UV-Vis spectroscopy over time.

5.3 Results and Discussion

For surface chemical modification studies, polymer nanocapsules were prepared by employing the previously reported method (Scheme 5.1).^{106,110} The chemical composition of the freshly made polymer nanocapsules was confirmed through ¹H NMR, FT-IR analysis, and solvent dispersibility tests with respect to those published before.

Hydrolysis of the *t*-butyl group of the polymer nanocapsules was achieved by refluxing in a water/methanol mixture using Ba(OH)₂, produced *in situ* from BaO, as the base catalyst.¹¹¹ As the reaction progressed, it can be observed that the initial more heterogeneous reaction mixture gradually turned into a more gel like mixture. The reaction mixture was then acidified and the polymer product was purified through dialysis and dried at ambient conditions. ¹H NMR spectrum of the polymer product showed distinctive peaks at 0.8 – 1.3 ppm corresponding to the hydrocarbon polymer backbone which remained. In contrast to the polymer nanocapsules before the hydrolysis, the peak at 1.5 ppm assigned to the *t*-butyl group disappeared in the product, indicating that it was successfully hydrolyzed. The peaks at 2.9 and 3.0 ppm were

assigned to the methylenes next to a carbonyl and a tetra-coordinated amine ($-\text{NH}_4^+$).¹⁰⁰ They appeared to be sharpened after the hydrolysis, supporting the notion that with the bulky *t*-butyl groups hydrolyzed these groups become more mobile and accessible to the solvents. This observation is also supported by the subsequent thermal analyses. FT-IR of the nanoparticles further confirmed the success of the synthetic modification with the disappearance of C–O–C stretching at 1176 cm^{-1} that is part of the ester, as well as a significant decrease in the intensity of the C–H stretching ranging from $2800\text{--}3000\text{ cm}^{-1}$, indicative of loss of the *t*-butyl group (Figure 5.1b).

PEGylation of the polymer nanocapsules was achieved by attaching PEG₄₀₀ to the polymer via an acid catalyzed esterification reaction with an excess of -OH terminated PEG₄₀₀. The freeze dried product showed a distinctive ¹H NMR signature at 3.6 ppm, which corresponds to the protons of the $-\text{OCH}_2\text{CH}_2\text{O}-$ segment of the PEG. This is further supported by FT-IR analysis with an increase in intensity of the C–H stretching at 2874 cm^{-1} as well as the appearance C–O–C stretching at 1220 and 1162 cm^{-1} corresponding to the ester and ether moieties on the surface of the nanoparticles (Figure 5.1c).

The two types of surface modified polymer nanocapsules were subjected to thermometric analyses. DSC thermograms were taken over the range of -25 to $120\text{ }^\circ\text{C}$ at a scan rate of $10^\circ\text{C}/\text{min}$. The data collected for the two types of material is shown in Figure 5.2. The DSC data of the original material exhibits two glass transitions (T_g 's) representative of two polymer domains. The first T_g occurs at $\sim -1\text{ }^\circ\text{C}$ was assigned to the poly(allylamine), PAA, segment which is in accordance with other published data, while the second T_g at $\sim 55\text{ }^\circ\text{C}$ was assigned to the poly(*t*-butyl acrylate) segment.^{110,112}

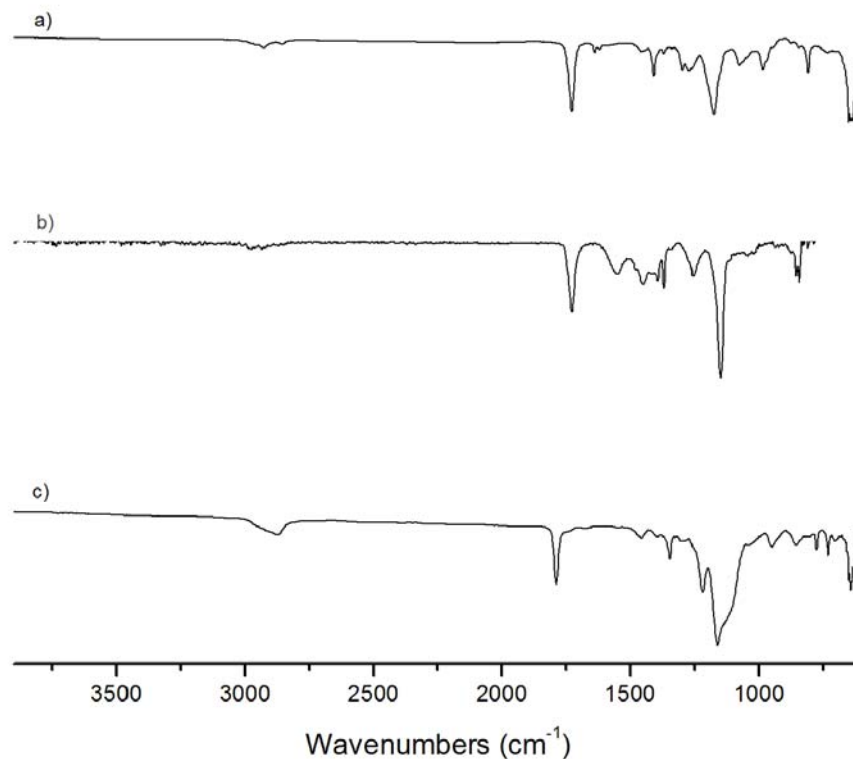


Figure 5.1 FT-IR of the (a) unmodified, (b) hydrolyzed, and (c) PEGylated poly(allylamine)-g-poly(*t*-butylacrylate) polymer nanocapsules.

For the hydrolyzed material, both of these T_g 's are well represented even with the conversion of the poly(*t*-butyl acrylate) segment to a poly(carboxylate) segment (Figure 5.2a). However, there appears to be a third T_g at ~ -22 °C. This maybe attributed to the fact that without the presence of the bulky *t*-butyl groups, the segments containing carboxylate groups are free to rotate along the polymer backbone. For PEG₄₀₀ coated coreshell material the T_g at ~ -1 °C corresponding to the PAA segment remains the same. However, the T_g representative of the poly(*t*-butyl acrylate) segment is shifted to a lower temperature with the exchange of PEG for the *t*-butyl group of the ester. This shift of the

T_g to $\sim 40^\circ\text{C}$ can be attributed to the amorphous nature of the PEG on the surface of the molecule (Figure 5.2b).

TGA of the surface modified polymer nanocapsules was also performed at a scan rate of $10^\circ\text{C}/\text{min}$ from $25\text{--}500^\circ\text{C}$. Similarly to unmodified polymer nanocapsules, the hydrolyzed material two distinct decomposition stages (Figure 5.3a). The first stage occurring at $\sim 250^\circ\text{C}$ is due to the loss of the carboxylate groups on the surface of the material representing 40% of the total weight of the material. The second stage occurring at $\sim 420^\circ\text{C}$ results in the decomposition of the internal segments of PAA, which represents 60%, the bulk, of the total weight composition of the material. For the PEG₄₀₀ coated polymer nanocapsules material, as expected, there were three distinct decomposition stages (Figure 5.3b). The first decomposition stage begins at $\sim 160^\circ\text{C}$ and corresponds to the PEG₄₀₀ layer, which represents 25% of the weight of the material. The second stage at $\sim 250^\circ\text{C}$ is the decomposition of the carboxyl group of the ester to which the PEG₄₀₀ is attached. This portion of the material represents 25% of its weight. The remaining 50% of material left, the PAA segments, undergoes decomposition at $\sim 420^\circ\text{C}$.

Changes to the surface structure of the polymer nanocapsules lead to changes in behavior across a series of different solvents (Table 5.1). Samples of the polymeric nanoparticles were exposed to solvent for 8 h at a time. It has been previously illustrated that the unmodified nanoparticles, due to the hydrophobic exterior attributed to the *t*-butyl groups of the ester, exhibited swelling in hydrophobic nonpolar solvents, such as toluene, over time.¹¹⁰ Upon hydrolysis of the *t*-butyl groups the surface of the polymer nanocapsules becomes more hydrophilic with formation of carboxylate anions.

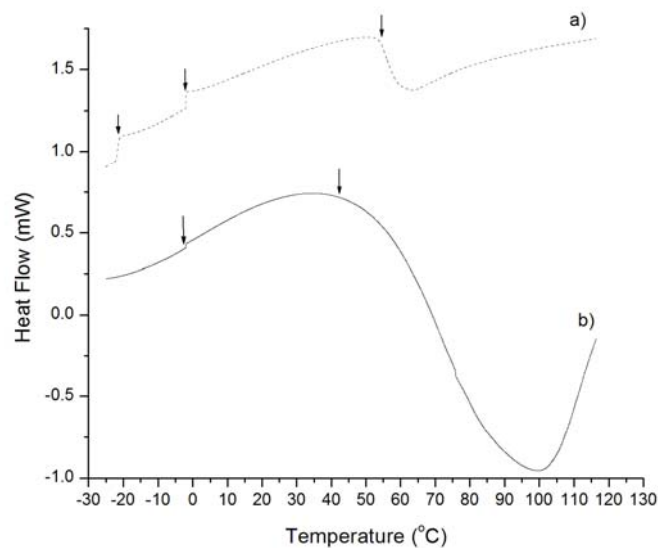


Figure 5.2 The DSC measurements of (a) hydrolyzed and (b) PEGylated poly-(allylamine)-*g*-poly(*t*-butylacrylate) polymer nanocapsules with arrows indicating glass transition states (T_g 's).

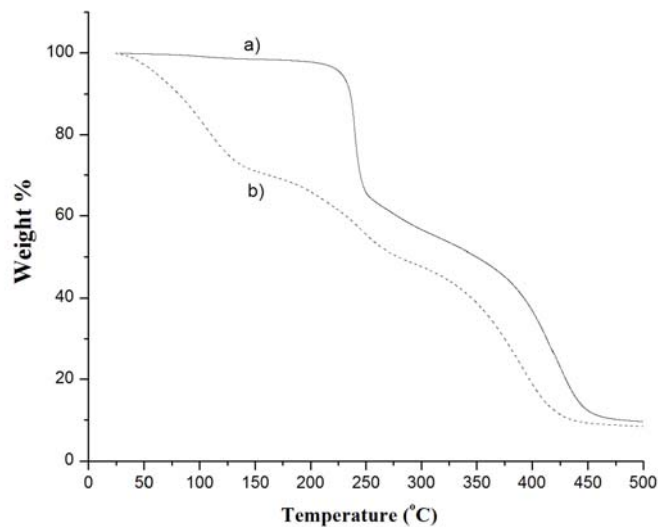


Figure 5.3 The TGA measurements of (a) hydrolyzed and (b) PEGylated poly-(allylamine)-*g*-poly(*t*-butylacrylate) polymer nanocapsules.

No longer exhibiting swelling in toluene, the material exhibits partial swelling in more polar organic solvents such as ethyl acetate, DMF and THF indicating some solubility. Yet, it still remained insoluble in water exhibiting little to no swelling. With the addition of a layer of PEG₄₀₀ to the surface of the polymer nanocapsules, the behavior of the nanocapsules significantly changes across the whole range of solvents tested with the exception of petroleum ether. This is due to the amphiphilic nature of the PEG₄₀₀ in the creation of a multilayered/multiphase nanoparticle as depicted in Scheme 5.1.

Table 5.1 The behavior of the polymer nanocapsules exposed to different solvents over an 8 h period at 25°C.

Solvents	Coreshell	Hydrolyzed coreshell	Hydrolyzed coreshell +PEG₄₀₀
DMF	Insoluble	Swells	Swells
DMSO	Swells	Swells	Swells
Toluene	Swells	Insoluble	Swells
Dichloromethane	Swells	Insoluble	Slight Swelling
Ethanol	Insoluble	Insoluble	Slight Swelling
Ethyl Acetate	Insoluble	Swells	Slight Swelling
Water	Insoluble	Insoluble	Slight Swelling
Petroleum Ether	Insoluble	Insoluble	Insoluble
Acetone	Insoluble	Insoluble	Slight Swelling
THF	Insoluble	Swells	Slight Swelling
Diethyl Ether	Insoluble	Insoluble	Slight Swelling

The above-mentioned spectroscopic and thermal characterizations provide support for the successes in the surface modifications of the polymer nanocapsules. The original PAA-g-poly(*t*-butyl acrylate) cross-linked comb copolymer core-shell

architecture are shown to be robust and suitable for post synthetic surface modifications without losing the overall micelle morphology and dispensability. The results from two typical modifications demonstrate that the surface properties, including solubility and biocompatibility, of these nanocapsules can easily be manipulated to suit a number of uses. One use, as a controlled release nanocarrier for small molecule imaging and therapeutic agents, was further investigated.

When observing the release profiles of nanocapsules, one must consider the type of device category that it falls under. Typically, nanodelivery systems fall under two categories, matrix-based or membrane controlled devices. A matrix-based device is one in which the reagent is actually contained within the polymer matrix and is slowly released as the matrix degrades or activated by a change in the surrounding environment, such as pH. In membrane controlled devices, the drug resides in a reservoir adjacent to the polymer matrix backbone or shell which acts as the rate controlling membrane.¹¹⁴ Our system, falling into the later category, should be a porous material due to its comb architecture. If this is so, then the release of the reagents from the core of these nanocapsules should be governed by diffusion following Fick's law. For this reason, the results of our work were fitted to the selected equation,¹¹⁵

$$W_t/W_\infty = kt^n$$

where W_t/W_∞ is the fractional release at time t , k is the rate constant and exponent n , the diffusion coefficient. The diffusion coefficient is the factor that dictates the mechanism

of diffusional transport involved. When $n = 0.5$, this mechanism of transport is Fickian. When $n = 1$ or that in between, the release is considered zero order or anomalous.¹¹⁶

Both types of surface modified nanocapsules were loaded with small guest molecules, with known UV-Vis absorbance spectra, by soaking the polymer nanocapsules in the solutions of the guest molecules in organic solvents. The polymer nanocapsules loaded with the guest molecules were then washed and dried for releasing studies. In the releasing studies, the loaded polymer nanocapsules were quantified and redispersed in aqueous buffer solutions with gentle shaking on a vortexer (Fisher). The amounts of the guest molecules diffused into the supernatant buffer solutions at each of the given time intervals were quantified via UV-Vis absorbance measurements of the guest molecules in the supernatant liquids. The first reagent, fluorescein, was selected representative of an imaging reagent. For the hydrolyzed nanocapsules, releasing equilibrium was reached rapidly between the internal concentration of the reagent within the nanocapsules and the surrounding solution within ~ 1 min (Figure 5.4). However, for the PEG₄₀₀ coated nanocapsules the amount of time required to attain equilibrium was nearly 3 times that of the hydrolyzed surface. Of the two modifications, it not only better fit the modeled equation with a more acceptable range of error but it behaves similarly to previously published results on such systems (Figure 5.5).¹⁰⁵ The discrepancy between the two different nanocapsules and their surfaces can be explained by the fact that for the hydrolyzed surface, there is a limited hydrophobic barrier through which the anionically charged fluorescein must travel through. This is not the case for the PEG₄₀₀ coated nanocapsules where the charged molecule must travel through the amphiphilic layer of poly(ethylene glycol).

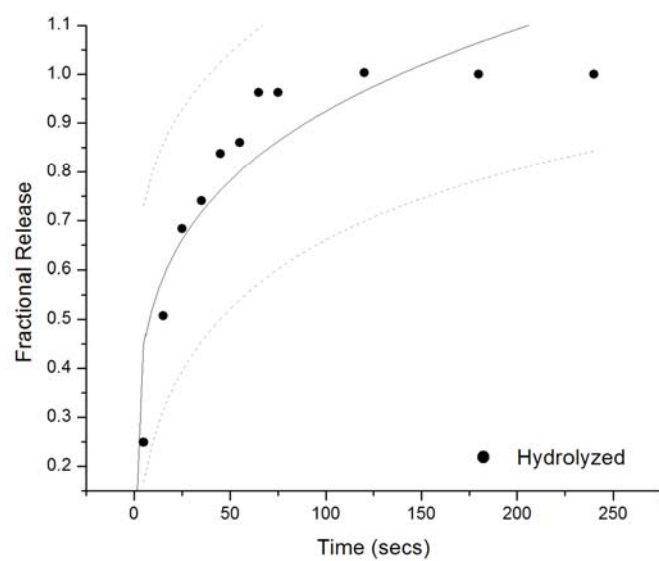


Figure 5.4 Fluorescein release profile for the hydrolyzed polymer nanocapsules with range of error denoted as space between dotted lines.

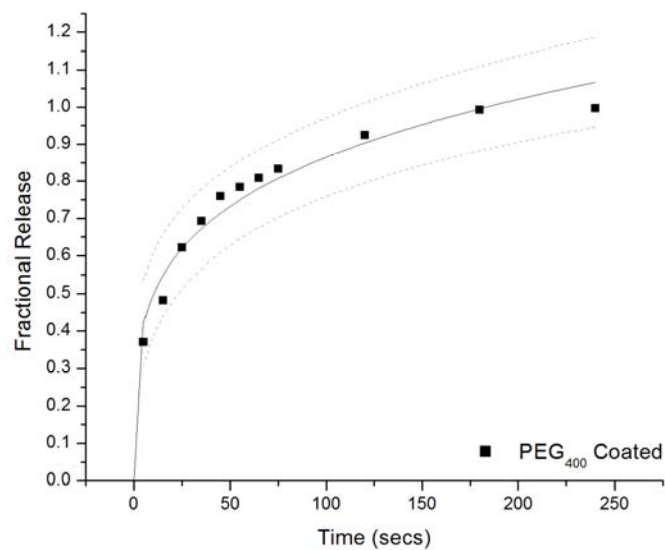


Figure 5.5 Fluorescein release profiles for the PEGylated polymer nanocapsules with range of error denoted as space between dotted lines.

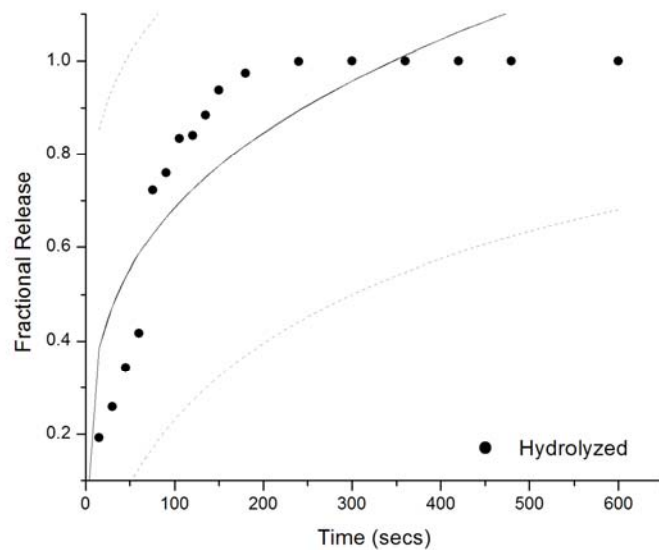


Figure 5.6 5-Fluorouracil release profiles for hydrolyzed polymer nanocapsules with range of error denoted as space between dotted lines.

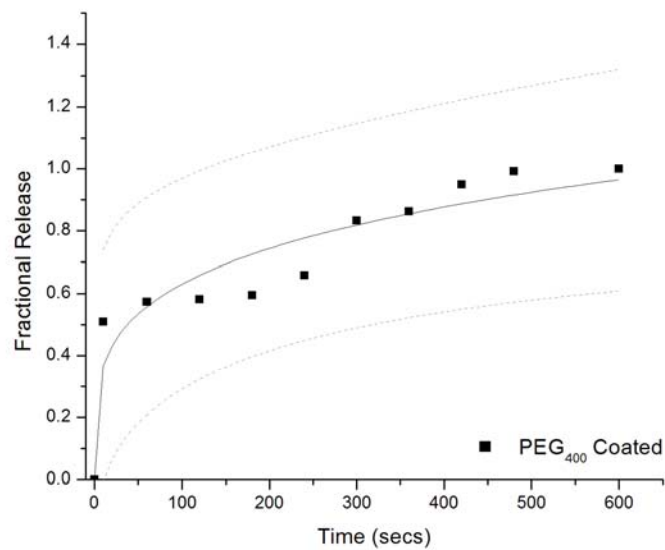


Figure 5.7 5-Fluorouracil release profiles for PEGylated polymer nanocapsules with range of error denoted as space between dotted lines.

The second guest molecule tested was 5-fluorouracil, which represents a small molecule cancer reagent. Release until equilibrium from the hydrolyzed nanocapsules again occurred at a much faster rate than the PEG₄₀₀ coated nanocapsules and does not provide a proper fit to the modeled equation (Figure 5.6). Though the amount of time for release until reaching equilibrium was significantly longer for the PEG₄₀₀ coated nanocapsules, the system does not appear to fit the modeled equation as well (Figure 5.7). The release system itself appears biphasic having two different release rates and two distinct times.¹¹⁷ This may stem from the fact that 5-fluorouracil has no moieties that exhibit a charge at physiological pH, 7.4. This being the case, the initial rate of release as the molecule diffuses through the hydrophobic backbone is dependent upon the initial swelling of the nanocapsule and should be greater than that of the second rate which is diffusion dependent as the molecule travels through the charged surface of the hydrolyzed nanocapsule or the amphiphilic surface of the PEG₄₀₀ coated nanocapsules.¹⁰⁵ The results from fitting the data to the selected equation were obtained and are listed in Table 5.2.

Table 5.2 The releasing results fitted to $W_t/W_\infty = kt^n$ based on a non-linear fit using Microcal Origin version 6 software.

Nanocapsule Type	Guest Molecules	Parameters		R ²
		k	n	
Hydrolyzed	Flourescein	0.3054	0.24047	0.81413
	5-Fluorouracil	0.16896	0.30416	0.74832
PEGylated	Flourescein	0.287	0.23952	0.95561
	5-Fluorouracil	0.21214	0.23674	0.79091

5.4 Conclusions and Future Work

In conclusion, it was found that the polymer nanocapsules are more effective carriers for negative charged small molecules in aqueous solutions at pH 7.4. This is most likely due to the quaternary ammonium groups that reside within the internal structure of the nanocapsule, which help to stabilize the negative charge. The fast releasing rates of the guest molecules was mostly attributed to the small size of the polymer nanocapsules (60-100 nm) used in this study. However, the results also indicated that the thin shells of the polymer nanocapsules may have defects that lowered the diffusion barrier of the guest molecules from releasing out of the capsule. For future studies, increasing the molecular weight of the acrylic segment of the polymer nanocapsules to reinforce the shell structures may help to increase the diffusion barrier. In addition, the above results are encouraging for the use of these polymer nanocapsules for the delivery of negatively charged DNA and RNA molecules.

REFERENCES

1. Lehn, J.M. *Supramolecular Chemistry: Concepts and Perspectives*; VCH Verlagsgesellschaft: Weinheim, Germany, 1995; Chapter 1.
2. Voet, D.; Voet, J.G.; Pratt, C.W. *Fundamentals of Biochemistry*, 2nd ed.; John Wiley & Sons: Hoboken, New Jersey, U.S.A., 2006; pp 103-162.
3. Voet, D.; Voet, J.G.; Pratt, C.W. *Fundamentals of Biochemistry*, 2nd ed.; John Wiley & Sons: Hoboken, New Jersey, U.S.A., 2006; pp 835-841.
4. Tredgold, R.H. *Order in thin organic films*; Cambridge University Press: Cambridge, London, 1994; pp 2-5.
5. Langmuir, I. *J. Am. Chem. Soc.* **1917**, *39*, 1848.
6. Blodgett, K.B. *J. Am. Chem. Soc.* **1935**, *57*, 1007.
7. Bigelow, W.C.; Pickett, D.L.; Zisman, W.A. *J. Colloid Interface Sci.* **1946**, *1*, 513.
8. Schreiber, F. *J. Phys: Cond. Matt.* **2004**, *16(28)*, 883.
9. Nuzzo, R.G.; Allara, D.L. *J. Am. Chem. Soc.* **1983**, *105*, 4481.
10. Nuzzo, R.G.; Zegarski, B.R.; Dubois, L.H. *J. Am. Chem. Soc.* **1987**, *109*, 733-740.
11. Nuzzo, R.G.; Fusco, F.A.; Allara, D.L. *J. Am. Chem. Soc.* **1987**, *109*, 2365.
12. Bain, C.D.; Biebuyck, H.A.; Whitesides, G.M. *Langmuir* **1989**, *5(3)*, 723-727.
13. de la Llave, E.; Ricci, A.; Calvo, E.J.; Scherlis, D.A. *J. Phys. Chem. C* **2008**, *112*, 17614.
14. Dubois, L.H.; Zegarski, B.R.; Nuzzo, R.G.; *J. Am. Chem. Soc.* **1990**, *112*, 575.
15. Sung, I.H.; Kim, D.E. *Tribology Letters* **2004**, *17(4)*, 843.

16. Laguna, A. *Modern Supramolecular Gold Chemistry: Gold-Metal Interactions and Applications*; VCH Verlagsgesellschaft: Weinheim, Germany, 2008; pp 165.
17. Rubahn, H.G. *Basics of Nanotechnology*, 3rd ed.; VCH Verlagsgesellschaft: Weinheim, Germany, 2008; pp 12.
18. Ahmadi, T.S.; Logunov, S.L.; El-Sayed, M.A. In *Nanostructured Materials: Clusters, Composites, and Thin Films*; Shalaev, V.M.; Moskovits, M., Eds.; ACS Symposium Series 679; American Chemical Society: Washington, DC, 1997, pp 125-140.
19. Haes, A.J.; Chang, L.; Klein, W.L.; Van Duyne, R.P. *JACS* **2005**, *127*, 2264.
20. Gomez, R. *Biomed. Microdevices* **2001**, *3(3)*, 201-209.
21. Prasad, S.; Bothara, M.; Reddy, R.; Carruthers, J.; Barrett, T. *Mater. Res. Soc. Symp. Proc.* **2008**, *1095*, 1-8.
22. Hahn, J.; Lieber, C.M. *NanoLetters* **2004**, *4(1)*, 51-54.
23. Vidic, J.; Pla-Roca, M.; Grosclaude, J.; Persuy, M.A.; Monnerie, R.; Caballero, D.; Errachid, A.; Hou, Y.; Jaffrezic-Renault, N.; Salesse, R.; Pajot-Augy, E.; Samitier, J. *Anal. Chem.* **2007**, *79*, 3280-3290.
24. Baldrich, E.; Laczka, O.; Del Campo, F.J.; Munoz, F.X. *J. of Immun. Methods* **2008**, *336*, 203-212.
25. Porter, M.D.; Bright, T.B.; Allara, D.L.; Chidsey, C.E.D. *J. Am. Chem. Soc.* **1987**, *109*, 3559.
26. Shewmake, T.A.; Solis, F.J.; Gillies, R.J.; Caplan, M.R. *Biomacromolecules* **2008**, *9(11)*, 3057.
27. Hu, J. Liu, Y.; Khemtong, C.; El Khoury, J.M.; McAfoos, T.J.; Taschner, I.S. *Langmuir* **2004**, *20*, 4933-38.
28. Kittredge, K.W.; Minton, M.A.; Fox, M.A.; Whitesell, J.K. *Helv. Chim. Acta* **2002**, *85*, 788.
29. Lindgren, G. *Chemica Scripta* **1976**, *9*, 220-226.
30. Khemtong, C.; Hu, J. *J. Sulfur Chem.* **2005**, *26*, 105-109.
31. Khemtong, C.; Banerjee, D.; Liu, Y.; El Khoury, J.M.; Rinaldi, P.L.; Hu, J. *Supramolecular Chem.* **2005**, *17(4)*, 335.

32. Venkataraman, L.; Klare, J.E.; Tam, I.W.; Nuckolls, C.; Hybertsen, M.S.; Steigerwald, M.L. *NanoLetters* **2006**, *6*(3), 458.
33. Laibinis, P.E.; Whitesides, G.M.; Allara, D.L.; Tao, Y.T.; Parikh, A.N.; Nuzzo, R.G. *J. Am. Chem. Soc* **1991**, *113*(19), 7152-7167.
34. Chidsey, C.E.D.; Loiacono, D.N. *Langmuir* **1990**, *6*(3), 682-691.
35. Carrillo, I.; Quintana, C.; Esteva, A.M.; Hernandez, L.; Hernandez, P. *Electroanalysis* **2008**, *20*(24), 2614-2620.
36. Bozic, R.G.; West, A.C.; Levicky, R. *Sensors and Actuators B* **2008**, *133*, 510.
37. Chidsey, C.E.D. *Science* **1991**, *251*(4996), 919-922.
38. Li, T.T.T.; Weaver, M.J. *J. Am. Chem. Soc* **1984**, *106*, 6107.
39. Finklea, H.O.; Hanshew, D.D. *J. Am. Chem. Soc* **1992**, *114*(9), 3174.
40. Chidsey, C.E.D.; Bertozzi, C.R.; Putvinski, T.M.; Mujscce, A.M. *J. Am. Chem. Soc* **1990**, *112*(11), 4301-4306.
41. Greenler, R.G. *J. Phys. Chem.* **1966**, *44*, 310.
42. Golden, W.G. *Fourier Transform Infrared Spectroscopy*, Vol. 4; Academic Press: New York, New York, U.S.A., 1985; pp 313.
43. Slater, D.A.; Hollins, P.; Chesters, M.A.; Pritchard, J.; Martin, D.H.; Surman, M.; Shaw, D.A.; Munro, I.H. *Rev. Sci. Instrum.* **1992**, *63*, 1547.
44. Liu, Y. Application of Supramolecular Chemistry in the Catalytic Transition Metal/Polycarbodiimide Nanocomposite and the Photoactive Surface Patterning. Ph.D. Dissertation, The University of Akron, Akron, OH, December 2003.
45. Cotton, F.A.; Reid, A.H. *Acta Cryst.* **1985**, *41*, 686.
46. Ulman, A. *Chem. Rev.* **1996**, *96*, 1533.
47. Bain, C. D.; Troughton, E. B.; Tao, Y. T.; Evall, J.; Whitesides, G. M.; Nuzzo, R. G. *J. Am. Chem. Soc.* **1989**, *111*, 321.
48. Bain, C. D.; Whitesides, G. M. *Angew. Chem., Int. Ed. Engl.* **1989**, *28*, 506.
49. Mazur, M.; Kryszinski, P. *Langmuir* **2001**, *17*, 7093-7101.

50. Anne, A.; Moiroux, J. *Macromolecules* **1999**, *32*, 5829-5835.
51. a) Minko, S.; Muller, M.; Motornov, M.; Nitschke, M.; Grundke, K.; Stamm, M. *J. Am. Chem. Soc.* **2003**, *125*, 3896-3900. b) Ionov, L.; Minko, S.; Stamm, M.; Gohy, J.; Jerome, R.; Scholl, A. *J. Am. Chem. Soc.* **2003**, *125*, 8302-8306. c) Julthongpiput, D.; Lin, Y. H.; Teng, J.; Zubarev, E. R.; Tsukruk, V. V. *J. Am. Chem. Soc.* **2003**, *125*, 15912-15921. d) von Werne, T. A.; Germack, D. S.; Hagberg, E. C.; Sheares, V. V.; Hawker, C. J.; Carter, K. R. *J. Am. Chem. Soc.* **2003**, *125*, 3831-3838.
52. Finklea, H. O. In *Electroanalytical Chemistry*; Bard, A. J., Rubinstein, J., Eds.; Marcel Dekker: New York, 1996; Vol. 19, p 109.
53. Kanazawa, H. *Anal. Bioanal. Chem.* **2004**, *378*, 46-48.
54. a) Ichimura, K.; Oh, S. K.; Nakagawa, M. *Science* **2000**, *288*, 1624-1626. b) Ionov, L.; Stamm, M.; Diez, S. *Nano Lett.* **2006**, *6*, 1982-1987.
55. Ionov, L.; Houbenov, N.; Sidorenko, A.; Stamm, M.; Minko, S. *Adv. Funct. Mater.* **2006**, *16*, 1153-1160.
56. a) Ionov, L.; Sapra, S.; Synytska, A.; Rogach, A. L.; Stamm, M.; Diez, S. *Adv. Mater.* **2006**, *18*, 1453-1457. b) Tokareva, I.; Minko, S.; Fendler, J. H.; Hutter, E. *J. Am. Chem. Soc.* **2004**, *126*, 15950-15951. c) Westenhoff, S.; Kotov, N. A. *J. Am. Chem. Soc.* **2002**, *124*, 2448-2449. d) Lin, Y. H.; McConney, M. E.; LeMieux, M. C.; Peleshanko, S.; Jiang, C. Y.; Singamaneni, S.; Tsukruk, V. V. *Adv. Mater.* **2006**, *18*, 1157-1161. e) Tokareva, I.; Tokarev, I.; Minko, S.; Hutter, E.; Fendler, J. H. *Chem. Commun.* **2006**, 3343-3345.
57. a) Motornov, M.; Sheparovych, R.; Lupitsky, R.; MacWilliams, E.; Hoy, O.; Luzinov, I.; Minko, S. *Adv. Funct. Mater.* **2007**, *17*, 2307; b) Fujii, S.; Armes, S. P.; Binks, B. P.; Murakami, R. *Langmuir* **2006**, *22*, 6818-6825.
58. a) Hoffman, A. S.; Stayton, P. S.; Press, O.; Murthy, N.; Lackey, C. A.; Cheung, C.; Black, F.; Campbell, J.; Fausto, N.; Kyriakides, T. R.; Bornstein, P. *Polym. Adv. Technol.* **2002**, *13*, 992-999; b) Lata, S.; Piehler, J. *Anal. Chem.* **2005**, *77*, 1096-1105.
59. Nealy, P. F.; Black, A. J.; Wilbur, J. L.; Whitesides, G. M. *Micro- and Nanofabrication Techniques Based on Self-assembled Monolayers in Molecular Electronics*; Jortner, J.; Ratner, M. Eds.; Blackwell Science, **1997**.
60. Wang, H.; Design, Synthesis, and Supramolecular Surface Chemistry of Bi- and Tridentate Surface Anchors for Nanoscience and Nanobiotechnology. Ph.D. Dissertation, The University of Akron, Akron, OH, August 2007.

61. Matyjaszewski, K.; Xia, J. *Chem. Rev.* **2001**, *101*(9), 2924.
62. a) Shon, Y. S.; Mzzitelli, C.; Murray, R. W. *Langmuir*, **2001**, *17*, 7735. b) Troughton, E. B.; Bain, C. D.; Whitesides, G. M.; Nuzzo, R. G.; Allara, D. L.; Porter, M. D. *Langmuir*, **1988**, *4*, 365. c) Li, X. M.; De Jong, M. R.; Inoue, K.; Shinkai, S.; Huskens, J.; Reinhoudt, D. N. *J. Mater. Chem.* **2001**, *11*, 1919. d) Brousseau, L. C.; Ovak, J. P.; Marinkos, S. M.; Feldheim, D. L.; *Adv Mater.* **1999**, *11*, 447. e) Maye, M. M.; Chun, S. C.; Han, L.; Rabinovich, D.; Zhong, C. *J. Am. Chem. Soc.* **2002**, *124*, 4958.
63. Dolog, I.; Mallik, R. R.; Mozyński, A.; Hu, J.; Wang, H. *Surface Science*, **2006**, *600*, 2972–2979.
64. Bao, Z. Y.; Bruening, M. L.; Baker, G. L. *J. Am. Chem. Soc.* **2006**, *128*, 9056-9060.
65. Zhou, F.; Hu, H. Y.; Yu, B.; Osborne, V. L.; Huck, W. T. S.; Liu, W. M. *Anal. Chem.* **2007**, *79*, 176-182.
66. Jones, D. M.; Huck, W. T. S. *Adv. Mater.* **2001**, *13*, 1256.
67. Du, J.; Armes, S. P. *J. Am. Chem. Soc.* **2005**, *127*, 12800.
68. Zhang, Q. L.; Xia, F.; Sun, T. L.; Song, W. L.; Zhao, T. Y.; M. C. Liu, M.C.; Jiang, L. *Chem. Commun.*, **2008**, 1199.
69. Matyjaszewski, K.; Miller, P. J.; Shukla, N.; Immaraporn, B.; Gelman, A.; Luokala, B. B.; Siclovan, T. M.; Kickelbick, G.; Vallant, T.; Hoffmann, H.; Pakula, T. *Macromolecules* **1999**, *32*, 8716.
70. Husemann, M.; Mecerreyes, D.; Hawker, C. J.; Hedrick, J. L.; Shah, R.; Abbott, N. L. *Angew. Chem., Int. Ed.*, **1999**, *38*, 647.
71. Motornov, M.; Sheparovych, R.; Tokarev, I.; Roiter, Y.; Minko, S. *Langmuir* **2007**, *23*, 13.
72. Szleifer, I.; Carignano, M. A. Tethered Polymer Layers. *Adv. Chem. Phys.* **1996**, *94*, 165.
73. Tam, T. K.; Ornatska, M.; Pita, M.; Minko, S.; Katz, E. *J. Phys. Chem. C*, **2008**, *112*, 8438.
74. Salata, O.V. *J. Nanobiotech.* **2004**, *2*.

75. Caruthers, S.D.; Wickline, S.A.; Lanza, G.M. *Curr. Opin. Biotechnol.* **2007**, *18*, 26.
76. Erickson, D.; Mandal, S.; Yang, A.H.J.; Cordovez, B. *Microfluid Nanofluid* **2008**, *4*, 33–52.
77. Kim, D.K.; Kerman, K.; Saito, M.; Sathuluri, R.R.; Endo, T.; Yamamura, S.; Kwon, Y.; Tamiya, E. *Anal. Chem.* **2007**, *79*, 1855–1864.
78. Khan, J.A.; Pillai, B.; Das, T.K.; Singh, Y.; Maiti, S. *ChemBioChem.* **2007**, *8*, 1239.
79. Fox, M.A.; Whitesell, J.K.; Hu, J.; Zhang, J.; Liu, F.; Kittredge, K. *J. Am. Chem. Soc.* **2001**, *123*, 1462.
80. Mirkin, C.A.; Cao, Y.C.; Jin, R.; Nam, J.M.; Thaxton, C.S. *J. Am. Chem. Soc.* **2003**, *125*, 14676.
81. Barchi, J.J.; Svarovsky, S.A.; Szekely, Z. *Tetrah: Asym.* **2005**, *16*, 587.
82. Mammen, M.; Choi, S.K.; Whitesides, G.M. *Angew. Chem. Int. Ed.* **1998**, *37*, 2754–2794.
83. Shewmake, T.A.; Solis, F.J.; Gillies, R.J.; Caplan, M.R. *Biomacromolecules* **2008**, *9(11)*, 3057.
84. Khemtong, C. Synthesis and Supramolecular Chemistry of 2,4,9-Trithiaadamantane Derivatives. Ph.D. Dissertation, University of Akron, Akron, OH, August 2005.
85. Rudd, P.M.; Elliott, T.; Cresswell, P.; Wilson, I.A.; Dwek, R.A. *Science* **2001**, *291*, 2370.
86. Reitter, J.N.; Means, R.E.; Desrosiers, R.C. *Nature Med.* **1998**, *4*, 679.
87. Orntoft, T.F.; Vestergaard, E.M. *Electrophoresis* **1999**, *20*, 364–365.
88. Reitter, J.N.; Means, R.E.; Desrosiers, R.C. *Nature Med.* **1998**, *4*, 679.
89. Balasubramanian, R.; Guo, R.; Mills, A.J.; Murray, J.W. *J. Am. Chem. Soc.* **2005**, *127*, 8126.
90. Jacobson, K.; Papahadjopoulos, D. *Biochemistry* **1975**, *14(1)*, 155.
91. Panicker, L. *J. Coll. Sur. B: Biointerfaces* **2008**, *61*, 146.

92. Panyam, J.; Labhasetwar, V. *Adv. Drug Delivery Rev.* **2003**, *55*, 329
93. Haag, R. *Angew. Chem. Int. Ed.* **2004**, *43*, 278.
94. Babu, V.R.; Sairam, M.; Hosamani, K.M.; Aminabhavi, T.M. *Int. J. Pharm.* **2006**, *325*, 55.
95. Gillies, E.R.; Frechet, J.M.J. *Chem. Commun.* **2003**, 1640.
96. Wooley, K.L. *J. Polym. Sci. A: Polym. Chem.* **2000**, *38*, 1397.
97. Koh, A.Y.C.; Saunders, B.R. *Chem. Commun.* **2000**, 2461.
98. Li, Z.C.; Jin, W.; Li, F.M. *React. Funct. Polym.* **1999**, *42*, 21.
99. Murthy, V.S.; Rana, R.K.; Wong, M.S. *J. Phys. Chem. B* **2006**, *110*, 25619-25627.
100. Thompson, C.J.; Ding, C.; Qu, X.; Yang, Z.; Uchegbu, I.F.; Tetley, L.; Cheng, W.P. *Colloid Polym. Sci.* **2008**, *286*, 1511-1526.
101. Werle, M.; Takeuchi, H. *Sci. Pharm.* **2008**, *76*, 751-160.
102. Zhang, B.; Ji, W.; Liu, W.; Yao, K. *Int. J. of Pharmaceutics* **2007**, *331*, 116-122.
103. Lu, M.Z.; Lan, H.L.; Wang, F.F.; Wang, Y.J. *J. Microencapsulation* **2000**, *17*(2), 245-251.
104. Chorny, M.; Fishbein, I.; Alferiev, I.; Levy, R.J. *Molecular Pharmaceutics* **2009**, *6*(5), 1380-1387.
105. Crisante, F.; Francolini, I.; Bellusci, M.; Martinelli, A.; D'Ilario, L.; Piozzi, A. *Eur. J. of Pharm. Sci.* **2009**, *36*, 555-564.
106. Sarkar, D.; El Khoury, J.M.; Lopina, S.T.; Hu, J. *Macromolecules* **2005**, *38*, 8603-8605.
107. Moghimi, S.M.; Hunter, A.C.; Murray, J.C. *Pharma. Rev.* **2001**, *53*(2), 296.
108. Rameez, S.; Alost, H.; Palmer, A.F. *Bioconjugate Chem.* **2008**, *19*, 1025.
109. Yan, G.P.; Hua, L.; Cheng, S.X.; Bottle, S.E.; Wang, X.G.; Yew, Y.K.; Zhou, R.Z. *J. Appl. Polym. Sci.* **2004**, *92*, 3869.

110. Sarkar, D.; El Khoury, J.M.; Lopina, S.T.; Hu, J. *J. App. Polym. Sci.* **2007**, *104*, 1905-1911.
111. Anderson, M.O.; Moser, J.; Sherrill, J.; Guy, R.K. *Synlett* **2004**, *13*, 2391-2393.
112. Zhang, Z.; Feng, S.S. *Biomacromolecules* **2006**, *7*, 1139-1146.
113. Huh, K.M.; Lee, S.C.; Cho, Y.W.; Lee, J.; Jeong, J.H.; Park, K. *J. Controlled Release* **2005**, *101*, 59-68.
114. Lee, A.J.; King, J.R.; Hibberd, S. *IMA J. of Mathe. Appl. Med. & Bio.* **1998**, *15*, 136.
115. Davidson, G.W.R.; Peppas, N.A. *J. Controlled Release* **1986**, *3*, 265.
116. Bajpai, A.J.; Chouboy, J. *J. Appl. Polym. Sci.* **2006**, *101*, 2323.
117. Tzafriri, A.R.; Lerner, E.I.; Flashner-Barak, M.; Hinchcliffe, M.; Ratner, E.; Parnas, H. *Clin. Cancer Research* **2005**, *826(11)*, 829.